

**MASTER**

**Measurement system design for an automatic guided vehicle**

Visser, H.M.C.

*Award date:*  
2000

[Link to publication](#)

**Disclaimer**

This document contains a student thesis (bachelor's or master's), as authored by a student at Eindhoven University of Technology. Student theses are made available in the TU/e repository upon obtaining the required degree. The grade received is not published on the document as presented in the repository. The required complexity or quality of research of student theses may vary by program, and the required minimum study period may vary in duration.

**General rights**

Copyright and moral rights for the publications made accessible in the public portal are retained by the authors and/or other copyright owners and it is a condition of accessing publications that users recognise and abide by the legal requirements associated with these rights.

- Users may download and print one copy of any publication from the public portal for the purpose of private study or research.
- You may not further distribute the material or use it for any profit-making activity or commercial gain

Eindhoven University of Technology  
Department of Electrical Engineering  
Division of Measurement and Control Systems  
Control Systems Group

**TU/e** technische  
universiteit  
eindhoven

# **Measurement system design for an Automatic Guided Vehicle**

by Ing. H.M.C. Visser

Master of Science Thesis  
carried out from September 1999 till August 2000

commissioned by Prof. Dr. Ir. P.P.J. van den Bosch (TUE)  
under supervision of Ir. D. de Bruin (TUE)

date: August 28, 2000

The Department of Electrical Engineering of the Eindhoven University of Technology accepts no responsibility for the contents of M.Sc. Theses or reports on practical training periods.

# Abstract

In and around the city of Eindhoven in The Netherlands, a new kind of public transportation system is going to be used. This new system consists amongst others of articulated and double articulated commuter buses, equipped with all-wheel steering for high maneuverability at bus stops and in curves. For human drivers it is impossible to steer such a complex vehicle sufficiently accurate by hand. Therefore, the buses have to be equipped with an automatic guidance system that steers the vehicles along the bus lanes.

The Control Systems Group of the Eindhoven University of Technology is doing research on the measurement and control system of the vehicle.

The automatic guidance system has to consist of a reliable measurement system. Only with a reliable measurement system, it is possible to steer the vehicle along the bus lane correctly. This report describes the design of a measurement system for the automatic guidance system where the vehicles can be equipped with.

The guidance system is designed in such a way that the vehicle is guided laterally. For the lateral guidance of the vehicle it is important that position and speed of the vehicle are determined with respect to the path that has to be followed. The path that has to be followed will be formed by a track of magnets. This is a track in which permanent magnets are mounted in the road surface at fixed distances of each other. These permanent magnets will be detected by magnetometers in the vehicle. The measurement system or the observer is designed according to the theory of Kalman filtering. In the design of the observer a lot of kinematics of the vehicle are involved. The kinematic equations of the vehicle are described as well as a state-space description of the kinematic equations.

The lateral position and velocity of the vehicle can be estimated with an accelerometer, which measures the lateral acceleration of the vehicle. The velocity estimates are obtained by integrating the measurements of the accelerometer once, whereas the estimates of the deviations are obtained by integrating the accelerometer data twice. The estimates show deviations with respect to the true values caused by measurement noise. The estimates can be updated and corrected with use of the measurement data coming from the magnetometers, which measure the lateral deviation of the vehicle. With this estimation technique, which is completely independent of all vehicle parameters, it is possible to obtain estimates of the lateral deviation and velocity of the vehicle, which come close to the true lateral deviation and velocity of the vehicle. To make the estimates come closer to the true values, the observer can be improved by extending it with some sensors. The measurement data of these additional sensors can be used to do an extra update on the estimates, with the intention to improve the estimates. The sensors that are discussed to improve the observer are the integrating and rate gyroscope. Gyroscopes measure the orientation or the rate of change in orientation of the object on which they are mounted.

Simulation results show that gyroscopes are a good option for the improvement of the observer. For the implementation of the sensors in the observer, it is important to know their noise properties and that the noise can be characterized in the observer. It is described how to deal with sensor noise and how to obtain noise properties. Noise properties of the used sensors are extracted from their datasheets and simulations are carried out to show the behaviour of the observer with these sensors and their noise. Furthermore, the observer is described in a SISO and MIMO representation and the design of the observer is done according to the MIMO representation.



# Acknowledgements

*I would like to use this page of my report, to express my sincere gratitude to the people involved in my thesis.*

*First of all I would like to thank Prof. Dr. Ir. P.P.J. van den Bosch, who gave me the opportunity for working on this project.*

*I also would like to thank Ir. Dik de Bruin, who coached me during the months I was working on my thesis.*

*I would like to thank the involved employees of the Control Systems Group of the TUE who all contributed their own part to my thesis.*

*Finally I would like to thank my family and friends, who supported me during my entire period of study.*

*Henri Visser.*

# Table of contents

<b>1 INTRODUCTION.....</b>	<b>1</b>
1.1 PURPOSE OF INVESTIGATION .....	1
1.2 ASSIGNMENT.....	2
1.3 STRUCTURE OF THE REPORT.....	2
<b>2 KALMAN FILTERING THEORY.....</b>	<b>3</b>
2.1 DISCRETE-TIME MODELS .....	3
2.2 OBSERVER DESIGN .....	4
2.3 DISCRETE-TIME KALMAN FILTER .....	5
2.3.1 Derivation of Kalman filter equations.....	5
2.3.2 Interpretation.....	8
2.4 PRACTICAL APPLICATION OF KALMAN FILTERING.....	10
2.4.1 Multi-rate, delayed and nonsynchronous sampling.....	10
2.5 CONCLUSIONS.....	11
<b>3 KINEMATICS OF THE VEHICLE.....</b>	<b>13</b>
3.1 DEFINITION OF COORDINATE FRAMES .....	13
3.2 KINEMATIC EQUATIONS OF THE VEHICLE .....	14
3.3 CONCLUSIONS.....	19
<b>4 DESCRIPTION OF THE SIMULATION MODEL.....</b>	<b>21</b>
4.1 THE SIMULINK MODEL .....	21
4.2 EXPLANATION OF THE MODEL BLOCKS.....	22
<b>5 OBSERVER DESIGN .....</b>	<b>25</b>
5.1 INTRODUCTION .....	25
5.2 LATERAL VELOCITY AND POSITION ESTIMATION .....	25
5.2.1 Predictor equations.....	28
5.2.2 Corrector equations.....	29
5.3 SIMULATION RESULTS.....	34
5.4 CONCLUSIONS.....	36
<b>6 SENSOR EXTENSION OF OBSERVER.....</b>	<b>37</b>
6.1 GYROSCOPES .....	37
6.1.1 Integrating gyroscope.....	37
6.1.1.1 Simulation results.....	45
6.1.1.2 Conclusions.....	48
6.1.2 Rate gyroscope.....	48
6.1.2.1 Simulation results.....	52
6.1.2.2 Conclusions.....	56
6.2 CONCLUSIONS.....	56
<b>7 SENSOR NOISE AND COVARIANCE ANALYSIS.....</b>	<b>57</b>
7.1 FILTERING OF SENSOR NOISE.....	57
7.2 WHITE NOISE AND COLORED NOISE.....	61
7.3 BIAS AND DRIFT PROPERTIES OF THE SENSORS .....	62
7.4 COVARIANCE AND PSD OF THE NOISE OF USED SENSORS.....	66
7.4.1 Accelerometer noise .....	67
7.4.2 Gyroscope noise .....	68
7.5 SIMULATION RESULTS.....	69
7.6 CONCLUSIONS.....	71

<b>8 CONCLUSIONS AND RECOMMENDATIONS .....</b>	<b>73</b>
8.1 CONCLUSIONS .....	73
8.2 RECOMMENDATIONS .....	74
<b>REFERENCES.....</b>	<b>75</b>
<b>TABLE OF FIGURES.....</b>	<b>77</b>
<b>APPENDICES .....</b>	<b>79</b>
<b>APPENDIX 1: OBSERVER.M .....</b>	<b>81</b>
<b>APPENDIX 2: DATASHEET OF MSA100 .....</b>	<b>87</b>
<b>APPENDIX 3: DATASHEET OF KVH E•CORE 1000 .....</b>	<b>89</b>





# Chapter 1

## Introduction

### *1.1 Purpose of investigation*

The Dutch foundation HOV (= high quality public transport) has designed a double articulated lightweight bus with 4 independently steerable axles and independent drives on 6 of the 8 wheels. The bus is going to drive from the central station of Eindhoven to the centre of Veldhoven, the new district Meerhoven and Eindhoven Airport. The name of the vehicle is 'Phileas' and it is kind of a tram on pneumatic tires, where great importance is attached to comfort, speed, punctuality and easily getting on and off. **Figure 1-1** shows a picture of the vehicle that is described above.



**Figure 1-1: Picture of the vehicle named Phileas**

For human drivers, it is impossible to steer such a vehicle by hand. Therefore a control system to steer the vehicle has to be designed.

The Control Systems Group of the Eindhoven University of Technology is doing research on the measurement and control system of the vehicle.

For the lateral guidance of the vehicle it is important that position and speed of the vehicle are determined with respect to the path that has to be followed. The path will be formed by a track of magnets. This is a track in which permanent magnets are mounted in the road surface at fixed distances of each other. These permanent magnets will be detected by magnetometers in the vehicle. Because of the fixed distance between the permanent magnets, the measurement data coming from the magnetometers will be available at discrete times only. With the use of additional sensors in the vehicle and in a model of the vehicle, it is possible to obtain measurement data at any required sampletime. With these additional sensors it is

possible to determine the speed and the position of the vehicle when the magnetometers are not on top of the permanent magnets.

## ***1.2 Assignment***

The assignment is to investigate which sensors can be used to realize a good measurement system. The way how the measurement signals from the different sensors can be combined, also has to be examined. The combination of sensors is also called sensor fusion. The found sensors have to be implemented in an observer in Simulink. According to simulation results, conclusions will be drawn and recommendations will be done.

## ***1.3 Structure of the report***

The observer is designed according to a Kalman Filter. To understand the design of the observer according to Kalman Filtering a short introduction to Kalman Filtering Theory is given in Chapter 2.

Chapter 3 deals with the kinematics of the vehicle. It is understandable that there are a lot of kinematics involved in such a vehicle. These kinematics are also involved in the design of the observer. In Chapter 3 the kinematic model of the vehicle is described and the kinematic equations of the vehicle, which will come back in the design of the observer, are given.

The Simulink model in which the observer has to be implemented has been studied. This is done to understand the behaviour of the model. The Simulink model and its functionality are described in Chapter 4.

The actual design of the observer is handled in Chapter 5. A method is introduced to estimate the lateral velocity and position of the vehicle with respect to the path that has to be followed. According to some simulation results, the observer is evaluated.

The design of the observer can be improved by extending the observer with a sensor or several sensors. A few sensors, which can be used for this purpose and how they can be implemented in the design of the observer, are described in Chapter 6. The improvement of the observer with use of the sensors is evaluated by means of some simulation results.

When the sensors which are described in this report are implemented in the observer, it is important to know their noise properties and that the noise can be characterized in the observer. How to handle sensor noise and how to obtain noise covariances are aspects which are dealt with in Chapter 7. There is also said something about low-frequency sensor properties, like bias and drift.

Finally, the report is concluded with the conclusions and recommendations. The main conclusions which are drawn during the M.Sc. project and some recommendations for further research are described in Chapter 8.

# Chapter 2

## Kalman Filtering Theory

This chapter deals with the theory of Kalman filtering. An introduction to the theory of Kalman filtering is given to explain the observer design which is described later in this report.

Kalman filters have been employed very successfully in control and guidance systems since the sixties, with particular application to avionics and navigation. These filters can track signals of known structure accurately among noise and other signal components with different structure. Since there is some noise present in every real-world dynamic process and all observations are subject to noise, it would make sense to optimize the observer gains for the noise that is present in the input and in the output. The theory for accomplishing this optimization was first developed by R.E. Kalman in 1960, and the resulting observer is known as the *Kalman filter*.

Because the observer is designed in discrete time, only the discrete-time Kalman filter will be discussed.

### 2.1 Discrete-time models

For a continuous-time process, with piecewise-constant (i.e., sampled and held) inputs, the model can be obtained from the continuous-time system (ref. [2]):

$$\dot{x} = Ax + Bu \quad (2-1)$$

The general solution to equation (2-1) is:

$$x(t + \tau) = e^{A\tau} x(t) + \int_t^{t+\tau} e^{A(t+\tau-\xi)} Bu(\xi) d\xi \quad (2-2)$$

Now suppose the input  $u(t)$  to equation (2-1) is piecewise-constant:

$$u(t) = u(nT) := u_n = \text{const.}, \text{ for } nT \leq t < (n+1)T \quad (2-3)$$

Evaluating equation (2-2) with  $t = nT$  and  $\tau = T$ , and using equation (2-3) gives:

$$x(nT + T) = e^{AT} x(nT) + \left( \int_{nT}^{nT+T} e^{A(nT+T-\xi)} B d\xi \right) u_n \quad (2-4)$$

The factor  $u_n$  is brought outside the integral because of the fact that  $u(t)$  is piecewise-constant.

Equation (2-4) can be written as:

$$x_{n+1} = \Phi x_n + \Gamma u_n \quad (2-5)$$

where:

$$x_n := x(nT) \quad (2-6)$$

$$\Phi := \Phi(T) = e^{AT} \quad (2-7)$$

$$\Gamma := \int_{nT}^{nT+T} e^{A(nT+T-\xi)} B d\xi = \int_0^T e^{A\lambda} B d\lambda = \frac{B}{A} (e^{AT} - I) = \frac{B}{A} (\Phi - I) \quad (2-8)$$

The *difference equation* or *recursion equation* (2-5) is the fundamental representation of a discrete-time system, and plays the same role as equation (2-1) does in a continuous-time system. In words, it can be read as “the state at the  $(n+1)$ st sampling instant is a linear combination of the state at the  $n$ th sampling instant and the (piecewise-constant) control during the  $n$ th sampling instant.”

## 2.2 Observer design

A full-order observer is a dynamic system of the same order as the process whose state is to be estimated. It is excited by the inputs and outputs of that process, and has the property that the estimation error, that means, the difference between the state  $x_n$  of the process and the state  $\tilde{x}_n$  of the observer, converges to zero as  $n \rightarrow \infty$  independent of the state of the process or its inputs and outputs.

Let the observer be defined by the general linear difference equation (ref. [2]):

$$\tilde{x}_{n+1} = F\tilde{x}_n + Ky_n + Hu_n \quad (2-9)$$

Now, the matrices  $F$ ,  $K$  and  $H$  have to be conditioned such that the requirements to a full-order observer are met. The conditions can be found by subtracting equation (2-9) from equation (2-5). This results in:

$$x_{n+1} - \tilde{x}_{n+1} = \Phi x_n + \Gamma u_n - F\tilde{x}_n - Ky_n - Hu_n \quad (2-10)$$

Let  $e_n$  be defined by:

$$e_n = x_n - \tilde{x}_n$$

Further, the observation  $y_n$  is given by:

$$y_n = Cx_n$$

From equation (2-10) can be obtained:

$$e_{n+1} = Fe_n + (\Phi - KC - F)x_n + (\Gamma - H)u_n \quad (2-11)$$

Thus, in order to meet the requirements to a full-order observer, the transition matrix  $F$  of the observer must be stable, that means, the eigenvalues of  $F$  must lie within the unit circle, and moreover, the following must hold:

$$F := \hat{\Phi} = \Phi - KC \quad (2-12)$$

$$H = \Gamma \quad (2-13)$$

According to these relations, the observer can be expressed as follows:

$$\tilde{x}_{n+1} = \Phi \tilde{x}_n + \Gamma u_n + K(y_n - C\tilde{x}_n) \quad (2-14)$$

It can be seen from equation (2-14) that the observer has the same dynamics as the underlying process, except that it has an additional input:

$$K(y_n - C\tilde{x}_n)$$

The role of this additional input can be interpreted as that of driving the error  $e_n$  to zero.

So, the observer design reduces to the selection of the gain matrix  $K$  such that the eigenvalues of  $\hat{\Phi} = \Phi - KC$  lie at suitable locations within the unit circle.

For both single- and multiple-output processes the observer gain matrix can be selected to make the observer a Kalman filter, that means, a filter producing the estimate  $\tilde{x}$  in a least squares sense of the estimation error or in other words, a minimum variance estimator.

## 2.3 Discrete-time Kalman filter

The optimum observer is defined as the one that has the smallest covariance matrix of the estimation error.

### 2.3.1 Derivation of Kalman filter equations

To derive the equations of the optimum observer, that is, the Kalman filter, it is supposed that the plant dynamics are modeled by the (possibly time-varying) dynamics (ref. [2]):

$$x_{n+1} = \Phi_n x_n + \Gamma_n u_n + v_n \quad (2-15)$$

In this equation  $v_n$  is a random noise process having the following statistical properties:

1. The noise has a mean of zero:

$$E\{v_n\} = 0$$

2.  $v_n$  and  $v_k$  are uncorrelated for  $n \neq k$ , that means:

$$E\{v_n v_k^T\} = 0, \text{ for } n \neq k$$

- 3.

$$E\{v_n v_n^T\} = V_n$$

A discrete-time random process, or, in other words, a random sequence, with the properties described above may be referred to as “sampled white noise” with zero-mean and covariance matrix  $V_n$ .

The observations are given by the following equation:

$$y_n = C_n x_n + w_n \quad (2-16)$$

In this equation  $w_n$  is sampled white noise with covariance matrix:

$$W_n = E\{w_n w_n^T\}$$

Furthermore,  $v_n$  and  $w_n$  are uncorrelated:

$$E\{v_n w_k^T\} = 0 \text{ for all } n, k \quad (2-17)$$

The observer for this process is defined by (ref. [2]):

$$\tilde{x}_{n+1} = \Phi_n \tilde{x}_n + \Gamma_n u_n + K_n (y_n - C_n \tilde{x}_n) \quad (2-18)$$

With the use of equation (2-15) and (2-18) the estimation error can be determined. The estimation error is defined by:

$$\tilde{e}_n := x_n - \tilde{x}_n \quad (2-19)$$

Upon this definition, the estimation error is given by:

$$\begin{aligned} \tilde{e}_{n+1} &= (\Phi_n - K_n C_n) \tilde{e}_n + v_n - K_n w_n \\ &= \tilde{\Phi}_n \tilde{e}_n + v_n \end{aligned} \quad (2-20)$$

where:

$$\tilde{\Phi}_n = \Phi_n - K_n C_n \quad (2-21)$$

$$v_n = v_n - K_n w_n \quad (2-22)$$

Toward the goal of minimizing the covariance matrix of the estimation error, the equation that governs its propagation is first developed. Then the gain matrix that minimizes the covariance matrix is found.

Using equation (2-20), the following can be written in preparation for deriving the covariance propagation equation:

$$\begin{aligned} \tilde{e}_{n+1} \tilde{e}_{n+1}^T &= (\tilde{\Phi}_n \tilde{e}_n + v_n) (\tilde{e}_n^T \tilde{\Phi}_n^T + v_n^T) \\ &= \tilde{\Phi}_n \tilde{e}_n \tilde{e}_n^T \tilde{\Phi}_n^T + v_n \tilde{e}_n^T \tilde{\Phi}_n^T + \tilde{\Phi}_n \tilde{e}_n v_n^T + v_n v_n^T \end{aligned} \quad (2-23)$$

Now, the expected value on both sides of equation (2-23) is taken, letting:

$$\tilde{P}_n = E\{\tilde{e}_n \tilde{e}_n^T\} \quad (2-24)$$

and with the note (ref. [2]) that  $E\{\tilde{e}_n v_n^T\} = 0$ , this results in:

$$\tilde{P}_{n+1} = \tilde{\Phi}_n \tilde{P}_n \tilde{\Phi}_n^T + \tilde{V}_n \quad (2-25)$$

In this equation  $\tilde{V}_n$  equals the following:

$$\begin{aligned} \tilde{V}_n &= E\{v_n v_n^T\} \\ &= E\{(v_n - K_n w_n)(v_n^T - w_n^T K_n^T)\} \\ &= V_n + K_n W_n K_n^T \end{aligned} \quad (2-26)$$

where the assumption is made that  $v_n$  and  $w_n$  are uncorrelated.

With use of equation (2-21) and (2-26), the following can be obtained from equation (2-25):

$$\tilde{P}_{n+1} = (\Phi_n - K_n C_n) \tilde{P}_n (\Phi_n^T - C_n^T K_n^T) + V_n + K_n W_n K_n^T \quad (2-27)$$

The objective now is to find the value of  $K_n$  that minimizes  $\tilde{P}_{n+1}$ . The optimum gain matrix is given by (ref. [2]):

$$\hat{K}_n = \Phi_n \tilde{P}_n C_n^T (C_n \tilde{P}_n C_n^T + W_n)^{-1} \quad (2-28)$$

The equation for the propagation of the minimum covariance matrix is:

$$\tilde{P}_{n+1} = \Phi_n \left\{ \tilde{P}_n - \tilde{P}_n C_n^T (C_n \tilde{P}_n C_n^T + W_n)^{-1} C_n \tilde{P}_n \right\} \Phi_n^T + V_n \quad (2-29)$$

This equation can be rewritten. Let  $\hat{K}_n$  be defined by:

$$\hat{K}_n := \Phi_n \tilde{K}_n \quad (2-30)$$

where:

$$\tilde{K}_n = \tilde{P}_n C_n^T (C_n \tilde{P}_n C_n^T + W_n)^{-1} \quad (2-31)$$

The *a posteriori* covariance matrix is defined as:

$$\hat{P}_n := \tilde{P}_n - \tilde{P}_n C_n^T (C_n \tilde{P}_n C_n^T + W_n)^{-1} C_n \tilde{P}_n = (I - \tilde{K}_n C_n) \tilde{P}_n \quad (2-32)$$

Now, equation (2-29) becomes:

$$\tilde{P}_{n+1} = \Phi_n \hat{P}_n \Phi_n^T + V_n \quad (2-33)$$

The gain matrix can also be expressed in terms of the *a posteriori* covariance matrix as follows:

$$\tilde{K}_n = \hat{P}_n C_n^T W_n^{-1} \quad (2-34)$$

### 2.3.2 Interpretation

For convenience, the equation of the observer (2-18) is repeated, but now with use of the optimized gain matrix:

$$\begin{aligned}\tilde{x}_{n+1} &= \Phi_n \tilde{x}_n + \Gamma_n u_n + \Phi_n \tilde{K}_n (y_n - C_n \tilde{x}_n) \\ &= \Phi_n \hat{x}_n + \Gamma_n u_n\end{aligned}\quad (2-35)$$

where:

$$\hat{x}_n = \tilde{x}_n + \tilde{K}_n (y_n - C_n \tilde{x}_n) \quad (2-36)$$

The intuitive interpretation is provided by the equations (2-35) and (2-36). The first of these equations is simply the equation of the dynamic process:

$$x_{n+1} = \Phi_n x_n + \Gamma_n u_n$$

with  $\hat{x}_n$  appearing in place of the state  $x_n$  on the right-hand side and with  $\tilde{x}_{n+1}$  appearing on the left. Since the observation  $y_{n+1}$  does not appear in equation (2-35), this equation can be regarded as a description of how the optimum state estimate  $\hat{x}_n$  propagates during the time interval between the  $n$ th and the  $(n+1)$ st observation, an interval during which no observations have occurred.

The effect of the  $n$ th observation is reflected in equation (2-36). This equation tells how the state estimate  $\tilde{x}_n$  prior to the observation is updated by the observation. First, the residual:

$$y_n - C_n \tilde{x}_n$$

is calculated. Then, the residual is multiplied by the gain matrix  $\tilde{K}_n$ . Finally, the result of the multiplication is added to the prior state estimate. All these operations occur at the instant of the  $n$ th observation. Thus,  $\tilde{x}_n$  can be interpreted as the optimum state estimate immediately before the  $n$ th observation, that is, the *a priori* state estimate. In the same way,  $\hat{x}_n$  can be interpreted as the optimum estimate of the state immediately after the  $n$ th observation, that is, the *a posteriori* state estimate. With the use of this interpretation, equation (2-36) shows how the new observation is used to get the *a posteriori* estimate from the *a priori* estimate, and equation (2-35) shows how that estimate propagates in time to give the *a priori* estimate of the state just before the  $(n+1)$ st observation.

The important relations of Kalman filtering are summarized in the next table, **Table 2-1**.



Update for	State	Covariance
Observation	$\hat{x}_n = \tilde{x}_n + \tilde{K}_n (y_n - C_n \tilde{x}_n)$	$\hat{P}_n = (I - \tilde{K}_n C_n) \tilde{P}_n$
Time	$\tilde{x}_{n+1} = \Phi_n \hat{x}_n + \Gamma_n u_n$	$\tilde{P}_{n+1} = \Phi_n \hat{P}_n \Phi_n^T + V_n$
$\tilde{K}_n = \tilde{P}_n C_n^T (C_n \tilde{P}_n C_n^T + W_n)^{-1} = \hat{P}_n C_n^T W_n^{-1}$		

**Table 2-1: Important relations for a discrete-time Kalman filter**

The procedure for a discrete-time Kalman filter is also shown in the flowchart of **Figure 2-1**.

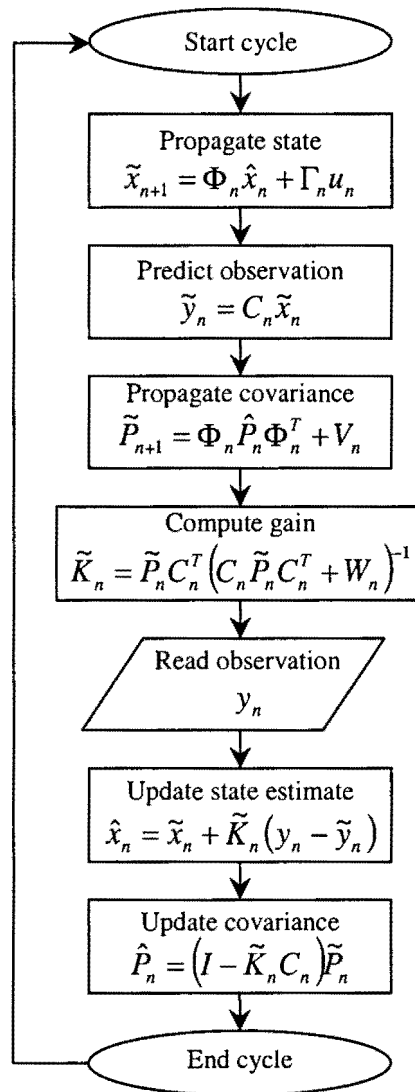


**Figure 2-1: Flowchart for a discrete-time Kalman filter**

The procedure shown in the flowchart above can be used even if the schedule of observations is not known in advance. In particular, the procedure is valid for applications in which observations are made at random instants.

## 2.4 Practical application of Kalman filtering

In reference [2] a practical application of Kalman filtering techniques is described which is very useful for the observer design which is dealt with in this report. This practical application is related to problems where multi-rate, delayed and nonsynchronous sampling is involved. The application as introduced in ref. [2] is discussed here.

### 2.4.1 Multi-rate, delayed and nonsynchronous sampling

An application of moderate complexity might involve the use of several sensors. The sensors may not all take their observations concurrently, but it is desired to integrate the observations optimally. A typical sampling pattern involving three sensors is illustrated in **Figure 2-2**.

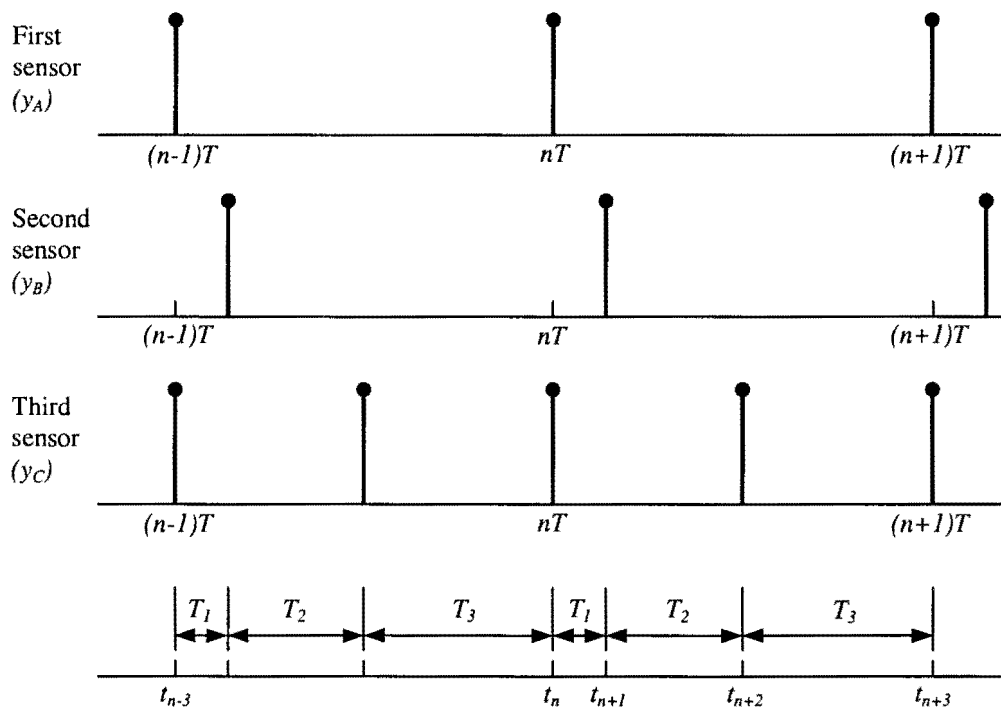


**Figure 2-2: Sampling pattern involving three sensors**

The first sensor, with output  $y_A$ , takes samples at multiples of  $T$  seconds. The second sensor, with output  $y_B$ , takes samples at the same rate, but these samples are offset from the first by  $T_1$  seconds. The third sensor, with output  $y_C$ , takes samples twice as frequently as the first two and is synchronized with the first sensor.

Merging the sampling schedules of the three sensors results in dividing the sampling interval into three subintervals of lengths  $T_1$ ,  $T_2$  and  $T_3$ , respectively. For the particular sampling pattern of **Figure 2-2**,  $T_1 + T_2 = T_3 = T/2$ . Thus each cycle has three sampling cases separated by intervals of different duration:

- *Case 1:* Sensors A and C operate simultaneously.
- *Case 2:* Sensor B operates alone.

- *Case 3*: Sensor C operates alone.

To merge the data from the sensors, the following relationships will be used:

$$\hat{x}_n = \tilde{x}_n + K_n (y_n - C_{AC} \tilde{x}_n)$$

$$\hat{x}_{n+1} = \tilde{x}_{n+1} + K_{n+1} (y_{n+1} - C_B \tilde{x}_{n+1})$$

$$\hat{x}_{n+2} = \tilde{x}_{n+2} + K_{n+2} (y_{n+2} - C_C \tilde{x}_{n+2})$$

Because  $y_n$  occurs for *Case 1* in which two sensors operate simultaneously, the observation matrix  $C_{AC}$  has two rows. The first contains the observation sensitivity coefficients for sensor A and the second for sensor C. The other two observation matrices  $C_B$  and  $C_C$  correspond to *Cases 2* and *3* in each of which there is only one observation and thus each has only one row.

Considering the observation cycle, the state update equation is written as follows:

$$\tilde{x}_{n+i} = \Phi_{\alpha_i} \hat{x}_{n+i-1} + \Gamma_{\alpha_i} u_{n+i-1}, \quad i = 1, 2, 3$$

where

$$\Phi_{\alpha_i} = e^{A T_i}$$

$$\Gamma_{\alpha_i} = \int_0^{T_i} e^{A \tau} B d\tau, \quad i = 1, 2, 3$$

After one observation cycle of three updates, the cycle would revert to the beginning. The cycle can be interpreted by expressing the procedure in words:

- Between samples, the state estimate and covariance matrix are propagated to the next sampling instant using the state transition matrix corresponding to the elapse of time between the samples.
- At sampling instants, the state estimate is updated using the current observation, the observation matrix and the gain matrix.

## 2.5 Conclusions

The theory of Kalman filtering is introduced. Kalman filters have been employed very successfully in control and guidance systems since the sixties, with particular application to avionics and navigation.

The discrete-time Kalman filter with its filtering equations is described, and an interpretation is given to the discrete-time Kalman filter or observer.

A Kalman filter seems to be very useful for applications in which multi-rate, delayed and nonsynchronous sampling is involved.



# Chapter 3

## Kinematics of the vehicle

There are a lot of kinematics involved in the vehicle. These kinematics are also involved in the observer design. This chapter discusses the kinematics of the vehicle. First, a frame model of the vehicle and three types of coordinate frames will be introduced and then the equations of the kinematics are presented.

### 3.1 Definition of coordinate frames

There will be used three types of coordinate frames to explain the kinematics which are involved in the observer design. These coordinate frames are shown in the vehicle model of **Figure 3-1**.

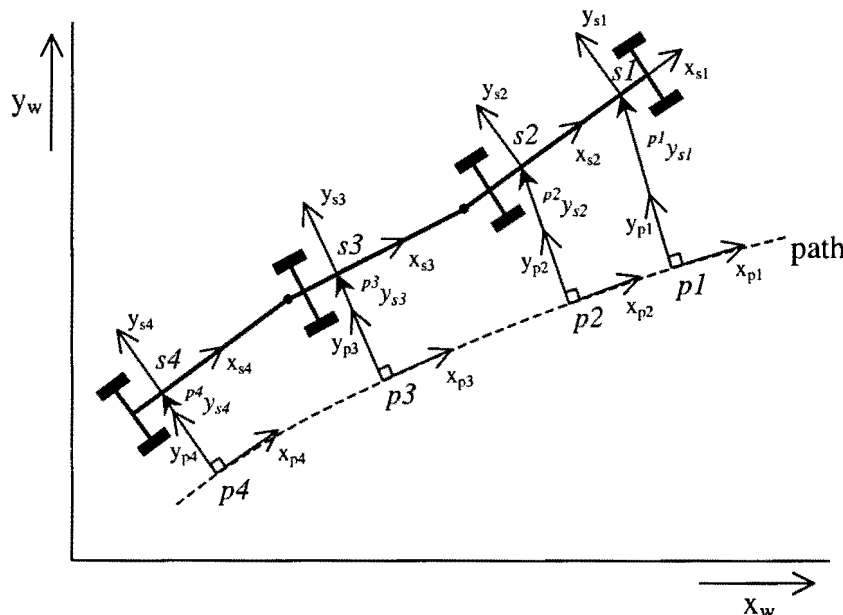


**Figure 3-1: Model of vehicle with sensor configuration**

The coordinate frames are the world fixed coordinate frame  $w$ , the vehicle fixed frames  $s_i$  and the path frames  $p_i$ . The frames  $p_i$  are thought to move along the desired path, adjacent to the frames  $s_i$ , such that the extension of the  $y$ -axis of frame  $p_i$  goes through the origin of frame  $s_i$ . The  $x$ -axes of the frames  $s_i$  are directed along the longitudinal axes of the carriages on which the frames are fixed. The  $x$ -axes of the frames  $p_i$  are directed along the tangent of the path at the origin of frame  $p_i$ , such that the  $y$ -axis of frame  $p_i$  points to the origin of frame  $s_i$ . The origins of the frames  $s_i$  are the points where the different sensors are mounted, so that the  $s_i$  frames are also called the *sensor frames*. The sensor configuration is also shown in **Figure 3-1**. The frames  $p_i$  and  $s_i$  are unity frames and they represent the orientation of the different frames. The distances  $p^i y_{s_i}$  are defined as the  $y$ -component of the vector pointing from

the origin of the path fixed frames  $pi$  to the origin of the vehicle fixed frames  $si$ . So, the label  ${}^{pi}y_{si}$  denotes the  $y$ -coordinate of frame  $si$  with respect to frame  $pi$ .

### 3.2 Kinematic equations of the vehicle

Now that the coordinate frames of the vehicle model are defined, the equations of the kinematics can be presented.

Let  ${}^w x_{si}$  and  ${}^w y_{si}$  denote the position of the origin of frame  $si$  expressed in frame  $w$ , then the velocity of frame  $si$  expressed in the directions of frame  $w$  becomes:

$${}^w \dot{x}_{si} = {}^{si}v_{x_{si}} \cos {}^w \varepsilon_{si} - {}^{si}v_{y_{si}} \sin {}^w \varepsilon_{si} \quad (3-1a)$$

$${}^w \dot{y}_{si} = {}^{si}v_{x_{si}} \sin {}^w \varepsilon_{si} + {}^{si}v_{y_{si}} \cos {}^w \varepsilon_{si} \quad (3-1b)$$

In this equation,  ${}^{si}v_{x_{si}}$  and  ${}^{si}v_{y_{si}}$  are the velocities of frame  $si$  with respect to frame  $w$ , but in the directions of frame  $si$ . Furthermore,  ${}^w \varepsilon_{si}$  denotes the orientation of frame  $si$  with respect to frame  $w$ .

By differentiating equation (3-1) with respect to time, the following result can be obtained:

$${}^w \ddot{x}_{si} = {}^{si}\dot{v}_{x_{si}} \cos {}^w \varepsilon_{si} - {}^{si}\dot{v}_{y_{si}} \sin {}^w \varepsilon_{si} - \left( {}^{si}v_{x_{si}} \sin {}^w \varepsilon_{si} + {}^{si}v_{y_{si}} \cos {}^w \varepsilon_{si} \right) {}^w \dot{\varepsilon}_{si} \quad (3-2a)$$

$${}^w \ddot{y}_{si} = {}^{si}\dot{v}_{x_{si}} \sin {}^w \varepsilon_{si} + {}^{si}\dot{v}_{y_{si}} \cos {}^w \varepsilon_{si} + \left( {}^{si}v_{x_{si}} \cos {}^w \varepsilon_{si} - {}^{si}v_{y_{si}} \sin {}^w \varepsilon_{si} \right) {}^w \dot{\varepsilon}_{si} \quad (3-2b)$$

An acceleration sensor or accelerometer mounted on the vehicle in frame  $si$ , with its sensitive axis directed along the  $y$ -axis of frame  $si$ , will measure the lateral acceleration  $a_{y_{si}}$ , which is given by the following equation:

$$a_{y_{si}} = {}^w \ddot{y}_{si} \cos {}^w \varepsilon_{si} - {}^w \ddot{x}_{si} \sin {}^w \varepsilon_{si} \quad (3-3)$$

Substitution of equation (3-2) into equation (3-3) results in:

$$\begin{aligned} a_{y_{si}} &= \left\{ {}^{si}\dot{v}_{x_{si}} \sin {}^w \varepsilon_{si} + {}^{si}\dot{v}_{y_{si}} \cos {}^w \varepsilon_{si} + \left( {}^{si}v_{x_{si}} \cos {}^w \varepsilon_{si} - {}^{si}v_{y_{si}} \sin {}^w \varepsilon_{si} \right) {}^w \dot{\varepsilon}_{si} \right\} \cos {}^w \varepsilon_{si} - \\ &\quad \left\{ {}^{si}\dot{v}_{x_{si}} \cos {}^w \varepsilon_{si} - {}^{si}\dot{v}_{y_{si}} \sin {}^w \varepsilon_{si} - \left( {}^{si}v_{x_{si}} \sin {}^w \varepsilon_{si} + {}^{si}v_{y_{si}} \cos {}^w \varepsilon_{si} \right) {}^w \dot{\varepsilon}_{si} \right\} \sin {}^w \varepsilon_{si} \\ &= {}^{si}\dot{v}_{y_{si}} \left( \cos {}^w \varepsilon_{si} \right)^2 + {}^{si}\dot{v}_{x_{si}} \left( \cos {}^w \varepsilon_{si} \right)^2 {}^w \dot{\varepsilon}_{si} + {}^{si}\dot{v}_{y_{si}} \left( \sin {}^w \varepsilon_{si} \right)^2 + {}^{si}\dot{v}_{x_{si}} \left( \sin {}^w \varepsilon_{si} \right)^2 {}^w \dot{\varepsilon}_{si} \\ &= {}^{si}\dot{v}_{y_{si}} \left\{ \left( \cos {}^w \varepsilon_{si} \right)^2 + \left( \sin {}^w \varepsilon_{si} \right)^2 \right\} + {}^{si}\dot{v}_{x_{si}} {}^w \dot{\varepsilon}_{si} \left\{ \left( \cos {}^w \varepsilon_{si} \right)^2 + \left( \sin {}^w \varepsilon_{si} \right)^2 \right\} \\ &= {}^{si}\dot{v}_{y_{si}} + {}^{si}\dot{v}_{x_{si}} {}^w \dot{\varepsilon}_{si} \end{aligned} \quad (3-4)$$

The velocity  ${}^{pi}\dot{y}_{si}$  of frame  $si$  with respect to the path frame  $pi$  and in the direction perpendicular to the tangent of the path as shown in **Figure 3-1** is given by:

$${}^{pi}\dot{y}_{si} = {}^{si}v_{y_{si}} \cos {}^{pi} \varepsilon_{si} + {}^{si}v_{x_{si}} \sin {}^{pi} \varepsilon_{si} \quad (3-5)$$

In this equation  ${}^{pi}\epsilon_{si}$  is the yaw deviation of frame  $si$  with respect to the tangent of the path. The tangent of the path is lying along the  $x$ -axis of frame  $pi$ . The path and the vehicle-referenced coordinates are illustrated in more detail in **Figure 3-2**.

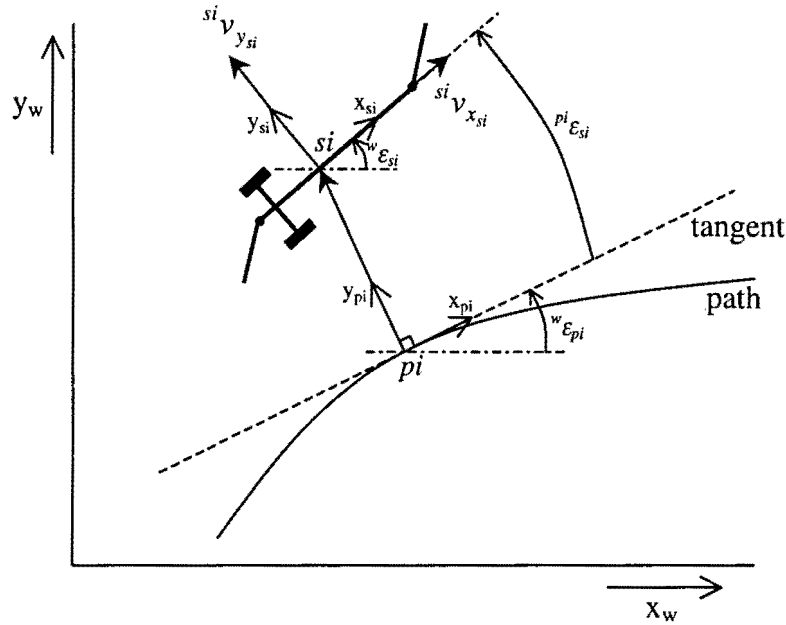


**Figure 3-2: Path and vehicle referenced coordinates**

Taking the time derivative of equation (3-5) yields:

$${}^{pi}\ddot{y}_{si} = {}^{si}\dot{v}_{y_{si}} \cos {}^{pi}\epsilon_{si} + {}^{si}\dot{v}_{x_{si}} \sin {}^{pi}\epsilon_{si} + {}^{pi}\dot{\epsilon}_{si} \left( {}^{si}v_{x_{si}} \cos {}^{pi}\epsilon_{si} - {}^{si}v_{y_{si}} \sin {}^{pi}\epsilon_{si} \right) \quad (3-6)$$

Now, it is assumed that the yaw deviations and the longitudinal acceleration are small. With these assumptions, equation (3-6) can be written as:

$$\begin{aligned} {}^{pi}\ddot{y}_{si} &\approx \dot{v}_{ys} + v_{xs} {}^{pi}\dot{\epsilon}_{si} \\ &= {}^{si}\dot{v}_{y_{si}} + {}^{si}v_{x_{si}} \left( {}^w\dot{\epsilon}_{si} - {}^w\dot{\epsilon}_{pi} \right) \\ &= a_{y_{si}} - {}^{si}v_{x_{si}} {}^w\dot{\epsilon}_{pi} \end{aligned} \quad (3-7)$$

Here  ${}^w\dot{\epsilon}_{pi}$  is the yaw rate of frame  $pi$ , which is defined in **Figure 3-2**. Equation (3-7) shows that the acceleration of frame  $si$  with respect to frame  $pi$  can be obtained from the reading of the accelerometer, the longitudinal velocity and the yaw rate of the path fixed frame  $pi$ .

Equation (3-7) can be written in a state-space form. After adding measurement noises, equation (3-7) can be expressed as:

$$\dot{\mathbf{x}}_{si} = \mathbf{A}\mathbf{x}_{si} + \mathbf{B}u_{si} + \mathbf{B}_w w_{si} \quad (3-8a)$$

$$y_{si} = \mathbf{C}\mathbf{x}_{si} + v_{si} \quad (3-8b)$$

In this equation the different variables are defined as:

$$\mathbf{x}_{si} = \begin{bmatrix} {}^{pi}y_{si} & {}^{pi}\dot{y}_{si} \end{bmatrix}^T$$

$$u_{si} = a_{y_{si}} - {}^{si}v_{x_{si}} \cdot {}^w\dot{\epsilon}_{pi}$$

$$\mathbf{B} = \mathbf{B}_w = \begin{bmatrix} 0 & 1 \end{bmatrix}^T$$

$$\mathbf{A} = \begin{bmatrix} 0 & 1 \\ 0 & 0 \end{bmatrix}$$

$$\mathbf{C} = \begin{bmatrix} 1 & 0 \end{bmatrix}$$

Furthermore, the measurement noise coming from the accelerometer as well as error in the measurement of the longitudinal velocity of the vehicle are denoted by  $w_{si}$  in equation (3-8). Further in equation (3-8),  $y_{si}$  is the lateral position error between the vehicle frame  $si$  and the path frame  $pi$  and in the direction perpendicular to the tangent of the path. The lateral position errors are measured by the magnetometers which are mounted at the origins of the  $si$ -frames on the vehicle. The magnetometer measurement noise and the noise due to magnet misalignment are denoted by  $v_{si}$ .

Equation (3-8) can be worked out for the complete sensor configuration of the vehicle. The complete sensor configuration consists of two sensor frames at the tractor, one sensor frame at the first semitrailer and one sensor frame at the second semitrailer. Equation (3-8a) is worked out for the four sensor frames as follows:

$$\dot{\mathbf{x}}_{s1} = \begin{bmatrix} {}^{p1}\dot{y}_{s1} \\ {}^{p1}\ddot{y}_{s1} \end{bmatrix} = \begin{bmatrix} 0 & 1 \\ 0 & 0 \end{bmatrix} \cdot \begin{bmatrix} {}^{p1}y_{s1} \\ {}^{p1}\dot{y}_{s1} \end{bmatrix} + \begin{bmatrix} 0 \\ 1 \end{bmatrix} \cdot u_{s1} + \begin{bmatrix} 0 \\ 1 \end{bmatrix} \cdot w_{s1} \quad (3-9a)$$

$$\dot{\mathbf{x}}_{s4} = \begin{bmatrix} {}^{p4}\dot{y}_{s4} \\ {}^{p4}\ddot{y}_{s4} \end{bmatrix} = \begin{bmatrix} 0 & 1 \\ 0 & 0 \end{bmatrix} \cdot \begin{bmatrix} {}^{p4}y_{s4} \\ {}^{p4}\dot{y}_{s4} \end{bmatrix} + \begin{bmatrix} 0 \\ 1 \end{bmatrix} \cdot u_{s4} + \begin{bmatrix} 0 \\ 1 \end{bmatrix} \cdot w_{s4} \quad (3-9d)$$

The same can be done for equation (3-8b). This results in the following:

$$y_{s1} = \begin{bmatrix} 1 & 0 \end{bmatrix} \cdot \begin{bmatrix} {}^{p1}y_{s1} \\ {}^{p1}\dot{y}_{s1} \end{bmatrix} + v_{s1} \quad (3-10a)$$

$$y_{s4} = \begin{bmatrix} 1 & 0 \end{bmatrix} \cdot \begin{bmatrix} {}^{p4}y_{s4} \\ {}^{p4}\dot{y}_{s4} \end{bmatrix} + v_{s4} \quad (3-10d)$$



Equations (3-9) and (3-10) are written in a single-input single-output (SISO) representation. In a case like this it is often more convenient to use a multiple-input multiple-output (MIMO) representation. Furthermore, equations (3-9) and (3-10) are perfectly suitable for such a representation. Rewriting the equations (3-9) and (3-10) in a MIMO representation, gives the following result:

$$\dot{\mathbf{x}} = \begin{bmatrix} p^1 \dot{y}_{s1} \\ p^1 \ddot{y}_{s1} \\ p^2 \dot{y}_{s2} \\ p^2 \ddot{y}_{s2} \\ p^3 \dot{y}_{s3} \\ p^3 \ddot{y}_{s3} \\ p^4 \dot{y}_{s4} \\ p^4 \ddot{y}_{s4} \end{bmatrix} = \begin{bmatrix} 0 & 1 & 0 & 0 & 0 & 0 & 0 & 0 \\ 0 & 0 & 0 & 0 & 0 & 0 & 0 & 0 \\ 0 & 0 & 0 & 1 & 0 & 0 & 0 & 0 \\ 0 & 0 & 0 & 0 & 0 & 0 & 0 & 0 \\ 0 & 0 & 0 & 0 & 0 & 1 & 0 & 0 \\ 0 & 0 & 0 & 0 & 0 & 0 & 0 & 0 \\ 0 & 0 & 0 & 0 & 0 & 0 & 0 & 1 \\ 0 & 0 & 0 & 0 & 0 & 0 & 0 & 0 \end{bmatrix} \cdot \begin{bmatrix} p^1 y_{s1} \\ p^1 \dot{y}_{s1} \\ p^2 y_{s2} \\ p^2 \dot{y}_{s2} \\ p^3 y_{s3} \\ p^3 \dot{y}_{s3} \\ p^4 y_{s4} \\ p^4 \dot{y}_{s4} \end{bmatrix} + \begin{bmatrix} 0 & 0 & 0 & 0 \\ 1 & 0 & 0 & 0 \\ 0 & 0 & 0 & 0 \\ 0 & 1 & 0 & 0 \\ 0 & 0 & 0 & 0 \\ 0 & 0 & 1 & 0 \\ 0 & 0 & 0 & 0 \\ 0 & 0 & 0 & 1 \end{bmatrix} \cdot \begin{bmatrix} u_{s1} \\ u_{s2} \\ u_{s3} \\ u_{s4} \end{bmatrix} + \begin{bmatrix} 0 & 0 & 0 & 0 \\ 1 & 0 & 0 & 0 \\ 0 & 0 & 0 & 0 \\ 0 & 1 & 0 & 0 \\ 0 & 0 & 0 & 0 \\ 0 & 0 & 1 & 0 \\ 0 & 0 & 0 & 0 \\ 0 & 0 & 0 & 1 \end{bmatrix} \cdot \begin{bmatrix} w_{s1} \\ w_{s2} \\ w_{s3} \\ w_{s4} \end{bmatrix} \quad (3-11)$$

$$\mathbf{y} = \begin{bmatrix} y_{s1} \\ y_{s2} \\ y_{s3} \\ y_{s4} \end{bmatrix} = \begin{bmatrix} 1 & 0 & 0 & 0 & 0 & 0 & 0 & 0 \\ 0 & 0 & 1 & 0 & 0 & 0 & 0 & 0 \\ 0 & 0 & 0 & 0 & 1 & 0 & 0 & 0 \\ 0 & 0 & 0 & 0 & 0 & 0 & 1 & 0 \end{bmatrix} \cdot \begin{bmatrix} p^1 y_{s1} \\ p^1 \dot{y}_{s1} \\ p^2 y_{s2} \\ p^2 \dot{y}_{s2} \\ p^3 y_{s3} \\ p^3 \dot{y}_{s3} \\ p^4 y_{s4} \\ p^4 \dot{y}_{s4} \end{bmatrix} + \begin{bmatrix} v_{s1} \\ v_{s2} \\ v_{s3} \\ v_{s4} \end{bmatrix} \quad (3-12)$$

With the use of this representation, equation (3-8) now becomes:

$$\dot{\mathbf{x}} = \mathbf{A}_m \mathbf{x} + \mathbf{B}_m \mathbf{u} + \mathbf{B}_{mw} \mathbf{w} \quad (3-13a)$$

$$\mathbf{y} = \mathbf{C}_m \mathbf{x} + \mathbf{v} \quad (3-13b)$$

where:

$$\dot{\mathbf{x}} = \begin{bmatrix} p^1 \dot{y}_{s1} & p^1 \ddot{y}_{s1} & p^2 \dot{y}_{s2} & p^2 \ddot{y}_{s2} & p^3 \dot{y}_{s3} & p^3 \ddot{y}_{s3} & p^4 \dot{y}_{s4} & p^4 \ddot{y}_{s4} \end{bmatrix}^T ;$$

$$\mathbf{x} = \begin{bmatrix} \rho^1 y_{s1} & \rho^1 \dot{y}_{s1} & \rho^2 y_{s2} & \rho^2 \dot{y}_{s2} & \rho^3 y_{s3} & \rho^3 \dot{y}_{s3} & \rho^4 y_{s4} & \rho^4 \dot{y}_{s4} \end{bmatrix}^T;$$

$$\mathbf{u} = \begin{bmatrix} u_{s1} & u_{s2} & u_{s3} & u_{s4} \end{bmatrix}^T;$$

$$\mathbf{w} = \begin{bmatrix} w_{s1} & w_{s2} & w_{s3} & w_{s4} \end{bmatrix}^T;$$

$$\mathbf{y} = \begin{bmatrix} y_{s1} & y_{s2} & y_{s3} & y_{s4} \end{bmatrix}^T;$$

$$\mathbf{v} = \begin{bmatrix} v_{s1} & v_{s2} & v_{s3} & v_{s4} \end{bmatrix}^T;$$

$$\mathbf{A}_m = \begin{bmatrix} 0 & 1 & 0 & 0 & 0 & 0 & 0 & 0 \\ 0 & 0 & 0 & 0 & 0 & 0 & 0 & 0 \\ 0 & 0 & 0 & 1 & 0 & 0 & 0 & 0 \\ 0 & 0 & 0 & 0 & 0 & 0 & 0 & 0 \\ 0 & 0 & 0 & 0 & 0 & 1 & 0 & 0 \\ 0 & 0 & 0 & 0 & 0 & 0 & 0 & 0 \\ 0 & 0 & 0 & 0 & 0 & 0 & 0 & 1 \\ 0 & 0 & 0 & 0 & 0 & 0 & 0 & 0 \end{bmatrix};$$

$$\mathbf{B}_m = \mathbf{B}_{mw} = \begin{bmatrix} 0 & 0 & 0 & 0 \\ 1 & 0 & 0 & 0 \\ 0 & 0 & 0 & 0 \\ 0 & 1 & 0 & 0 \\ 0 & 0 & 0 & 0 \\ 0 & 0 & 1 & 0 \\ 0 & 0 & 0 & 0 \\ 0 & 0 & 0 & 1 \end{bmatrix};$$

$$\mathbf{C}_m = \begin{bmatrix} 1 & 0 & 0 & 0 & 0 & 0 & 0 & 0 \\ 0 & 0 & 1 & 0 & 0 & 0 & 0 & 0 \\ 0 & 0 & 0 & 0 & 1 & 0 & 0 & 0 \\ 0 & 0 & 0 & 0 & 0 & 0 & 1 & 0 \end{bmatrix}.$$

The observation matrix  $\mathbf{C}_m$  consists of four rows. Each row contains the observation sensitivity coefficients for a particular sensor at the vehicle frame  $si$ . So, the first row contains the observation sensitivity coefficients for the sensor at vehicle frame  $s1$  and the fourth row contains the observation sensitivity coefficients for the sensor at vehicle frame  $s4$ . Therefore, the observation matrix  $\mathbf{C}_m$  can also be expressed as:

$$\mathbf{C}_m = [\mathbf{C}_{s1} \quad \mathbf{C}_{s2} \quad \mathbf{C}_{s3} \quad \mathbf{C}_{s4}]^T$$

where  $\mathbf{C}_{s1} = [1 \ 0 \ 0 \ 0 \ 0 \ 0 \ 0 \ 0]$  is the observation matrix for the sensor at vehicle frame  $s1$  and  $\mathbf{C}_{s4} = [0 \ 0 \ 0 \ 0 \ 0 \ 0 \ 1 \ 0]$  is the observation matrix for the sensor at vehicle frame  $s4$ . The other two observation matrixes  $\mathbf{C}_{s2}$  and  $\mathbf{C}_{s3}$  can be obtained from  $\mathbf{C}_m$  and speak for themselves.

### ***3.3 Conclusions***

After the definition of the different coordinate frames involved in the kinematics of the vehicle, the kinematic equations of the vehicle can be formed. From the kinematic equations a model description can be obtained in a state-space form. The model description is formed by the model equations which describe the model. The model equations can be worked out for the complete sensor configuration of the vehicle. This can be done in a single-input single-output (SISO) representation or in a multiple-input multiple-output (MIMO) representation. It seems that the model equations lend themselves perfectly for a description in a MIMO representation.



# Chapter 4

## Description of the simulation model

To evaluate the sensors they have to be implemented in an observer. The observer is implemented in an existing Simulink model. To understand the working of the model, it will be described in this chapter. First, the Simulink model will be introduced and then the different model blocks or subsystems are discussed.

### 4.1 The Simulink model

As was mentioned before the observer will be implemented in an existing Simulink model. The model is developed by my coach during his doctoral research. The Simulink block diagram of the model is illustrated in **Figure 4-1**.

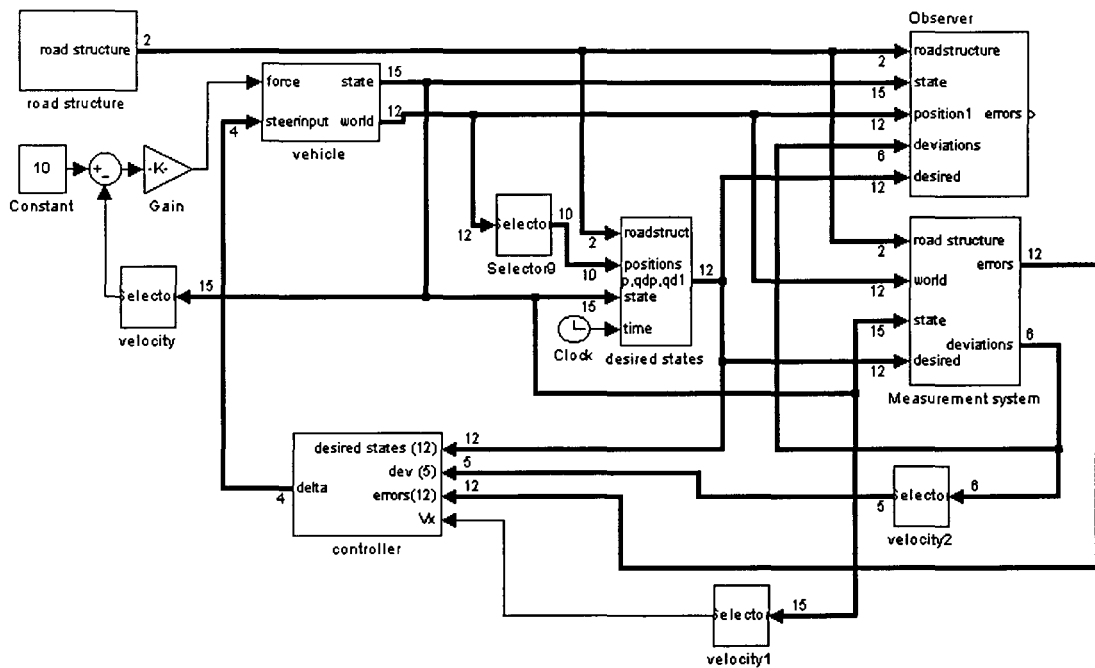


**Figure 4-1: Block diagram of the Simulink model**

The model simulates a driving vehicle. The vehicle consists of a tractor and two semitrailers which are connected through two articulation points. The vehicle maintains a constant velocity and it drives along a desired path. The path is formed by a straight line and a curve with a given radius. The vehicle is controlled by means of its steering angle.

The Simulink model consists of many blocks and subsystems. **Figure 4-1** shows the main blocks of the model and is therefore the upper layer of the model. The main blocks and an explanation of their functionality will be given in the next paragraph.

## 4.2 Explanation of the model blocks

In this section an explanation of the functionality of the different model blocks is given. This is done to illustrate how simulations are run and to give some understanding in the simulation model. Thus, now a description of the model blocks will be given together with an explanation of their functionality.

See **Figure 4-1** for the names of the different model blocks.

### Road structure

- In this block the trajectory of the road is defined. The length of the straight line and the radius of the curve can be entered in this block. These values will be used for the calculation of the desired states in the model.

### Vehicle

- This block contains the transformation of the steer- and force-inputs into states of the vehicle. The states of the vehicle are its position and its velocity with respect to the path reference frame. Furthermore, the block outputs the yaw and its first and second derivatives with respect to the path reference frame together with the second derivative of the position with respect to the path reference frame. To obtain the positions of the vehicle with respect to the world reference frame a transformation is also made between the states of the vehicle and the world reference frame.

### Desired states

- The desired states of the vehicle are calculated in this model block. The inputs of the block are the road structure, the positions of the vehicle with respect to the world reference frame, the states of the vehicle and the simulation clock. The desired states are the states of the vehicle when the vehicle drives ideal along the desired path with no deviations. This is not true in practice, so there is always a difference between the desired states and the true states of the vehicle.

### Measurement system

- This block forms the measurement system of the model. The block has the road, the positions of the vehicle with respect to the world reference frame called world, the true states of the vehicle and the desired states as its input. The block outputs the errors and the deviations, which are fed back to the controller so that the measurement system is in closed loop. With deviations is meant the smallest difference in position of the vehicle and the desired path in the direction that is perpendicular to the tangent of the path. The errors are the deviations in the yaw and the yaw rate of the vehicle. The measurement system is a continuous-time system and it assumes that the deviation from the path as well as the time derivative of the deviation are continuously available for the controller. The time derivative of the deviation however can not be measured directly. Furthermore, the deviation can only be measured at discrete times when magnetic markers are used. Besides this, the effect of disturbances and noise coming from the sensors is not taken into account in this system. These aspects are taken along in the observer design.

**Controller**

- In this block the controller of the system is implemented. The vehicle is controlled by means of its steering angle and it has 4 independently steerable axles. So, the controller calculates independently the 4 steering angles of the steerable axles out of the desired states, the deviations, the errors and the driving speed. The steering angles are fed into the vehicle block. The control of steering angles is to achieve that the driven route of the vehicle approaches the desired path as close as possible.

**Observer design**

- This is the main block of the Simulink model in relation to the assignment. This block contains the implementation of the designed observer. The block has as its input the road structure, the states of the vehicle, the positions of the vehicle with respect to the world reference frame called world, the deviations from the path and the desired states. Its output is the same as the errors output of the measurement system, only the output of the observer is calculated in a complete different way. Further, the output of the observer is not fed into any other block, so the observer is in open loop. In this way the performance of the observer can be compared with the performance of the measurement system. The observer design will be discussed in detail in a later stage of this report.

The observer is designed according to a Kalman Filter. To understand the observer design according to Kalman Filtering a short introduction to Kalman Filtering Theory was given in Chapter 2.





# Chapter 5

## Observer design

### 5.1 Introduction

The observer has to estimate the velocity of the deviation and the deviation itself of the vehicle. There are different methods to do this. There is an article (ref. [9]) in which a passivity-based observer has been discussed. This observer estimates both positions and velocities of a tractor semitrailer vehicle. However, this kind of observer has a few disadvantages. First, it relies on complete knowledge of vehicle parameters like mass, centre of gravity and cornering stiffnesses. Because there might be a large uncertainty in these parameters in practice, it can not be guaranteed that the estimated positions and velocities converge to the real positions and velocities. Another disadvantage is that this method relies in fact on accurate position measurements. In this case however, there are discrete markers like permanent magnets used for position measurements. The passivity-based observer simply ignores the discrete nature of the magnetic markers and assumes that the deviation stays constant in between the magnets, where the position can not be measured. In this report another technique is used for the observer design. The method which is used here combines the discrete magnetic markers with acceleration measurements according to a Kalman filtering technique. The method can also be extended with the measurements of additional sensors. This estimation technique is completely independent of all vehicle parameters. Moreover, the effects of disturbances are also taken into account by the observer. The observer design with its estimation technique according to Kalman filtering is described in this chapter.

### 5.2 Lateral velocity and position estimation

The goal of the observer is to give continuous estimates of the velocity and the deviation of the sensors with respect to the desired path which is formed by the track of magnets. The velocity estimates are obtained by integrating the measurement of  ${}^{pi} \ddot{y}_{si}$  once, whereas the estimates of the deviations are obtained by integrating  ${}^{pi} \ddot{y}_{si}$  twice. Everytime a magnet passes by, a correction will be made to the estimates to correct for measurement noise and accelerometer drift.

The observer has to be implemented on a digital system, so that the estimates are given at discrete time intervals. This is where a complication is introduced into the estimation scheme by the discrete nature of the magnetic markers. The magnetic markers, laid on the road centerline at fixed intervals, provide the lateral position errors only when the magnetometers on the vehicle are approximately above a marker. If the system is discretized with a sampling time in the range at which the lateral position measurements become available, large estimation errors will be introduced. Therefore the sampling interval chosen for reading accelerometer measurements and estimating lateral velocity and position is fixed at  $\Delta$ , which is set to 5 msecs. This value is small enough to allow accurate estimation. However, this also means that

magnetometer measurements are not available at every sampling instant  $\Delta$ , but after every  $n$  sample times, where  $n$  keeps varying with the velocity of the vehicle.

The problems arising out of this non-availability of measured data are addressed by the use of a multi-rate estimation scheme which is described in section 2.4.1. The model equations are simply integrated when measurements are not available, and measurement information is used when it becomes available at a marker.

Now, the model equations can be discretized. But first, the structure of the discrete time Kalman filter, according to which the observer is designed, will be given. The structure of the discrete time Kalman filter (ref. [3]) is depicted in **Figure 5-1**.

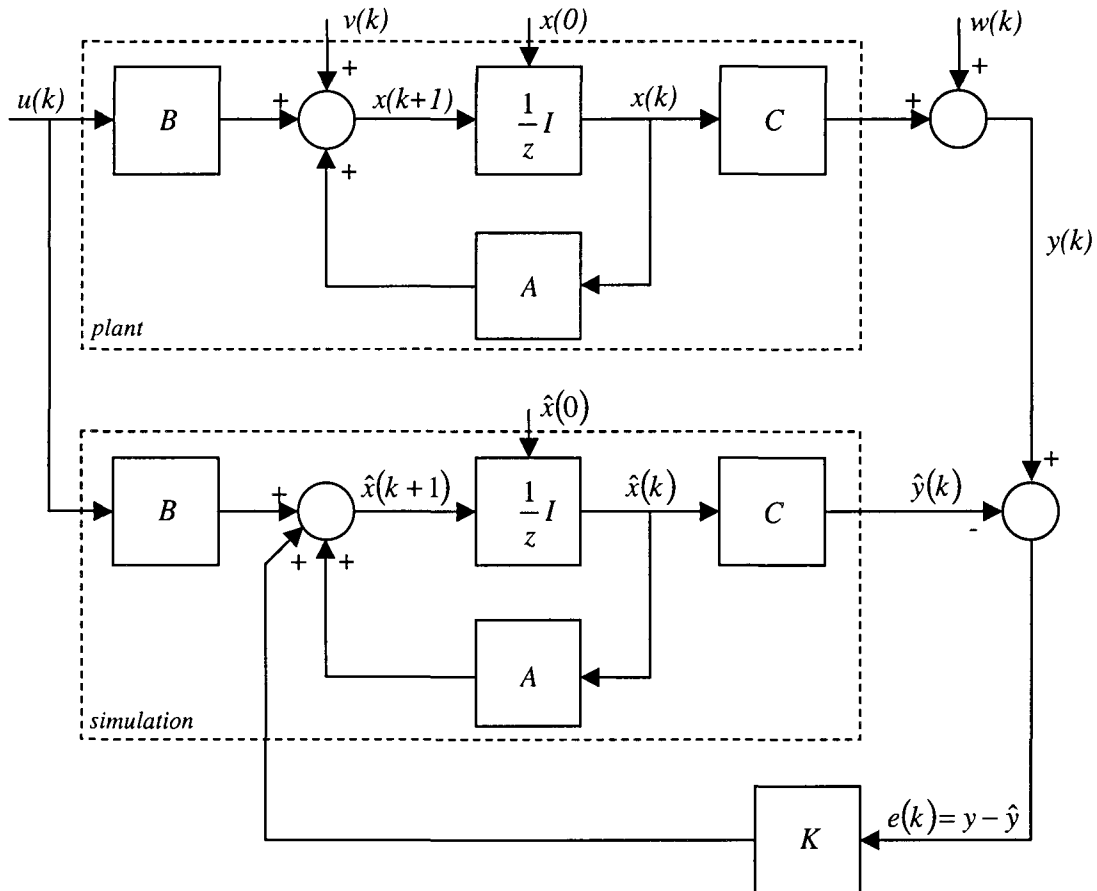


**Figure 5-1: Discrete time Kalman filter**

For this discrete time Kalman filter, the following general equations hold. The equations are written in vector- and matrixform.

$$\mathbf{x}(k+1) = \mathbf{A}\mathbf{x}(k) + \mathbf{B}\mathbf{u}(k) + \mathbf{v}(k) \quad (5-1)$$

$$\mathbf{y}(k) = \mathbf{C}\mathbf{x}(k) + \mathbf{w}(k) \quad (5-2)$$

$$\hat{\mathbf{x}}(k+1) = \mathbf{A}\hat{\mathbf{x}}(k) + \mathbf{B}\mathbf{u}(k) + \mathbf{K}(\mathbf{y}(k) - \hat{\mathbf{y}}(k)) \quad (5-3)$$

$$\hat{\mathbf{y}}(k) = \mathbf{C}\hat{\mathbf{x}}(k) \quad (5-4)$$

In **Figure 5-1**, the upper outlined block is the *plant* and is the modelled behaviour of the real system. The lower outlined block is the *simulation* and it simulates the behaviour of the real system. Actually, the behaviour of the *plant* is also simulated in the situation here. The *plant* and the *simulation* are both excited with the same input signal  $u(k)$ . The lower outlined block (*simulation*) is actually the observer of the real system and it estimates the state  $\hat{x}(k+1)$ . The purpose of the observer is to estimate the state so that the estimated state  $\hat{x}(k+1)$  and the real state  $x(k+1)$  approximate each other as close as possible.

Now that the structure of the discrete time Kalman filter has been described, the model equations can be discretized. First, equation (3-8a) will be discretized with sample time  $\Delta$ . According to ref. [4] this results in:

$$\mathbf{x}_{si}(k+1) = \mathbf{A}_d \mathbf{x}_{si}(k) + \mathbf{B}_d u_{si}(k) + \mathbf{B}_{wd} w_{d_{si}}(k) \quad (5-5)$$

In this equation is:

$$\mathbf{A}_d = e^{A\Delta} \quad (5-6a)$$

$$\mathbf{B}_d = \int_0^\Delta e^{A\tau} \mathbf{B} d\tau \quad (5-6b)$$

$$\mathbf{B}_{wd} = \int_0^\Delta e^{A\tau} \mathbf{B}_w d\tau \quad (5-6c)$$

Assuming the signal  $u_{si}(t)$  to be piecewise-constant, then:

$$u_{si}(k) = \frac{1}{\Delta} \int_{t_k}^{t_k+\Delta} u_{si}(t) dt \approx u_{si}(t_k) \quad (5-6d)$$

Ref. [4] says that,

$$w_{d_{si}}(k) = \frac{1}{\Delta} \int_{t_k}^{t_k+\Delta} w_{si}(t) dt \quad (5-6e)$$

Furthermore,  $k$  is the  $k^{\text{th}}$  sampling instant and  $t_k$  is the corresponding time. The average of the accelerometer reading over one sampling period is used as the input in equation (5-5).

The other equation in (3-8), equation (3-8b), is now replaced by (ref. [4]):

$$y_{si}(t_j) = \mathbf{C} \mathbf{x}_{si}(t_j) + v_{d_{si}}(t_j), \quad j=0,1,2,\dots \quad (5-7)$$

where  $t_j$  is the time when the magnetometer at the vehicle frame  $si$  is on the  $j^{\text{th}}$  magnetic marker, and  $v_{d_{si}}(t_j)$  is the magnetometer noise from the magnetometer at the vehicle frame  $si$ . Furthermore,  $\mathbf{C} = [1 \ 0]$  is the observation matrix for the magnetometer at vehicle frame  $si$ .

From the previous it follows that:

$$0 < (k+1)\Delta \leq t_{j+1} - t_j, \quad k = 0, \dots, n_j - 1$$

where  $t_{j+1}$  is the time when the  $(j+1)^{\text{th}}$  magnetic marker measurement is available, and  $n_j$  is the number of complete sample times counted between the  $j^{\text{th}}$  and  $(j+1)^{\text{th}}$  magnetic marker measurements. Then the following holds:

$$(t_j + n_j \Delta) \leq t_{j+1} < (t_j + (n_j + 1)\Delta) \quad (5-8)$$

Now that the model equations are discretized, the predictor and the corrector equations can be presented.

## 5.2.1 Predictor equations

Every sampling instant  $k$  after the  $j^{\text{th}}$  marker, until  $k = n_j - 1$ , the following predictor equation is used (chapter 2 and ref. [4]):

$$\tilde{\mathbf{x}}_{si}(k+1, t_j) = \mathbf{A}_d \tilde{\mathbf{x}}_{si}(k, t_j) + \mathbf{B}_d u_{si}(k), \quad k=0, \dots, n_j - 1 \quad (5-9a)$$

$$\tilde{\mathbf{x}}_{si}(0, t_j) = \hat{\mathbf{x}}_{si}(t_j, t_j) \quad (5-9b)$$

This equation represents the propagation of the state estimate. The time  $t_j$  is the time instant the magnetometer at vehicle frame  $si$  crosses the  $j^{\text{th}}$  magnetic marker and  $n_j$  is the number of complete sample times counted between the  $j^{\text{th}}$  and the  $(j+1)^{\text{th}}$  magnetic marker measurements. The notation  $\tilde{\mathbf{x}}_{si}(k+1, t_j)$  means that the state estimate is made at instant  $k+1$ , while  $t_j$  indicates that for this estimate all real, measured outputs till time instant  $t_j$  are used.

According to equation (2-19), the estimation error is defined by:

$$\tilde{\mathbf{e}}_{si}(k) = \mathbf{x}_{si}(k) - \tilde{\mathbf{x}}_{si}(k) \quad (5-10)$$

and the covariance of the estimation error is defined by:

$$\tilde{\mathbf{P}}_{si}(k) = E\{\tilde{\mathbf{e}}_{si}(k)\tilde{\mathbf{e}}_{si}(k)^T\} \quad (5-11)$$

The covariance of the estimation error for the predictor equation (5-9) propagates as follows:

$$\tilde{\mathbf{P}}_{si}(k+1, t_j) = \mathbf{A}_d \tilde{\mathbf{P}}_{si}(k, t_j) \mathbf{A}_d^T + \mathbf{B}_{wd} W_{d_{si}} \mathbf{B}_{wd}^T \quad (5-12a)$$

$$\tilde{\mathbf{P}}_{si}(0, t_j) = \hat{\mathbf{P}}_{si}(t_j) \quad (5-12b)$$

In equation (5-12b),  $\hat{\mathbf{P}}_{si}(t_j)$  is the estimation error covariance at time  $t_j$  after incorporating the magnetic marker measurement at  $t_j$ . Furthermore,

$W_{d_{si}} = E\{w_{d_{si}}(k)w_{d_{si}}^T(k)\}$  is the covariance of the noise  $w_{d_{si}}(k)$  coming from the accelerometer at vehicle frame  $si$ .

After that equation (5-9) is updated  $n_j$  times, there still might be a small interval  $\Delta_t$ , smaller than  $\Delta$ , before which a magnetometer will pass over a magnetic marker and provide a measurement. This interval can be obtained from equation (5-8), and is given by:

$$\Delta_t = T_j - n_j \Delta, \quad T_j = t_{j+1} - t_j$$

The problem is now that the time  $T_j$  is not known in advance and that it is not easy to determine. If  $T_j$  could be determined, the predictor equation could be modified, taking into account the small time interval  $\Delta_t$ . The problem is not solved here, it is assumed that neglecting the time interval  $\Delta_t$  will not introduce that big errors in the prediction. The assumption is an acceptable one for low speeds of the vehicle. At low speeds the covered distance of the vehicle during one sampling instant  $\Delta$  is very small. This means that the covered distance during the time interval  $\Delta_t$ , which is smaller than  $\Delta$ , is also very small. It is assumed that the lateral velocity and position will not change that drastically in the time interval  $\Delta_t$ , so that the prediction does not have to be modified. At high speeds the same assumption is made. Suppose a maximum velocity of 20 m/s of the vehicle, then the covered distance of the vehicle during one sampling instant  $\Delta$  is 10 cm. At high speeds, the lateral velocity and position will also not change that drastically over such a short distance, so that the assumption which is made before is an acceptable one.

### 5.2.2 Corrector equations

When the magnetometer at the vehicle frame  $si$  is on top of a magnetic marker, the prediction which is made by equation (5-9) can be corrected. This is done in a few steps. First the Kalman gain is computed. This is done by the following equation:

$$\tilde{\mathbf{K}}_{si}(t_{j+1}) = \tilde{\mathbf{P}}_{si}(t_{j+1}, t_j) \mathbf{C}^T \left[ \mathbf{C} \tilde{\mathbf{P}}_{si}(t_{j+1}, t_j) \mathbf{C}^T + V_{d_{si}} \right]^{-1} \quad (5-13)$$

$V_{d_{si}} = E\{v_{d_{si}}(k)v_{d_{si}}^T(k)\}$  is the covariance of the noise  $v_{d_{si}}(k)$  due to magnet misalignment and magnetometer noise coming from the magnetometer at vehicle frame  $si$ .

Then a prediction is made of the observation or measurement from the magnetometer at the vehicle frame  $si$  at time instant  $t_{j+1}$ . To make the prediction, the following equation is used:

$${}^{pi} \tilde{y}_{si}(t_{j+1}, t_j) = \mathbf{C} \tilde{\mathbf{x}}_{si}(t_{j+1}, t_j) \quad (5-14)$$

Now, the prediction of equation (5-9) is corrected by the corrector equation, which is given by (chapter 2 and ref. [4]):

$$\hat{\mathbf{x}}_{si}(t_{j+1}, t_{j+1}) = \tilde{\mathbf{x}}_{si}(t_{j+1}, t_j) + \tilde{\mathbf{K}}_{si}(t_{j+1}) \left\{ {}^{pi} y_{si}(t_{j+1}) - \mathbf{C} \tilde{\mathbf{x}}_{si}(t_{j+1}, t_j) \right\} \quad (5-15)$$

This equation represents the update of the state estimate. The term  ${}^{pi} y_{si}(t_{j+1})$  in this equation is the measurement from the magnetometer at vehicle frame  $si$  at the time instant  $t_{j+1}$ .

At last the prediction of the covariance of the estimation error is corrected by the following equation:

$$\hat{\mathbf{P}}_{si}(t_{j+1}) = \tilde{\mathbf{P}}_{si}(t_{j+1}, t_j) - \tilde{\mathbf{K}}_{si}(t_{j+1}) \mathbf{C} \tilde{\mathbf{P}}_{si}(t_{j+1}, t_j) \quad (5-16)$$

The update of the covariance of the estimation error is expressed by this equation.

Just as in the continuous-time domain, the discrete-time model equations can be written in a MIMO representation. By rewriting equation (5-5) the following result can be obtained:

$$\mathbf{x}(k+1) = \mathbf{A}_{\text{md}} \mathbf{x}(k) + \mathbf{B}_{\text{md}} \mathbf{u}(k) + \mathbf{B}_{\text{mwd}} \mathbf{w}_d(k) \quad (5-17)$$

with:

$$\mathbf{x}(k+1) = \begin{bmatrix} p^1 y_{s1}(k+1) & p^1 y_{s1}(k+2) & \dots & p^4 y_{s4}(k+1) & p^4 y_{s4}(k+2) \end{bmatrix}^T;$$

$$\mathbf{x}(k) = \begin{bmatrix} p^1 y_{s1}(k) & p^1 y_{s1}(k+1) & \dots & p^4 y_{s4}(k) & p^4 y_{s4}(k+1) \end{bmatrix}^T;$$

$$\mathbf{A}_{\text{md}} = e^{\mathbf{A}_m \Delta};$$

$$\mathbf{B}_{\text{md}} = \int_0^{\Delta} e^{\mathbf{A}_m \tau} \mathbf{B}_m d\tau;$$

$$\mathbf{B}_{\text{mwd}} = \int_0^{\Delta} e^{\mathbf{A}_m \tau} \mathbf{B}_{\text{mw}} d\tau;$$

$$\mathbf{u}(k) = \begin{bmatrix} u_{s1}(k) & u_{s2}(k) & u_{s3}(k) & u_{s4}(k) \end{bmatrix}^T;$$

$$\mathbf{w}_d(k) = \begin{bmatrix} w_{d,1}(k) & w_{d,2}(k) & w_{d,3}(k) & w_{d,4}(k) \end{bmatrix}^T.$$

Model equation (5-7) can also be written in a MIMO representation. This results in:

$$\mathbf{y}(k) = \mathbf{C}_m \mathbf{x}(k) + \mathbf{v}_d(k) \quad (5-18)$$

where the index  $k$  is used instead of  $t_j$ , for the reason that it is now better visible that the equation is in the discrete-time domain. In this equation is:

$$\mathbf{y}(k) = \begin{bmatrix} y_{s1}(k) & y_{s2}(k) & y_{s3}(k) & y_{s4}(k) \end{bmatrix}^T;$$

$$\mathbf{v}_d(k) = \begin{bmatrix} v_{d,1}(k) & v_{d,2}(k) & v_{d,3}(k) & v_{d,4}(k) \end{bmatrix}^T;$$

and

$$\mathbf{C}_m = \begin{bmatrix} 1 & 0 & 0 & 0 & 0 & 0 & 0 & 0 \\ 0 & 0 & 1 & 0 & 0 & 0 & 0 & 0 \\ 0 & 0 & 0 & 0 & 1 & 0 & 0 & 0 \\ 0 & 0 & 0 & 0 & 0 & 0 & 1 & 0 \end{bmatrix}.$$

Equation (5-18) suggests that the measurements coming from the magnetometers are available all at the same time. In practice this is not the case. This is taken care of in the formation of the predictor and corrector equations.

The predictor and corrector equations which are described before, hold for the discrete-time model equations in the SISO representation. When you want to apply the predictor and corrector equations to the discrete-time model equations in the

MIMO representation, they have to be adjusted. The equations can be adjusted in the following way. First, the predictor equation (5-9) which represents the propagation of the state estimate is adjusted as follows:

$$\tilde{\mathbf{x}}(k+1, t_j) = \mathbf{A}_{\text{md}} \tilde{\mathbf{x}}(k, t_j) + \mathbf{B}_{\text{md}} \mathbf{u}(k), \quad k=0, \dots, n_j-1 \quad (5-19a)$$

$$\tilde{\mathbf{x}}(0, t_j) = \hat{\mathbf{x}}(t_j, t_j) \quad (5-19b)$$

The covariance of the estimation error for the predictor equation (5-19) propagates now as:

$$\tilde{\mathbf{P}}(k+1, t_j) = \mathbf{A}_{\text{md}} \tilde{\mathbf{P}}(k, t_j) \mathbf{A}_{\text{md}}^T + \mathbf{B}_{\text{mwd}} \mathbf{W}_d \mathbf{B}_{\text{mwd}}^T \quad (5-20a)$$

$$\tilde{\mathbf{P}}(0, t_j) = \hat{\mathbf{P}}(t_j) \quad (5-20b)$$

where:

$$\mathbf{W}_d = E\{\mathbf{w}_d(k) \mathbf{w}_d^T(k)\} = \text{diag} [W_{d_{s1}} \quad W_{d_{s2}} \quad W_{d_{s3}} \quad W_{d_{s4}}]^T$$

Adjusting the computation of the Kalman gain which is used in the corrector equation (5-15) results in:

$$\tilde{\mathbf{K}}_i(t_{j+1}) = \tilde{\mathbf{P}}(t_{j+1}, t_j) \mathbf{C}_{\text{mi}}^T [\mathbf{C}_{\text{mi}} \tilde{\mathbf{P}}(t_{j+1}, t_j) \mathbf{C}_{\text{mi}}^T + \mathbf{V}_d]^{-1} \quad (5-21)$$

where:

$$\mathbf{V}_d = E\{\mathbf{v}_d(k) \mathbf{v}_d^T(k)\} = \text{diag} [V_{d_{s1}} \quad V_{d_{s2}} \quad V_{d_{s3}} \quad V_{d_{s4}}]^T$$

and with the matrix  $\mathbf{C}_{\text{mi}}$  equal to the matrix  $\mathbf{C}_{\text{m}}$ , but with the  $i^{\text{th}}$  row equal to the matrix  $\mathbf{C}_{\text{si}}$  and the rest of the matrix  $\mathbf{C}_{\text{m}}$  contains zeros. This distinction has to be made because the measurements coming from the magnetometers are not available all at the same time.

After adjustment, equation (5-14) becomes:

$${}^p \tilde{\mathbf{y}}_{\text{is}}(t_{j+1}, t_j) = \mathbf{C}_{\text{mi}} \tilde{\mathbf{x}}(t_{j+1}, t_j) \quad (5-22)$$

with:

$${}^p \tilde{\mathbf{y}}_{\text{is}}(t_{j+1}, t_j) = [{}^{p1} \tilde{y}_{s1}(t_{j+1}, t_j) \quad 0 \quad 0 \quad 0]^T$$

for  $i = 1$ , which means that the measurement from the magnetometer at vehicle frame  $s1$  is available, and:

$${}^p \tilde{\mathbf{y}}_{\text{is}}(t_{j+1}, t_j) = [0 \quad 0 \quad 0 \quad {}^{p4} \tilde{y}_{s4}(t_{j+1}, t_j)]^T$$

for  $i = 4$ , which means that the measurement from the magnetometer at vehicle frame  $s4$  is available.

The predictor equation (5-19) is now corrected by the adjusted corrector equation, which is given by:

$$\hat{\mathbf{x}}(t_{j+1}, t_{j+1}) = \tilde{\mathbf{x}}(t_{j+1}, t_j) + \tilde{\mathbf{K}}_i(t_{j+1}) \{ {}^p \mathbf{y}_s(t_{j+1}) - \mathbf{C}_{mi} \tilde{\mathbf{x}}(t_{j+1}, t_j) \} \quad (5-23)$$

The term  ${}^p \mathbf{y}_s(t_{j+1})$  in this equation are the measurements from the magnetometers at the vehicle frames  $si$  at the time instant  $t_{j+1}$ . In the form of a matrix it is written as:

$${}^p \mathbf{y}_s(t_{j+1}) = \begin{bmatrix} {}^{p1} y_{s1}(t_{j+1}) & {}^{p2} y_{s2}(t_{j+1}) & {}^{p3} y_{s3}(t_{j+1}) & {}^{p4} y_{s4}(t_{j+1}) \end{bmatrix}^T$$

At last, the corrector equation to correct the prediction of the covariance of the estimation error is adjusted. This yields:

$$\hat{\mathbf{P}}(t_{j+1}) = \tilde{\mathbf{P}}(t_{j+1}, t_j) - \tilde{\mathbf{K}}_i(t_{j+1}) \mathbf{C}_{mi} \tilde{\mathbf{P}}(t_{j+1}, t_j) \quad (5-24)$$

The observer is designed according to the model equations, the predictor and the corrector equations in the MIMO representation.

Using the predictor and the corrector equations, the estimate  $\tilde{\mathbf{x}}_{si}(k+1, t_j)$  can be obtained when the magnetometers at the vehicle frames  $si$  are between magnetic markers and  $\hat{\mathbf{x}}_{si}(t_{j+1}, t_{j+1})$  can be obtained when the magnetometers are on top of a magnetic marker.

When one cycle of prediction and correction is run through, the cycle starts all over from the beginning. The procedure of a cycle is shown in the flowchart of **Figure 5-2**. Basically, this is the same flowchart of **Figure 2-1**, but with some modifications.



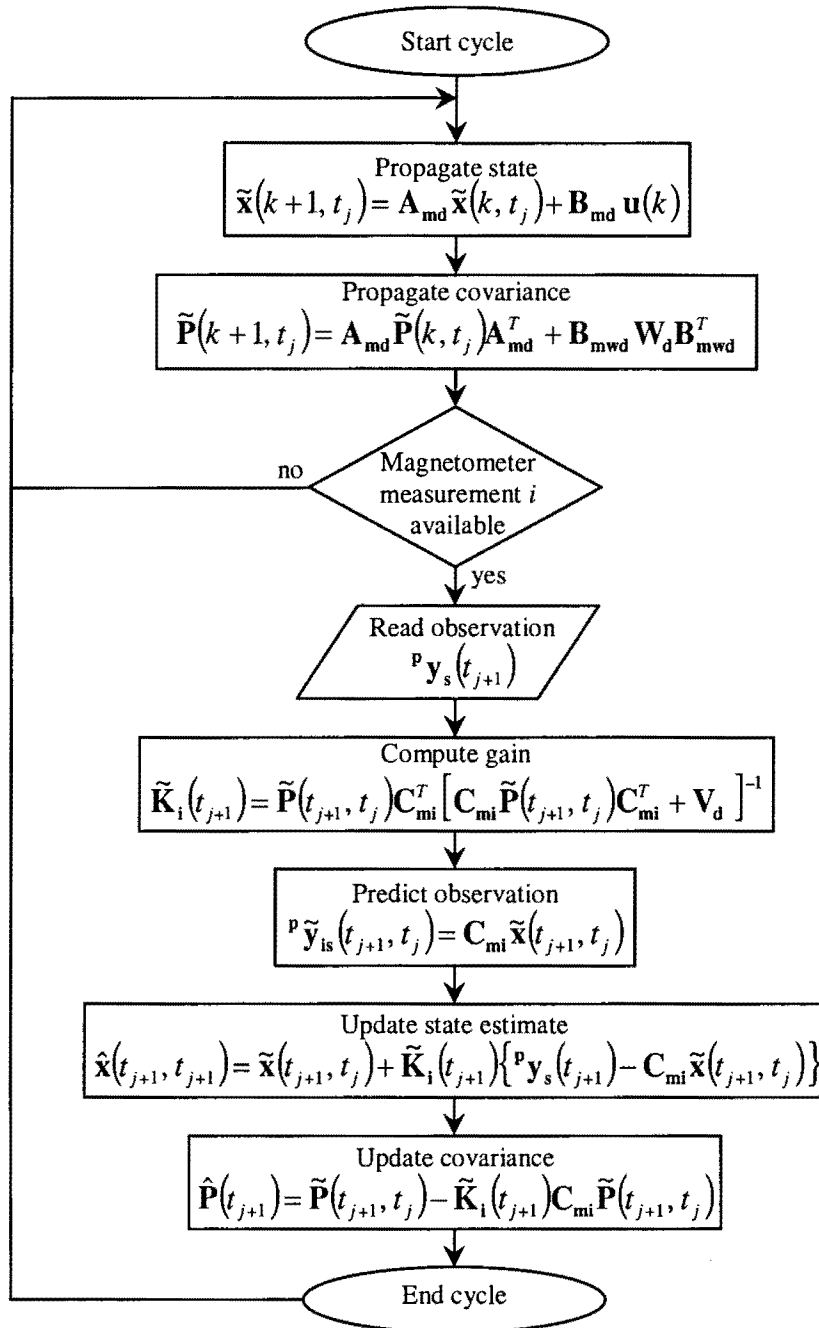


Figure 5-2: Flowchart of observer cycle

In one cycle the distance between two magnetic markers is covered. The cycle works as follows. Between magnetic markers the model equations are integrated to obtain a prediction of the state and a correction is made when the magnetometers are on top of a magnetic marker. When a magnetic marker is passed the cycle starts again with the prediction of the state. The procedure of one cycle can also be represented in a flowchart. The observer is designed according to the procedure which is given in the flowchart of **Figure 5-2**.

### 5.3 Simulation results

To evaluate the performance of the observer, some simulations are carried out. The simulations are conducted by use of the simulation model which is described in **Chapter 4**. The observer design is implemented in a Matlab-file. It is written as a S-function in a Matlab m-file. The Matlab-file in which the observer is implemented is given in **Appendix A**.

The simulations are carried out for a vehicle entering a curve with a radius of  $50\text{ m}$ . at a speed of  $10\text{ ms}^{-1}$ . The vehicle is equipped with a simple low gain PD-controller to provide large errors. Furthermore, the vehicle is equipped with one magnetometer and one accelerometer at each vehicle frame  $si$ , to provide lateral position error and lateral acceleration at the vehicle frames. For these simulations, the observer was implemented with a sampling time  $\Delta$  which was set to  $5\text{ ms}$ . and the distance between the magnetic markers was set to  $2\text{ m}$ . Band limited white noise was added to the acceleration signals applied to the observer to simulate the effect of accelerometer noise. Furthermore, noise was added to the magnetometer signals to simulate the effect of magnetic marker misalignment and magnetometer noise. The noise of the sensors, its value and its covariance are aspects which are discussed in detail in **Chapter 7**.

The next figures, **Figure 5-3** until **Figure 5-6**, show the estimated lateral velocity and the true lateral velocity as well as the estimated lateral deviation and the true lateral deviation. In each figure the estimated and true lateral velocity of vehicle frame  $si$  are depicted at the right side of the figure. At the left side of each figure the estimated and true lateral deviation of vehicle frame  $si$  are depicted.

As can be seen in this figures, the estimated lateral velocity approximates the true lateral velocity close, except for some deviations due to the magnetic marker misalignment and magnetometer noise as well as accelerometer noise. The figures also show that the estimated lateral deviation is close to the true lateral deviation, but here the measurement errors due to magnet misalignment and magnetometer noise as well as accelerometer noise are also visible.

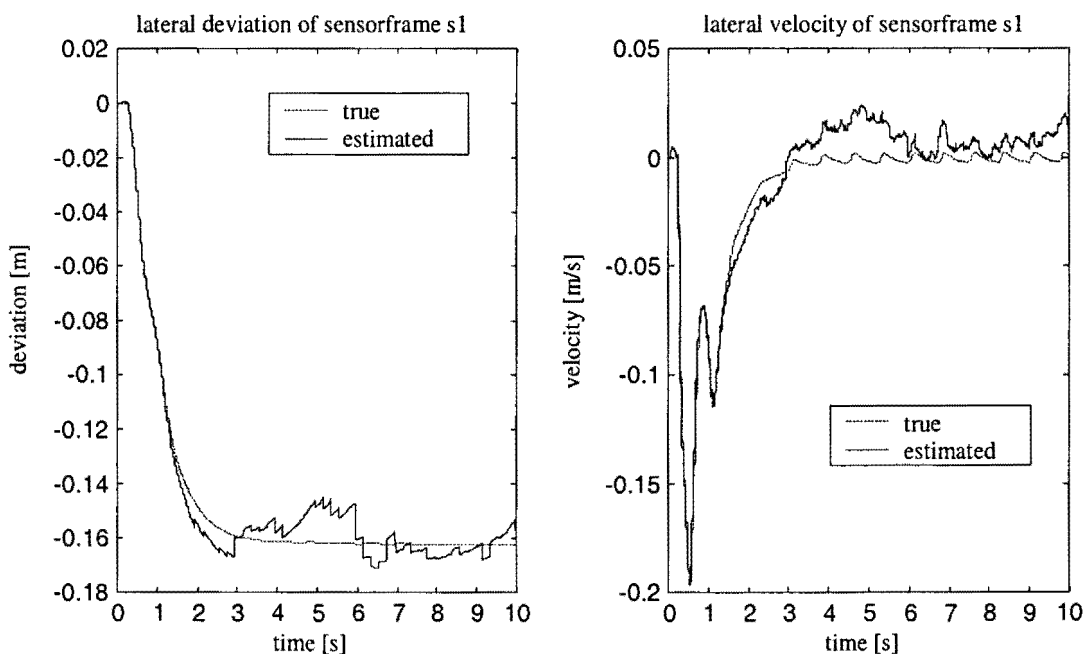


**Figure 5-3: Estimated and true lateral deviation and velocity of sensorframe  $s1$**

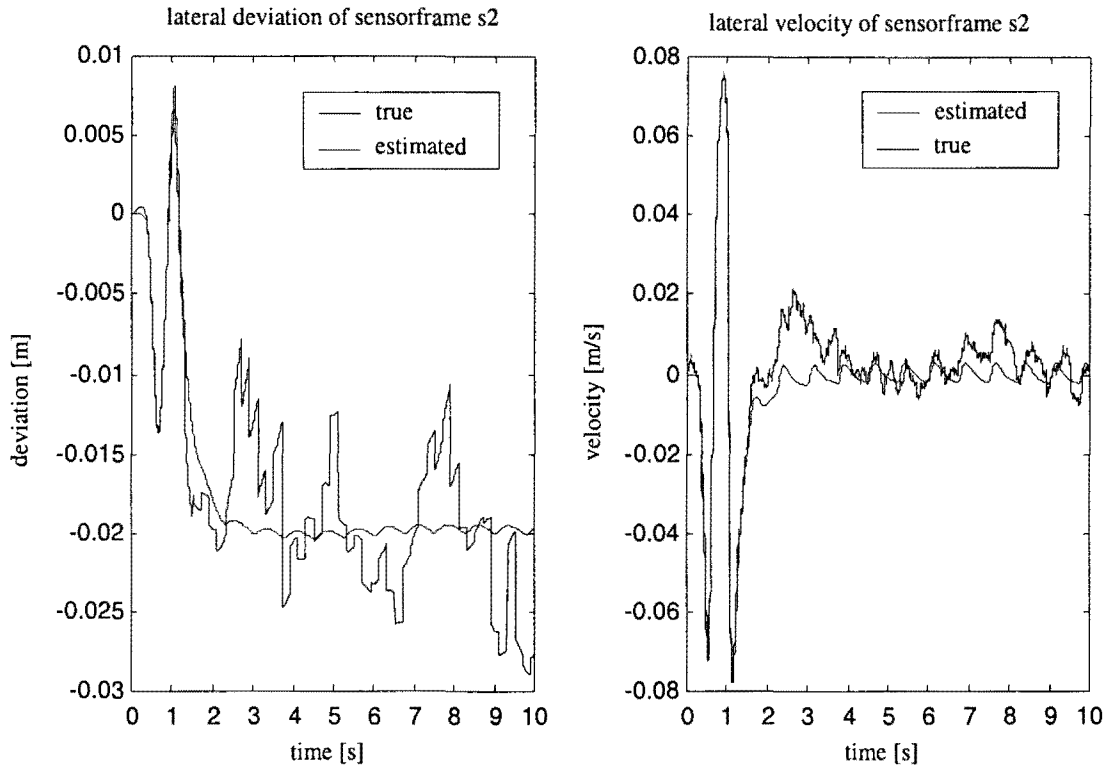


**Figure 5-4: Estimated and true lateral deviation and velocity of sensorframe  $s_2$**

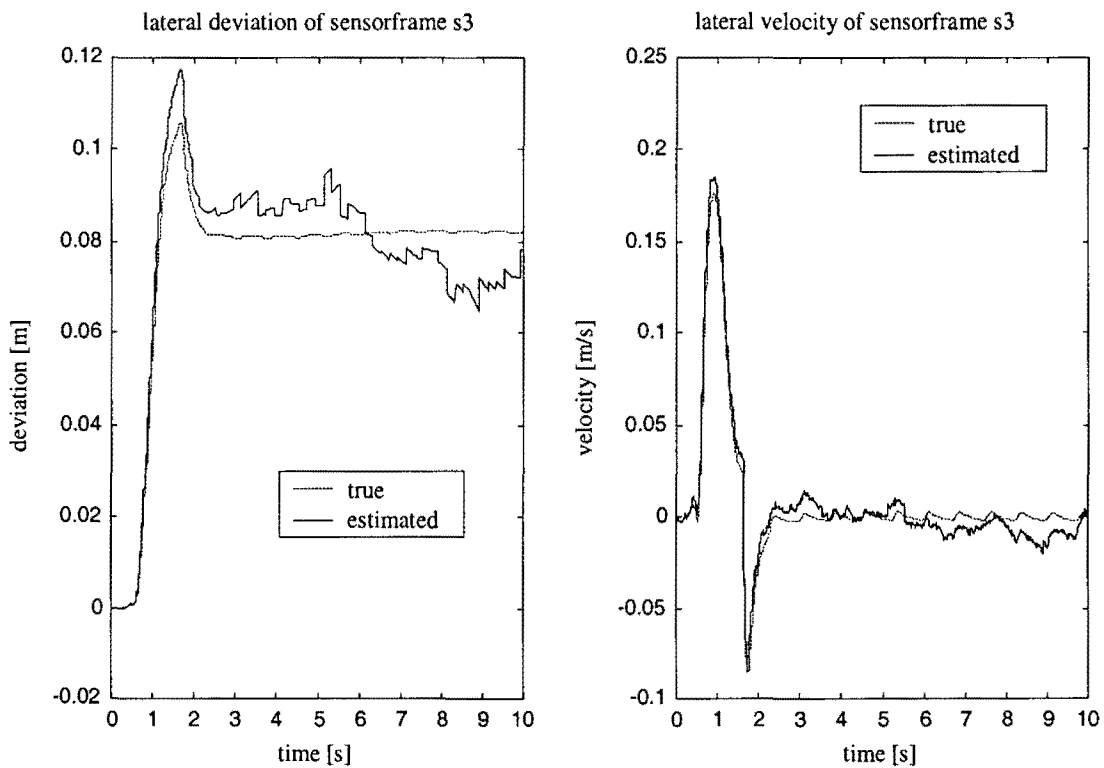


**Figure 5-5: Estimated and true lateral deviation and velocity of sensorframe  $s_3$**

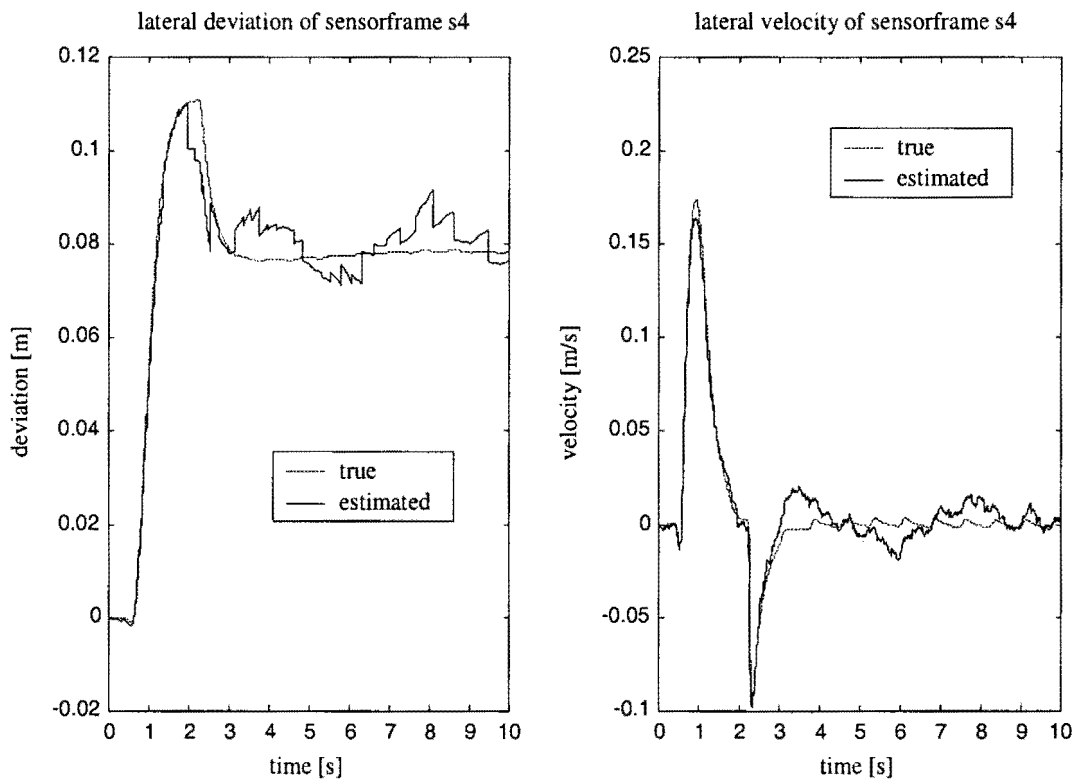


**Figure 5-6: Estimated and true lateral deviation and velocity of sensorframe s4**

The estimates of the states are close to the true states as can be seen in the figures above. But the figures also show that there are some deviations in the estimates which are caused by magnetic marker misalignment, magnetometer noise and accelerometer noise. To reduce the influence of these disturbances, the observer could be extended with other measurements of additional sensors. This is described in the next chapter.

## 5.4 Conclusions

An observer has been designed to estimate the lateral velocity and the lateral deviation of the vehicle. The method which is used combines the discrete magnetic markers with acceleration measurements according to a Kalman filtering technique.

This estimation technique is completely independent of all vehicle parameters. The lateral velocity and deviation are estimated by the predictor and corrector equations which are introduced in the Kalman filtering theory. The model equations, the predictor equations and the corrector equations are presented in a SISO and in a MIMO representation. The observer is designed according to the MIMO representation. Simulation results show that the estimated lateral velocity and deviation are close to the true lateral velocity and deviation, except for some deviations caused by sensor noise and magnet misalignment. The observer can be improved by the use of the measurements of additional sensors. The expectation is then that the deviations in the estimated states are reduced.

# Chapter 6

## Sensor extension of observer

To improve the observer it can be extended with additional sensors. Then the extra measurements which become available can be used to implement an extra correction step in the observer. The intention is that the measurements of these additional sensors are available at a much higher rate than the rate at which the measurements of the magnetometers are available. In this way the predictor equations of the observer can be corrected more often and the observer does not have to wait until the measurement of a magnetometer becomes available. Then it is possible to improve the estimated states so that they better approximate the true states.

### 6.1 Gyroscopes

Gyroscopes are instruments which are used to measure angular motion. Most of the gyroscopes are vibrating structure gyroscopes. Vibrating structure gyroscopes are solid state devices which provide an output voltage proportional to the rate of turn applied to the sensitive axis.

A vibrating structure gyroscope works on the basic principle of detecting coriolis forces. These forces are generated when a moving particle is rotated.

To use the coriolis effect to detect angular rotation, a solid structure is forced to vibrate normally at its resonant frequency. This is achieved by applying an alternating voltage to the primary electrodes. The vibration provides the structure with a linear velocity component. When the structure is rotated the coriolis forces cause the vibration motion of the structure to be coupled to another vibration mode or plane of the structure. The magnitude of this secondary vibration is proportional to the angular rate of turn. The vibrating technology can be very robust and available at low cost in contrast to traditionally gyroscopes which have been very fragile and expensive.

So, gyroscopes (also known as “rate gyros” or just “gyros”) can be used to measure the angular velocity of a vehicle. The angular velocity from the gyroscope can be integrated to provide the heading or orientation of the vehicle. The output of a gyroscope is also called “yaw rate” and the integrated output of a gyroscope is also called “yaw angle”. The angular velocity and the orientation of a vehicle are main aspects for the lateral control system of the vehicle. This is because any small momentary orientation error will cause a constantly growing lateral position error. Furthermore, a gyroscope is an inertial sensor which has the advantage that it is self-contained, that means, the sensor does not need any external references. Besides, a gyroscope is easy to mount at a vehicle, it can be pretty accurate and it is not that expensive anymore. For these reasons, the gyroscopes are chosen to analyse them as possible sensors for the extension of the observer.

#### 6.1.1 Integrating gyroscope

First, the integrating gyroscope which provides the orientation or the yaw angle of the vehicle is examined. For this, the vehicle with the sensor configuration which is

described before is extended with three integrating gyroscopes. One on the tractor and one on each semitrailer. The gyroscopes are mounted at the centres of gravity of the three carriages of an empty vehicle. For convenience, the vehicle sensorframe  $s_2$  is moved to the articulation point which connects the tractor and the first semitrailer. The model of the vehicle with its extended sensor configuration and the modification looks now as shown in **Figure 6-1**.

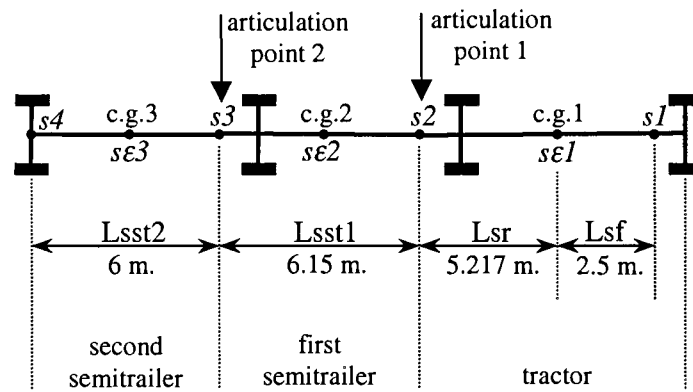


**Figure 6-1: Model of vehicle with extended sensor configuration**

The points which are denoted with  $sE1$ ,  $sE2$  and  $sE3$  in **Figure 6-1**, are the vehicle sensor frames of the (integrating) gyroscopes. Now the measurements of the gyroscopes can be used for an extra correction step in the observer. The output of an integrating gyroscope is the yaw angle of the vehicle carriage on which it is mounted. To do a correction step in the observer with the yaw angle, it is needed to make an estimate of the yaw angle. Because the states of the observer contain the lateral deviations of the vehicle frames  $s_i$  and you want to correct the states, it is obvious to estimate the yaw angle error and not the yaw angle. The yaw angle error is the difference between the actual yaw angle of a vehicle carriage and the desired yaw angle of the path. This is clarified in **Figure 6-2**.

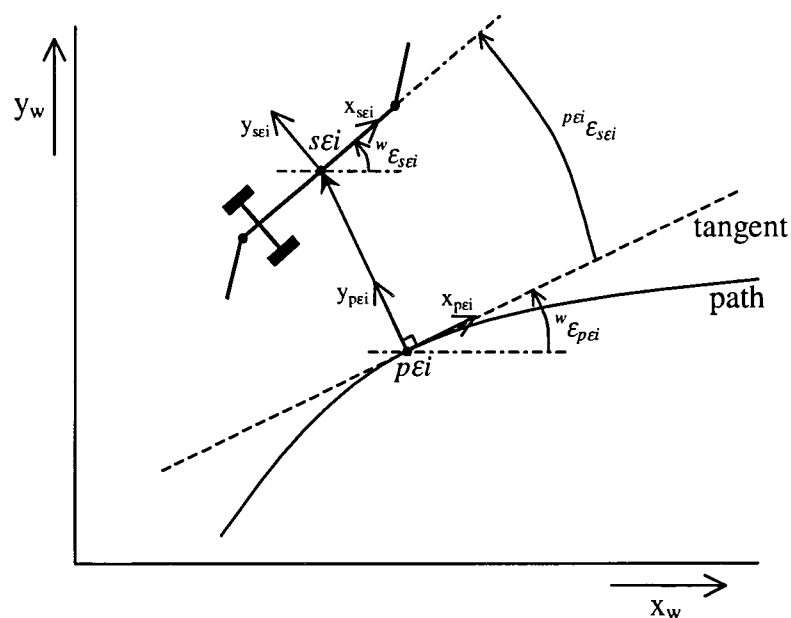


**Figure 6-2: Definition of yaw angle error of vehicle carriage**

In this figure the different angles are defined. The vehicle frames  $sei$  where the gyroscopes are mounted and the path frames  $p\epsilon i$  are shown. The actual yaw angle of a vehicle carriage is denoted by  ${}^w\epsilon_{sei}$  and the desired yaw angle of the tangent of the path with respect to the world is denoted by  ${}^w\epsilon_{p\epsilon i}$ . Furthermore, the yaw angle error which is the difference between the actual yaw angle of a vehicle carriage and the desired yaw angle of the path is denoted by  ${}^{p\epsilon i}\epsilon_{sei}$ .

Now that the yaw angle error is defined, a way to estimate the yaw angle error can be introduced. The yaw angle error can be estimated with the use of the estimated states of the observer. The estimated states of the observer namely contains the lateral deviation of the vehicle frame  $si$  with respect to the path and this information can be used for the estimation of the yaw angle error. For the estimation the definitions of **Figure 3-1** and the modified sensor configuration of **Figure 6-1** are used.

For this kind of vehicle it is supposed that the road curvature is kept small. That means that road curves are in the range of curves with a radius of 50 m. and bigger. Furthermore it is assumed that the lateral control of the vehicle is that good, that the yaw angle errors of the vehicle carriages will stay small. With the assumption of small road curvatures and the assumption that the yaw angle errors will stay small, the yaw angle error of the tractor can be estimated by the following equation:

$$\sin {}^{p\epsilon 1}\epsilon_{s\epsilon 1} = \frac{{}^{p1}y_{s1} - {}^{p2}y_{s2}}{L_{sf} + L_{sr}} \quad (6-1)$$

where  $L_{sf} + L_{sr}$  the distance is between the vehicle sensor frame  $s1$  and the vehicle sensor frame  $s2$ . With the assumption that the yaw angle error will stay small the following approximation can be applied:

$$\sin {}^{p\epsilon 1}\epsilon_{s\epsilon 1} \approx {}^{p\epsilon 1}\epsilon_{s\epsilon 1}, \quad \text{for small } {}^{p\epsilon 1}\epsilon_{s\epsilon 1}$$

With this approximation equation (6-1) becomes:

$${}^{p\epsilon 1}\epsilon_{s\epsilon 1} \approx \frac{{}^{p1}y_{s1} - {}^{p2}y_{s2}}{L_{sf} + L_{sr}} \quad (6-2)$$

This equation is used as a prediction of the observation from the integrating gyroscope at vehicle frame  $s\epsilon 1$ . Then the prediction of the observation is used in an extra correction step of the observer. If equation (6-2) is used in a corrector equation it has to be rewritten in the representation of equation (5-14). Rewriting equation (6-2) in the representation of equation (5-14) and in the discrete-time domain results in:

$${}^{p\epsilon 1}\tilde{\epsilon}_{s\epsilon 1}(k) = \mathbf{C}_{s\epsilon 1} \tilde{\mathbf{x}}(k) \quad (6-3)$$

where:

$$\mathbf{C}_{s\epsilon 1} = \begin{bmatrix} \frac{1}{L_{sf} + L_{sr}} & 0 & -\frac{1}{L_{sf} + L_{sr}} & 0 & 0 & 0 & 0 & 0 \end{bmatrix}$$

and:

$$\tilde{\mathbf{x}}(k) = \left[ {}^{p1}\tilde{y}_{s1}(k) \quad {}^{p1}\tilde{y}_{s1}(k+1) \quad \dots \quad {}^{p4}\tilde{y}_{s4}(k) \quad {}^{p4}\tilde{y}_{s4}(k+1) \right]^T$$

Furthermore, the tilde  $\sim$  denotes that the variables are estimates.

When the gyroscopes are implemented in the observer, the sampling interval chosen for reading gyroscope measurements is set to the same sampling interval as was chosen for reading accelerometer measurements and is fixed at  $\Delta$ , which was set to 5 ms. It is also assumed that the readings of the gyroscope measurement and the accelerometer measurement are synchronized, so that measurement data of the gyroscope is available at the same time instant as the measurement data of the accelerometer. In this way, every sampling instant  $k$  after the  $j^{\text{th}}$  magnetic marker, until  $k = n_j - 1$ , a prediction of the state can be made and at the same time a correction of the state can be made. When a magnetometer is on top of a magnetic marker another correction of the state is made as before. The big advantage of using an extra gyroscope is that the state can be corrected at a much higher rate than if only magnetometers are used.

The Kalman gain for the corrector equation of the integrating gyroscope at the tractor is given by:

$$\tilde{\mathbf{K}}_{se1}(k+1) = \tilde{\mathbf{P}}(k+1, t_j) \mathbf{C}_{se1}^T \left[ \mathbf{C}_{se1} \tilde{\mathbf{P}}(k+1, t_j) \mathbf{C}_{se1}^T + \mathbf{V}_{d_{se1}} \right]^{-1} \quad (6-4)$$

where  $\tilde{\mathbf{P}}(k+1, t_j)$  is given by equation (5-20a) and where  $\mathbf{V}_{d_{se1}} = E\{v_{d_{se1}}(k)v_{d_{se1}}^T(k)\}$  is the covariance of the noise  $v_{d_{se1}}(k)$  coming from the integrating gyroscope at vehicle frame  $se1$ . The state estimate is updated and corrected by the following equation:

$$\hat{\mathbf{x}}(k+1, t_j) = \tilde{\mathbf{x}}(k+1, t_j) + \tilde{\mathbf{K}}_{se1}(k+1) \left\{ {}^{pe1}\varepsilon_{se1}(k+1) - \mathbf{C}_{se1} \tilde{\mathbf{x}}(k+1, t_j) \right\} \quad (6-5)$$

The term  ${}^{pe1}\varepsilon_{se1}(k+1)$  in this equation is the measurement from the integrating gyroscope at vehicle frame  $se1$  at the sampling instant  $k+1$ , which is the actual yaw angle of the tractor, minus the desired yaw angle calculated at path frame  $pe1$ . So, the term  ${}^{pe1}\varepsilon_{se1}(k+1)$  represents the yaw angle error of the tractor. The update of the covariance of the estimation error will be:

$$\hat{\mathbf{P}}(k+1, t_j) = \tilde{\mathbf{P}}(k+1, t_j) - \tilde{\mathbf{K}}_{se1}(k+1) \mathbf{C}_{se1} \tilde{\mathbf{P}}(k+1, t_j) \quad (6-6)$$

The same can be done for the first semitrailer. However, the estimation of the yaw angle error of the first semitrailer is slightly different than the estimation of the yaw angle error of the tractor. This is because only the lateral deviation of one point on the first semitrailer is known, namely the lateral deviation of the vehicle frame  $s3$ . But to use the estimation as in equation (6-1), you need to know the lateral deviation of two points on the first semitrailer. The lateral deviation of a second point on the first semitrailer can be found by transformation of the lateral deviation of the vehicle frame  $s2$  to the lateral deviation of the vehicle frame  $s2$ , but then with respect to the first semitrailer. In this way it is possible to obtain the lateral deviation of two points on the first semitrailer and then an estimation can be made of the yaw angle error of the first semitrailer. Together with the measurement data of the integrating gyroscope on the first semitrailer another extra correction step can be made in the observer. It is first explained now how to transform the lateral deviation of vehicle frame  $s2$  to a lateral deviation of a point on the first semitrailer. This is done according to **Figure 6-3**. As



was noted before, the vehicle frame  $s_2$  is now positioned on the articulation point between the tractor and the first semitrailer. The accelerometer at vehicle frame  $s_2$  is mounted in that way that its sensitive axis would measure the lateral acceleration of vehicle frame  $s_2$  in the direction which is perpendicular to the longitudinal axis of the tractor.

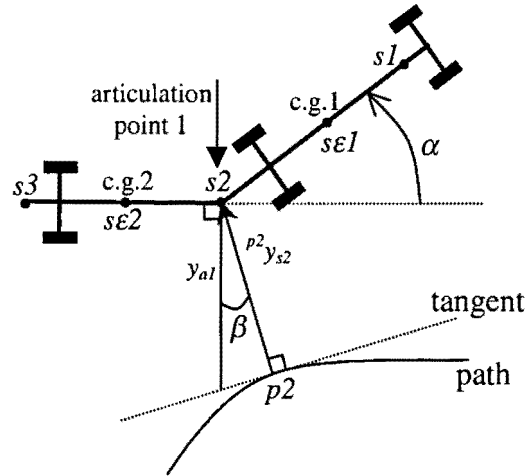


Figure 6-3: Transformation of lateral deviation  ${}^{p^2}y_{s2}$  to lateral deviation  $y_{a1}$

Figure 6-3 shows the tractor and the first semitrailer of the vehicle and the articulation point between them which is called *articulation point 1*. The angle which is denoted by  $\alpha$  represents the angle between the two carriages of the vehicle. This angle can be measured with an angular sensor or it can be obtained by taking the difference of the integrating gyroscope readings from the tractor and the first semitrailer. The angle  $\beta$  is the angle which defines the transformation of the lateral deviation  ${}^{p^2}y_{s2}$  to the lateral deviation  $y_{a1}$ . For small angles  $\alpha$  it can be said that:

$$\beta \approx \alpha$$

The lateral deviation  $y_{a1}$  can now be calculated as follows:

$$\begin{aligned} \cos \beta &= \frac{{}^{p^2}y_{s2}}{y_{a1}} \xrightarrow{\beta \approx \alpha} \cos \alpha = \frac{{}^{p^2}y_{s2}}{y_{a1}} \\ \Rightarrow y_{a1} \cos \alpha &= {}^{p^2}y_{s2} \\ \Rightarrow y_{a1} &= \frac{{}^{p^2}y_{s2}}{\cos \alpha} \end{aligned} \quad (6-7)$$

The yaw angle error of the first semitrailer can now be estimated by:

$$\sin {}^{p\epsilon 2} \epsilon_{s\epsilon 2} = \frac{y_{a1} - {}^{p^3}y_{s3}}{L_{sst1}} \quad (6-8)$$

With the assumption again that the yaw angle error will stay small, equation (6-8) can be approximated by:

$${}^{pE2}\mathcal{E}_{sE2} \approx \frac{y_{a1} - p^3 y_{s3}}{L_{Sst1}} \quad (6-9)$$

with  $y_{a1}$  given as in equation (6-7). Equation (6-9) can also be written in a matrix-form as in equation (6-3). This yields:

$${}^{pE2}\tilde{\mathcal{E}}_{sE2}(k) = \mathbf{C}_{sE2}(k) \tilde{\mathbf{x}}(k) \quad (6-10)$$

where:

$$\mathbf{C}_{sE2}(k) = \begin{bmatrix} 0 & 0 & \frac{1}{\cos\alpha(k) \cdot L_{Sst1}} & 0 & -\frac{1}{L_{Sst1}} & 0 & 0 & 0 \end{bmatrix}$$

Note that the matrix  $\mathbf{C}_{sE2}(k)$  is dependent of the sampling instant  $k$ , so that it is a time-variant matrix. This is because the angle  $\alpha$  between the tractor and the first semitrailer is in the matrix and this angle is not a constant, but it is a time-varying variable. For the implementation of this  $\mathbf{C}$ -matrix in the observer this has no consequences. This is because the  $\mathbf{C}$ -matrix is calculated on-line, so that each sampling instant  $k$  the right value for the variable  $\alpha$  is taken. In this way the  $\mathbf{C}$ -matrix varies through time, but every sampling instant  $k$  it yields the right matrix, which can be used in an extra correction step for the integrating gyroscope at the first semitrailer. The three equations for the extra correction step in the observer are going to be:

$$\tilde{\mathbf{K}}_{sE2}(k+1) = \tilde{\mathbf{P}}(k+1, t_j) \mathbf{C}_{sE2}^T(k+1) \left[ \mathbf{C}_{sE2}(k+1) \tilde{\mathbf{P}}(k+1, t_j) \mathbf{C}_{sE2}^T(k+1) + V_{d_{sE2}} \right]^{-1} \quad (6-11)$$

This is the Kalman gain for the corrector equation of the integrating gyroscope at the first semitrailer. Again,  $\tilde{\mathbf{P}}(k+1, t_j)$  is given by equation (5-20a) and

$V_{d_{sE2}} = E\{v_{d_{sE2}}(k)v_{d_{sE2}}^T(k)\}$  is the covariance of the noise  $v_{d_{sE2}}(k)$  coming from the integrating gyroscope at vehicle frame  $sE2$ . The state estimate is updated and corrected by the following equation:

$$\hat{\mathbf{x}}(k+1, t_j) = \tilde{\mathbf{x}}(k+1, t_j) + \tilde{\mathbf{K}}_{sE2}(k+1) \left\{ {}^{pE2}\mathcal{E}_{sE2}(k+1) - \mathbf{C}_{sE2}(k+1) \tilde{\mathbf{x}}(k+1, t_j) \right\} \quad (6-12)$$

The term  ${}^{pE2}\mathcal{E}_{sE2}(k+1)$  in this equation is the measurement from the integrating gyroscope at vehicle frame  $sE2$  at the sampling instant  $k+1$ , which is the actual yaw angle of the first semitrailer, minus the desired yaw angle calculated at path frame  $pE2$ . So, the term  ${}^{pE2}\mathcal{E}_{sE2}(k+1)$  represents the yaw angle error of the first semitrailer. The update of the covariance of the estimation error will be:

$$\hat{\mathbf{P}}(k+1, t_j) = \tilde{\mathbf{P}}(k+1, t_j) - \tilde{\mathbf{K}}_{sE2}(k+1) \mathbf{C}_{sE2}(k+1) \tilde{\mathbf{P}}(k+1, t_j) \quad (6-13)$$

The procedure for the correction step of the integrating gyroscope at the second semitrailer is actually the same as the procedure for the correction step of the integrating gyroscope at the first semitrailer. The estimation of the yaw angle error can also be done according to **Figure 6-3**, but with the modification that the tractor is

now the first semitrailer and the first semitrailer is now the second semitrailer. **Figure 6-3** with the necessary modifications is shown in **Figure 6-4**.

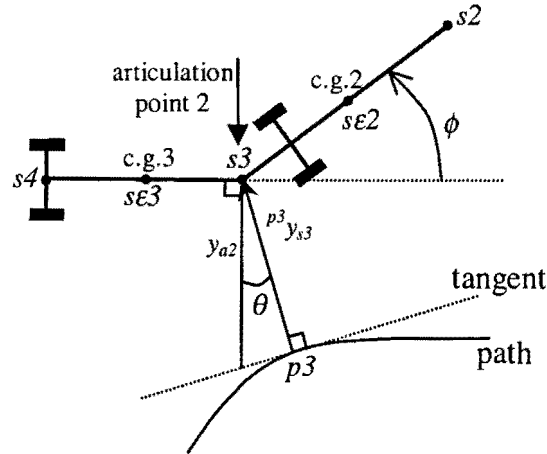


**Figure 6-4:** Transformation of lateral deviation  ${}^{p^3}y_{s3}$  to lateral deviation  $y_{a2}$

**Figure 6-4** shows the first and the second semitrailer of the vehicle and the articulation point between them which is called *articulation point 2*. The angle which is denoted by  $\phi$  represents the angle between the two carriages of the vehicle. This angle can be measured with an angular sensor or it can be obtained by taking the difference of the integrating gyroscope readings from the first and the second semitrailer. The angle  $\theta$  is the angle which defines the transformation of the lateral deviation  ${}^{p^3}y_{s3}$  to the lateral deviation  $y_{a2}$ . For small angles  $\phi$  it can be said that:

$$\theta \approx \phi$$

The equation for the lateral deviation  $y_{a2}$  now becomes:

$$\begin{aligned} \cos \theta &= \frac{{}^{p^3}y_{s3}}{y_{a2}} \xrightarrow{\theta \approx \phi} \cos \phi = \frac{{}^{p^3}y_{s3}}{y_{a2}} \\ \Rightarrow y_{a2} \cos \phi &= {}^{p^3}y_{s3} \\ \Rightarrow y_{a2} &= \frac{{}^{p^3}y_{s3}}{\cos \phi} \end{aligned} \quad (6-14)$$

The yaw angle error of the second semitrailer can now be estimated by:

$$\sin {}^{p\epsilon^3} \epsilon_{s\epsilon^3} = \frac{y_{a2} - {}^{p^4}y_{s4}}{Ls_{st2}} \quad (6-15)$$

We assume again that the yaw angle error will stay small, so that equation (6-15) can be approximated by the following equation:

$${}^{p\epsilon^3} \epsilon_{s\epsilon^3} \approx \frac{y_{a2} - {}^{p^4}y_{s4}}{Ls_{st2}} \quad (6-16)$$

with  $y_{a2}$  given as in equation (6-14). When equation (6-16) is written in a matrix-form the following result is obtained:

$${}^{p\mathcal{E}3}\tilde{\mathcal{E}}_{s\mathcal{E}3}(k) = \mathbf{C}_{s\mathcal{E}3}(k)\tilde{\mathbf{x}}(k) \quad (6-17)$$

where:

$$\mathbf{C}_{s\mathcal{E}3}(k) = \begin{bmatrix} 0 & 0 & 0 & 0 & \frac{1}{\cos\phi(k) \cdot L_{sst2}} & 0 & -\frac{1}{L_{sst2}} & 0 \end{bmatrix}$$

Note that also the matrix  $\mathbf{C}_{s\mathcal{E}3}(k)$  is dependent of the sampling instant  $k$ , so that it is a time-variant matrix. This has no consequences for the implementation of this C-matrix in the observer, because this C-matrix is also calculated on-line. The three equations for the extra correction step of the integrating gyroscope at the second semitrailer in the observer are stated by:

$$\tilde{\mathbf{K}}_{s\mathcal{E}3}(k+1) = \tilde{\mathbf{P}}(k+1, t_j) \mathbf{C}_{s\mathcal{E}3}^T(k+1) \left[ \mathbf{C}_{s\mathcal{E}3}(k+1) \tilde{\mathbf{P}}(k+1, t_j) \mathbf{C}_{s\mathcal{E}3}^T(k+1) + \mathbf{V}_{d_{s\mathcal{E}3}} \right]^{-1} \quad (6-18)$$

$$\hat{\mathbf{x}}(k+1, t_j) = \tilde{\mathbf{x}}(k+1, t_j) + \tilde{\mathbf{K}}_{s\mathcal{E}3}(k+1) \left\{ {}^{p\mathcal{E}3}\mathcal{E}_{s\mathcal{E}3}(k+1) - \mathbf{C}_{s\mathcal{E}3}(k+1) \tilde{\mathbf{x}}(k+1, t_j) \right\} \quad (6-19)$$

$$\hat{\mathbf{P}}(k+1, t_j) = \tilde{\mathbf{P}}(k+1, t_j) - \tilde{\mathbf{K}}_{s\mathcal{E}3}(k+1) \mathbf{C}_{s\mathcal{E}3}(k+1) \tilde{\mathbf{P}}(k+1, t_j) \quad (6-20)$$

Equation (6-18) is the Kalman gain for the corrector equation (6-19).

$\mathbf{V}_{d_{s\mathcal{E}3}} = E\{v_{d_{s\mathcal{E}3}}^T(k)v_{d_{s\mathcal{E}3}}(k)\}$  is the covariance of the noise  $v_{d_{s\mathcal{E}3}}(k)$  coming from the integrating gyroscope at vehicle frame  $s\mathcal{E}3$ . The term  ${}^{p\mathcal{E}3}\mathcal{E}_{s\mathcal{E}3}(k+1)$  in equation (6-19) is the measurement from the integrating gyroscope at vehicle frame  $s\mathcal{E}3$  at the sampling instant  $k+1$ , which is the actual yaw angle of the second semitrailer, minus the desired yaw angle calculated at path frame  $p\mathcal{E}3$ . So, the term  ${}^{p\mathcal{E}3}\mathcal{E}_{s\mathcal{E}3}(k+1)$  represents the yaw angle error of the second semitrailer. At last, equation (6-20) gives the update of the covariance of the estimation error.

The three correction steps which can be made with the measurement data of the three integrating gyroscopes are described now as three different steps. But the three different steps can also be combined to one step because the measurement data of the three integrating gyroscopes is available at the same sampling instant. The nine equations which are involved in the three different correction steps can then be combined to three equations which slightly differ from the equations in the individual correction steps. When combined, the equation for the Kalman gain which is used in the state update equation for the three integrating gyroscopes is given by:

$$\tilde{\mathbf{K}}_{se}(k+1) = \tilde{\mathbf{P}}(k+1, t_j) \mathbf{C}_{se}^T(k+1) \left[ \mathbf{C}_{se}(k+1) \tilde{\mathbf{P}}(k+1, t_j) \mathbf{C}_{se}^T(k+1) + \mathbf{V}_{d_{se}} \right]^{-1} \quad (6-21)$$

where  $\tilde{\mathbf{P}}(k+1, t_j)$  is given by equation (5-20a). Furthermore, in equation (6-21) is:

$$\mathbf{V}_{d_{se}} = \text{diag}[V_{d_{se1}} \quad V_{d_{se2}} \quad V_{d_{se3}}]^T \quad (6-22)$$

and:

$$\mathbf{C}_{se}(k) = \begin{bmatrix} \frac{1}{Lsf + Lsr} & 0 & -\frac{1}{Lsf + Lsr} & 0 & 0 & 0 & 0 & 0 \\ 0 & 0 & \frac{1}{\cos\alpha(k) \cdot Lsst1} & 0 & -\frac{1}{Lsst1} & 0 & 0 & 0 \\ 0 & 0 & 0 & 0 & \frac{1}{\cos\phi(k) \cdot Lsst2} & 0 & -\frac{1}{Lsst2} & 0 \end{bmatrix} \quad (6-23)$$

The matrix  $\mathbf{C}_{se}(k)$  is the observation matrix for the three integrating gyroscopes at the three vehicle carriages. The update of the state estimate using the measurements of the three integrating gyroscopes can also be combined. This results in:

$$\hat{\mathbf{x}}(k+1, t_j) = \tilde{\mathbf{x}}(k+1, t_j) + \tilde{\mathbf{K}}_{se}(k+1) \{ {}^{pe} \boldsymbol{\varepsilon}_{se}(k+1) - \mathbf{C}_{se}(k+1) \tilde{\mathbf{x}}(k+1, t_j) \} \quad (6-24)$$

The term  ${}^{pe} \boldsymbol{\varepsilon}_{se}(k+1)$  in this equation are the measurements from the integrating gyroscopes at the vehicle frames  $sei$  at the sampling instant  $k+1$ , which are the actual yaw angles of the three vehicle carriages, minus the desired yaw angles calculated at the path frames  $pei$ . It also can be written as:

$${}^{pe} \boldsymbol{\varepsilon}_{se}(k+1) = \left[ {}^{pe1} \varepsilon_{se1}(k+1) \quad {}^{pe2} \varepsilon_{se2}(k+1) \quad {}^{pe3} \varepsilon_{se3}(k+1) \right]^T$$

With the use of the Kalman gain matrix  $\tilde{\mathbf{K}}_{se}(k+1)$  and the observation matrix  $\mathbf{C}_{se}(k+1)$  the update of the covariance of the estimation error is given by:

$$\hat{\mathbf{P}}(k+1, t_j) = \tilde{\mathbf{P}}(k+1, t_j) - \tilde{\mathbf{K}}_{se}(k+1) \mathbf{C}_{se}(k+1) \tilde{\mathbf{P}}(k+1, t_j) \quad (6-25)$$

The extra correction step with the measurements of the three integrating gyroscopes is implemented in the observer. The expectation is that the estimates of the states better approximate the true states now, with less deviations.

### 6.1.1.1 Simulation results

The improvement of the observer with the integrating gyroscopes can be shown best when the distance between the magnetic markers is large and the velocity of the vehicle is low. In this way, the time between updates with measurement data coming from the magnetometers is large and there will be large errors in the state estimates. Using the measurement data coming from the integrating gyroscopes, it is possible to update the state estimate at a much higher frequency, so that the errors in the state estimates are a lot smaller. The Matlab-file in which the observer, including the correction steps from the integrating gyroscopes, is implemented is given in **Appendix A**.

The simulations to evaluate the improvement of the observer are carried out for a vehicle entering a curve with a radius of 150 m. at a speed of 10  $ms^{-1}$ . The vehicle is again equipped with a simple low gain PD-controller to provide large errors. Furthermore, the sensor configuration of the vehicle is extended with an integrating gyroscope at each vehicle carriage, to provide the yaw angle of each vehicle carriage.

For these simulations, the sample time  $\Delta$  of the observer was not changed and was set to 5 ms. and the distance between the magnetic markers was set to 10 m. Band limited white noise was added to the signals coming from the accelerometers, magnetometers and gyroscopes to simulate the effect of measurement noise and magnetic marker misalignment.

The results which come out of the simulations are given in **Figure 6-5** until **Figure 6-8**. The figures show the true lateral deviation and velocity of the different sensor frames. The estimated states of the observer, which are estimated with use of accelerometer and magnetometer measurement data, are also illustrated in the figures. Furthermore, the states of the observer which are corrected with use of measurement data coming from the integrating gyroscopes, are drawn in the figures too.

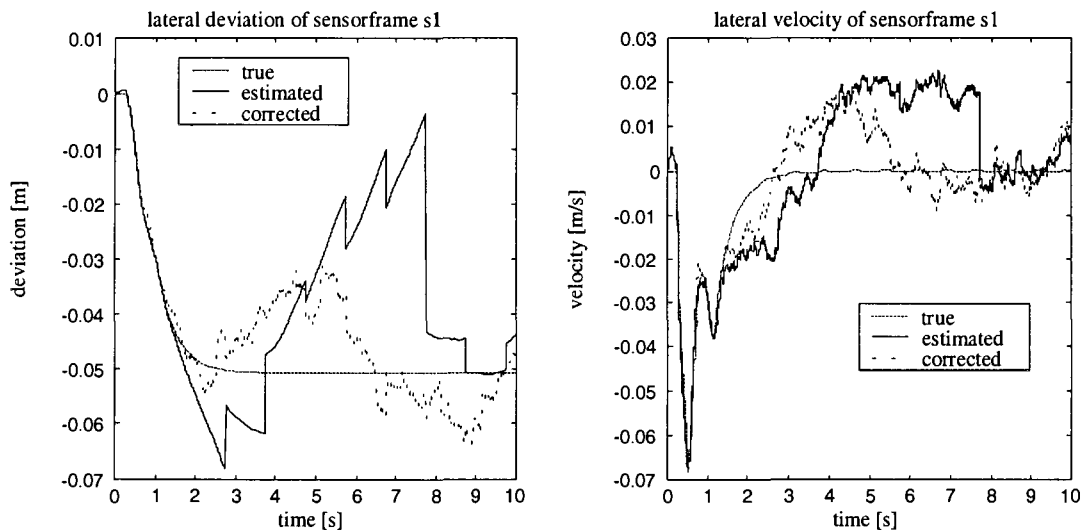


**Figure 6-5: Estimated, true and corrected lateral deviation and velocity of sensorframe s1**

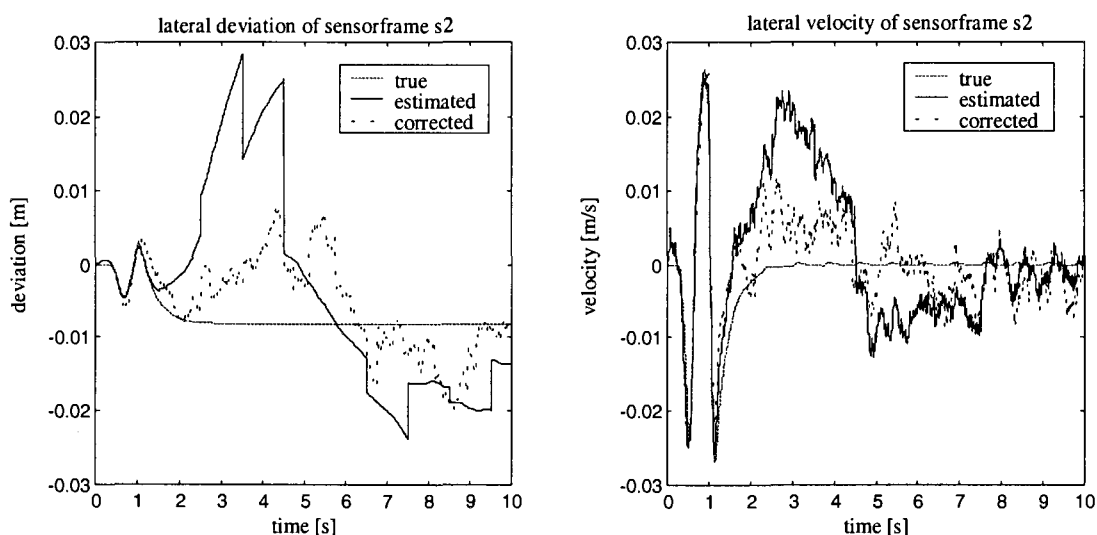


**Figure 6-6: Estimated, true and corrected lateral deviation and velocity of sensorframe s2**

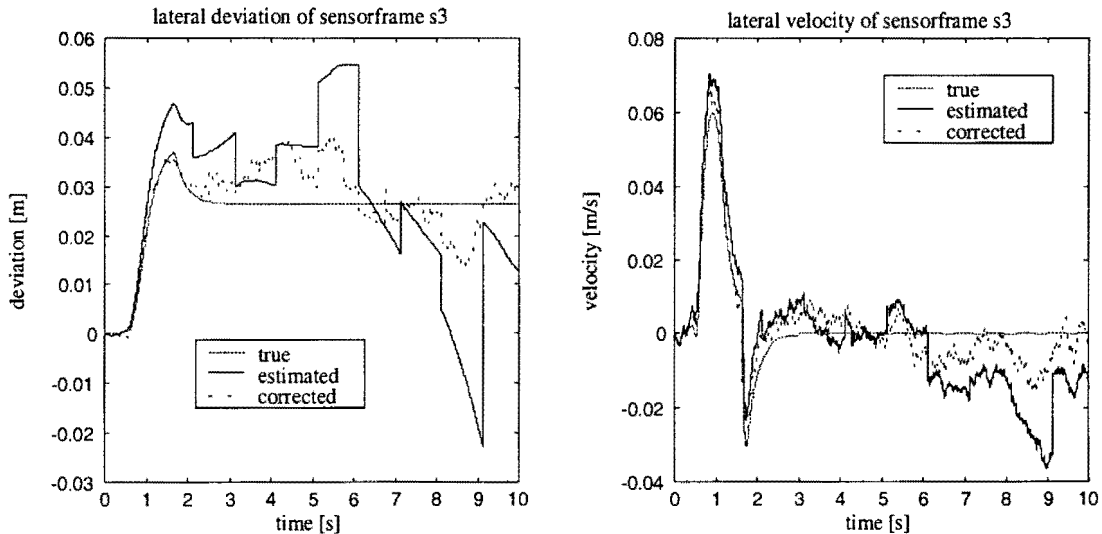


**Figure 6-7: Estimated, true and corrected lateral deviation and velocity of sensorframe s3**

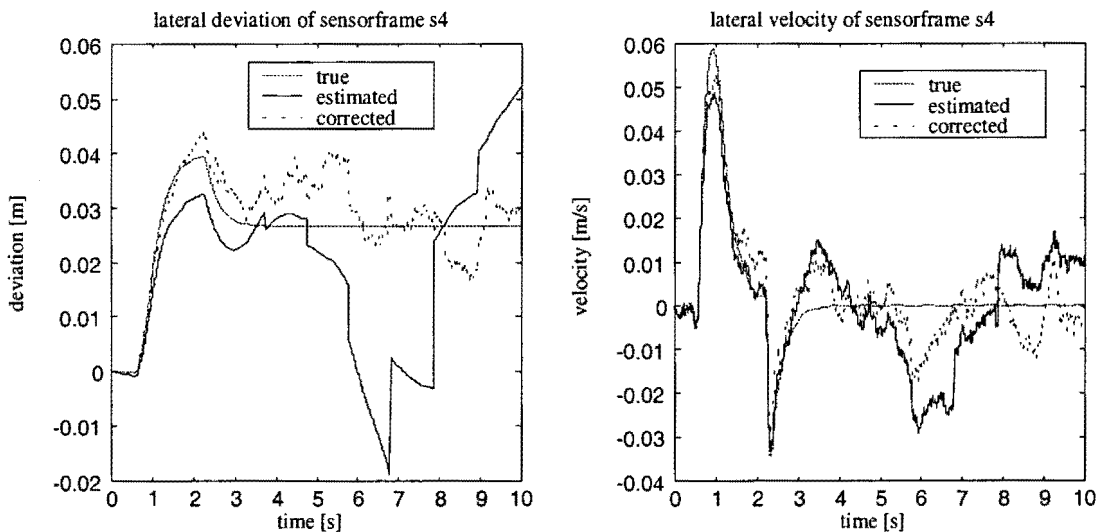


**Figure 6-8: Estimated, true and corrected lateral deviation and velocity of sensorframe s4**

It can be seen in the figures that the estimated states have large errors with respect to the true states. This is because the distance between the magnetic markers is large, which implies that the time between updates from the magnetometers is large. This causes large errors in the estimated states. It is possible to do extra updates on the estimated states with use of the integrating gyroscopes. The figures show that the estimated states after correction with the integrating gyroscopes, approximate the true states much closer. Especially at points where the estimated states without correction have their maxima, the improvement of the corrected states is large.

During some simulations it was noticed that the measured yaw error showed some drift with increasing time. This can have two reasons. It is possible that the desired yaw calculated at the path frames contains some deviations. These deviations are found back in the yaw error. Another possibility is that the drift is introduced with the integration process of the integrating gyroscope. The output of the integrating

gyroscope is namely obtained by integration of the measurement data of a rate gyroscope. Small errors and noise in the measurement data of the rate gyroscope can provide large errors in the integrated version of the rate gyroscope. If the measured yaw error shows drift, a reliable correction step with the integrating gyroscopes is not possible. It could be even so that the estimated states become worse after correction with use of measurement data coming from the integrating gyroscopes. Therefore, it has to be sure that the measurement of the yaw is reliable and the calculation of the yaw error is accurate.

### 6.1.1.2 Conclusions

The observer can be extended with integrating gyroscopes. The state estimates approximate the true states a lot better when the state estimates are extra updated with the measurement data coming from the integrating gyroscopes. So, integrating gyroscopes are a good option to improve the observer. However, integrating gyroscopes have a disadvantage. Because the signal of the rate gyroscope is integrated, the output of an integrating gyroscope can contain some errors or drift due to the integration. If this is the case, the measurement data coming from the integrating gyroscope is not reliable enough to use it in the observer. Therefore, it has to be sure that the output of the integrating gyroscope contains no errors before it is used as an extra correction step in the observer. The calculation of the desired yaw at the path frames also has to be accurate enough, otherwise the outcome of the yaw error contains some deviations, which also makes the correction step unreliable.

## 6.1.2 Rate gyroscope

Now, the rate gyroscope which provides the rate of the change in orientation or the yaw rate of the vehicle is examined. For this, the vehicle is equipped with three rate gyroscopes. The rate gyroscopes are mounted at the same place as where the integrating gyroscopes were mounted. The points which are denoted with  $s\epsilon 1$ ,  $s\epsilon 2$  and  $s\epsilon 3$  in **Figure 6-1**, are renamed by  $s\acute{\epsilon} 1$ ,  $s\acute{\epsilon} 2$  and  $s\acute{\epsilon} 3$  and they are the vehicle sensor frames of the rate gyroscopes. The measurements of the rate gyroscopes can be used for an extra correction step in the observer. The output of a rate gyroscope is the yaw rate of the vehicle carriage on which it is mounted. To do a correction step in the observer with the yaw rate, it is needed to make an estimate of the yaw rate. For the same reasons as with the integrating gyroscopes, not the yaw rate is estimated, but the yaw rate error is estimated. The yaw rate error is the difference between the actual yaw rate of a vehicle carriage and the desired yaw rate of the path. The yaw rate error of the tractor can be estimated by the following equation. This equation is obtained by taking the time derivative of equation (6-1).

$$\cos^{p\acute{\epsilon} 1} \epsilon_{s\acute{\epsilon} 1} \cdot \dot{\epsilon}_{s\acute{\epsilon} 1}^{p\acute{\epsilon} 1} = \frac{p^1 \dot{y}_{s1} - p^2 \dot{y}_{s2}}{Lsf + Lsr} \quad (6-26)$$

where  $\dot{\epsilon}_{s\acute{\epsilon} 1}^{p\acute{\epsilon} 1}$  the yaw rate error of the tractor is, which is the difference between the actual yaw rate of the tractor and the desired yaw rate of the path. Furthermore,  $p^1 \dot{y}_{s1}$



is the lateral velocity of vehicle frame  $s1$  with respect to the path frame  $p1$  and  ${}^{p2}\dot{y}_{s2}$  is the lateral velocity of vehicle frame  $s2$  with respect to the path frame  $p2$ . With the assumption that the yaw angle error stays small the following approximation can be applied:

$$\cos {}^{p\epsilon 1}\epsilon_{s\epsilon 1} \approx 1, \quad \text{for small } {}^{p\epsilon 1}\epsilon_{s\epsilon 1}$$

With this approximation equation (6-26) becomes:

$${}^{p\epsilon 1}\dot{\epsilon}_{s\epsilon 1} \approx \frac{{}^{p1}\dot{y}_{s1} - {}^{p2}\dot{y}_{s2}}{Lsf + Lsr} \quad (6-27)$$

This equation is used as a prediction of the observation from the rate gyroscope at vehicle frame  $s\epsilon 1$ .

Deriving an equation for the estimation of the yaw rate error of the first semitrailer, by differentiating equation (6-8) with respect to time, results in:

$$\cos {}^{p\epsilon 2}\epsilon_{s\epsilon 2} \cdot {}^{p\epsilon 2}\dot{\epsilon}_{s\epsilon 2} = \frac{\dot{y}_{a1} - {}^{p3}\dot{y}_{s3}}{Lsst1} \quad (6-28)$$

where  ${}^{p\epsilon 2}\dot{\epsilon}_{s\epsilon 2}$  the yaw rate error of the first semitrailer is, which is the difference between the actual yaw rate of the first semitrailer and the desired yaw rate of the path at path frame  $p\epsilon 2$ . Furthermore,  ${}^{p3}\dot{y}_{s3}$  is the lateral velocity of vehicle frame  $s3$  with respect to the path frame  $p3$ . The term  $\dot{y}_{a1}$  can be obtained by differentiating equation (6-7) with respect to time. This yields:

$$\dot{y}_{a1} = \frac{{}^{p2}\dot{y}_{s2}}{\cos \alpha} + {}^{p2}y_{s2} \frac{\sin \alpha}{\cos^2 \alpha} \dot{\alpha} \quad (6-29)$$

Thus, to transform the lateral velocity  ${}^{p2}\dot{y}_{s2}$  to the lateral velocity of vehicle frame  $s2$ , but perpendicular to the first semitrailer, the lateral deviation  ${}^{p2}y_{s2}$  and the angular velocity  $\dot{\alpha}$  also have to be taken into account according to equation (6-29). These variables are namely incorporated in the second term of equation (6-29). However, the variable  $\dot{\alpha}$  is very small and  $\dot{\alpha}$  even goes to zero when  $\alpha$  stays constant. Furthermore, the value of  $\sin \alpha$  will be very small, because  $\alpha$  is small. For these reasons, the term  ${}^{p2}y_{s2} \frac{\sin \alpha}{\cos^2 \alpha} \dot{\alpha}$  will be such small that it would nearly not contribute to the lateral velocity  $\dot{y}_{a1}$ . Therefore, this term will be neglected. With the assumption again that the yaw angle error will stay small, equation (6-28) can be approximated by:

$${}^{p\epsilon 2}\dot{\epsilon}_{s\epsilon 2} \approx \frac{\dot{y}_{a1} - {}^{p3}\dot{y}_{s3}}{Lsst1} \quad (6-30)$$

This equation is used as a prediction of the yaw rate error of the first semitrailer with  $\dot{y}_{a1}$  given as:

$$\dot{y}_{a1} = \frac{p^2 \dot{y}_{s2}}{\cos \alpha} \quad (6-31)$$

There also can be found an equation for the estimation of the yaw rate error of the second semitrailer. This equation is obtained by taking the time derivative of equation (6-15) and is given by:

$$\cos^{p\hat{e}3} \dot{\epsilon}_{s\hat{e}3} \cdot \dot{\epsilon}_{s\hat{e}3} = \frac{\dot{y}_{a2} - p^4 \dot{y}_{s4}}{L_{Sst2}} \quad (6-32)$$

where  ${}^{p\hat{e}3} \dot{\epsilon}_{s\hat{e}3}$  the yaw rate error of the second semitrailer is, which is the difference between the actual yaw rate of the second semitrailer and the desired yaw rate of the path at path frame  $p\hat{e}3$ . Furthermore,  ${}^{p4} \dot{y}_{s4}$  is the lateral velocity of vehicle frame  $s4$  with respect to the path frame  $p4$ . The term  $\dot{y}_{a2}$  can be obtained by taking the time derivative of equation (6-14). This results in:

$$\dot{y}_{a2} = \frac{p^3 \dot{y}_{s3}}{\cos \phi} + p^3 y_{s3} \frac{\sin \phi}{\cos^2 \phi} \dot{\phi} \quad (6-33)$$

For the same reasons as before, the second term in equation (6-33) will be neglected. If again the assumption is made that the yaw angle error will stay small, equation (6-32) can be approximated by the following equation:

$${}^{p\hat{e}3} \dot{\epsilon}_{s\hat{e}3} \approx \frac{\dot{y}_{a2} - p^4 \dot{y}_{s4}}{L_{Sst2}} \quad (6-34)$$

Equation (6-34) represents the prediction of the yaw rate error of the second semitrailer. In this equation is  $\dot{y}_{a2}$  given by:

$$\dot{y}_{a2} = \frac{p^3 \dot{y}_{s3}}{\cos \phi} \quad (6-35)$$

When the equations (6-27), (6-30) and (6-34) are combined and written in a matrix-form in the discrete-time domain, the following result can be obtained:

$${}^{p\hat{e}} \tilde{\mathbf{e}}_{s\hat{e}}(k+1) = \mathbf{C}_{s\hat{e}}(k) \tilde{\mathbf{x}}(k) \quad (6-36)$$

with  $\tilde{\mathbf{x}}(k)$  given as in equation (6-3) and where:

$${}^{p\hat{e}} \tilde{\mathbf{e}}_{s\hat{e}}(k+1) = \left[ {}^{p\hat{e}1} \tilde{\epsilon}_{s\hat{e}1}(k+1) \quad {}^{p\hat{e}2} \tilde{\epsilon}_{s\hat{e}2}(k+1) \quad {}^{p\hat{e}3} \tilde{\epsilon}_{s\hat{e}3}(k+1) \right]^T \quad (6-37)$$

and the C-matrix is given by:

$$\mathbf{C}_{s\dot{\epsilon}}(k) = \begin{bmatrix} 0 & \frac{1}{Lsf + Lsr} & 0 & -\frac{1}{Lsf + Lsr} & 0 & 0 & 0 & 0 \\ 0 & 0 & 0 & \frac{1}{\cos \alpha(k) \cdot Lsst1} & 0 & -\frac{1}{Lsst1} & 0 & 0 \\ 0 & 0 & 0 & 0 & 0 & \frac{1}{\cos \phi(k) \cdot Lsst2} & 0 & -\frac{1}{Lsst2} \end{bmatrix} \quad (6-38)$$

The matrix  $\mathbf{C}_{s\dot{\epsilon}}(k)$  is the observation matrix for the three rate gyroscopes at the three vehicle carriages.

The three rate gyroscopes can also be used for an extension of the observer. The measurement data coming from the three rate gyroscopes can be used to implement an extra correction step in the observer. The correction step with the three rate gyroscopes can be implemented in one step, because the measurement data from the three rate gyroscopes is available at the same sampling instant.

The three equations for the extra correction step in the observer which can be made with the measurement data from the three rate gyroscopes at the vehicle carriages are:

$$\tilde{\mathbf{K}}_{s\dot{\epsilon}}(k+1) = \tilde{\mathbf{P}}(k+1, t_j) \mathbf{C}_{s\dot{\epsilon}}^T(k+1) \left[ \mathbf{C}_{s\dot{\epsilon}}(k+1) \tilde{\mathbf{P}}(k+1, t_j) \mathbf{C}_{s\dot{\epsilon}}^T(k+1) + \mathbf{V}_{d_{s\dot{\epsilon}}} \right]^{-1} \quad (6-39)$$

where  $\tilde{\mathbf{P}}(k+1, t_j)$  is given by equation (5-20a). Furthermore, in equation (6-39) is:

$$\mathbf{V}_{d_{s\dot{\epsilon}}} = \text{diag} [V_{d_{s\dot{\epsilon}1}} \quad V_{d_{s\dot{\epsilon}2}} \quad V_{d_{s\dot{\epsilon}3}}]^T \quad (6-40)$$

In equation (6-40),  $\mathbf{V}_{d_{s\dot{\epsilon}}} = E\{\mathbf{v}_{d_{s\dot{\epsilon}}}(k) \mathbf{v}_{d_{s\dot{\epsilon}}}^T(k)\}$  is the covariance matrix of the noise coming from the rate gyroscopes at the vehicle frames  $s\dot{\epsilon}1$ ,  $s\dot{\epsilon}2$  and  $s\dot{\epsilon}3$ .

The Kalman gain which is calculated in equation (6-39) is used in the state update equation:

$$\hat{\mathbf{x}}(k+1, t_j) = \tilde{\mathbf{x}}(k+1, t_j) + \tilde{\mathbf{K}}_{s\dot{\epsilon}}(k+1) \left\{ \mathbf{p}^{\dot{\epsilon}} \dot{\boldsymbol{\epsilon}}_{s\dot{\epsilon}}(k+1) - \mathbf{C}_{s\dot{\epsilon}}(k+1) \tilde{\mathbf{x}}(k+1, t_j) \right\} \quad (6-41)$$

The term  $\mathbf{p}^{\dot{\epsilon}} \dot{\boldsymbol{\epsilon}}_{s\dot{\epsilon}}(k+1)$  in this equation are the measurements from the rate gyroscopes at the vehicle frames  $s\dot{\epsilon}i$  at the sampling instant  $k+1$ , which are the actual yaw rates of the three vehicle carriages, minus the desired yaw rates calculated at the path frames  $p\dot{\epsilon}i$ . It also can be written as:

$$\mathbf{p}^{\dot{\epsilon}} \dot{\boldsymbol{\epsilon}}_{s\dot{\epsilon}}(k+1) = \left[ p^{\dot{\epsilon}1} \dot{\epsilon}_{s\dot{\epsilon}1}(k+1) \quad p^{\dot{\epsilon}2} \dot{\epsilon}_{s\dot{\epsilon}2}(k+1) \quad p^{\dot{\epsilon}3} \dot{\epsilon}_{s\dot{\epsilon}3}(k+1) \right]^T$$

The update of the covariance of the estimation error can be obtained with the use of the Kalman gain matrix  $\tilde{\mathbf{K}}_{s\dot{\epsilon}}(k+1)$  and the observation matrix  $\mathbf{C}_{s\dot{\epsilon}}(k+1)$  and is given by:

$$\hat{\mathbf{P}}(k+1, t_j) = \tilde{\mathbf{P}}(k+1, t_j) - \tilde{\mathbf{K}}_{s\dot{\epsilon}}(k+1) \mathbf{C}_{s\dot{\epsilon}}(k+1) \tilde{\mathbf{P}}(k+1, t_j) \quad (6-42)$$

The extra correction step with the measurements of the three rate gyroscopes is implemented in the observer.

When the extra correction step(s) from the integrating and/or from the rate gyroscope(s) are/is implemented in the observer, the flowchart of **Figure 5-2** which shows the procedure of an observer cycle, has to be modified.

The flowchart of **Figure 5-2** with the modifications needed for the extra correction step(s) is shown in **Figure 6-9** on the next page.

There also have been made some changes in the notation of the predictor equations and of the corrector equations for the magnetometers in the flowchart of **Figure 6-9** in comparison with the notation which is used in the flowchart of **Figure 5-2**. This is done to make sure that the corrector equations for the integrating and rate gyroscopes fit in with the predictor equations and the corrector equations for the magnetometers in the right way.

### **6.1.2.1 Simulation results**

The simulations carried out to show the improvement of the observer with the rate gyroscopes are almost the same as the simulations which are described in section 6.1.1.1. The distance between the magnetic markers is again chosen large and the velocity of the vehicle is low. By choosing this so, large errors in the state estimates will appear. The large errors in the state estimates can be reduced by using the measurement data coming from the rate gyroscopes as an extra update of the state estimates. The Matlab-file which describes the observer, including the correction steps from the rate gyroscopes, is given in **Appendix A**.

The information used in the simulations is the same as the information used in the simulations with the integrating gyroscopes, with some little changes. For the simulations here, the vehicle is entering a curve with a radius of 100 m. at a speed of 5  $ms^{-1}$ . The distance between the magnetic markers was again set to 10 m. and the values of the noise used in the simulations were also not changed.

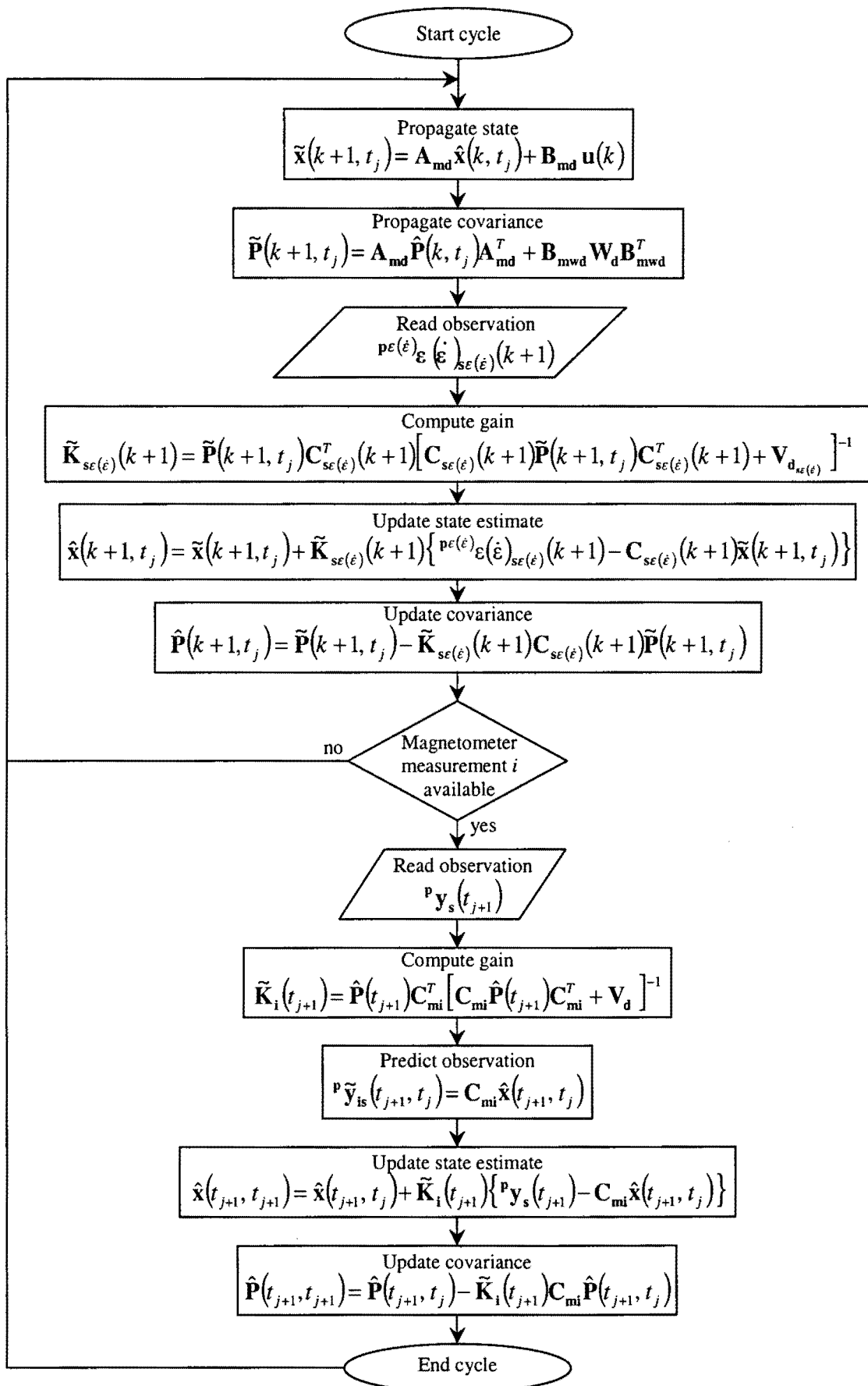
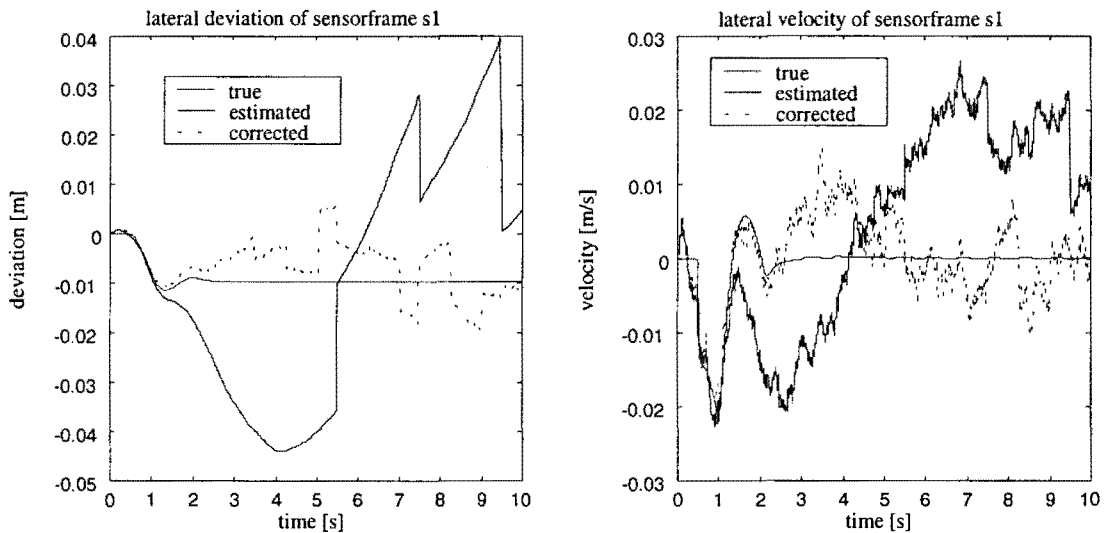
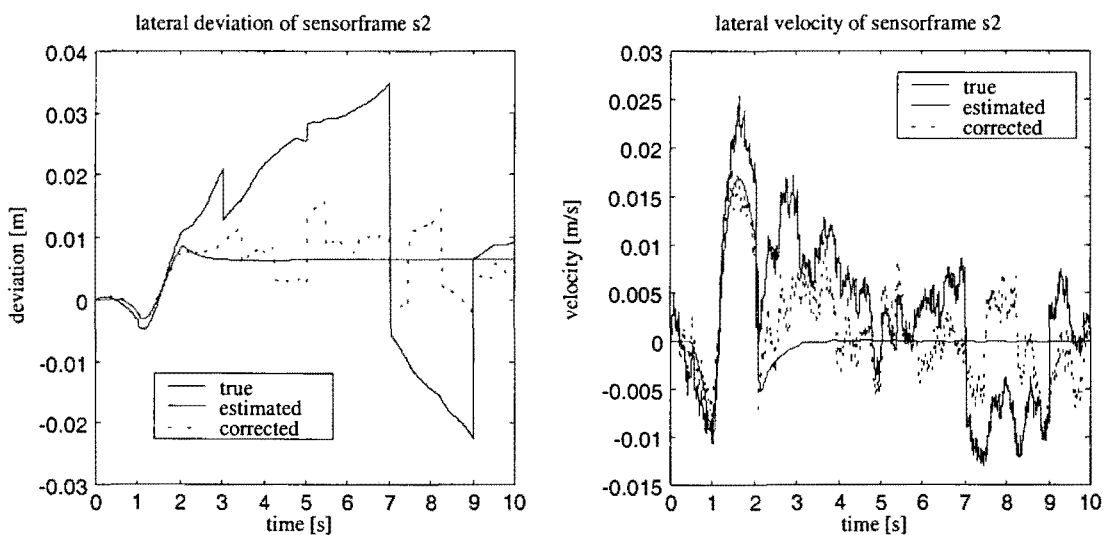


Figure 6-9: Flowchart of extended observer cycle

The simulation results are depicted in the next figures, **Figure 6-10** until **Figure 6-13**. The figures show the true lateral deviation and velocity of the different sensor frames as well as the estimated states of the observer. The estimated states of the observer are obtained with use of accelerometer and magnetometer measurement data. The states of the observer which have undergone an extra update with use of measurement data coming from the rate gyroscopes, are also given in the figures. These states are denoted with corrected states.



**Figure 6-10: True, estimated and rate gyro-corrected lateral deviation and velocity of sensorframe  $s1$**



**Figure 6-11: True, estimated and rate gyro-corrected lateral deviation and velocity of sensorframe  $s2$**

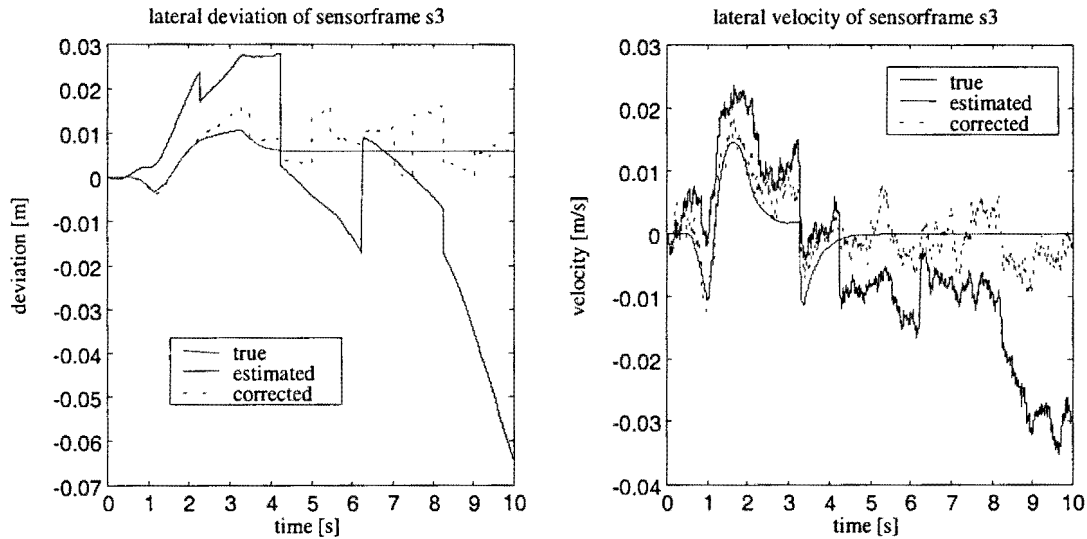


**Figure 6-12: True, estimated and rate gyro-corrected lateral deviation and velocity of sensorframe s3**

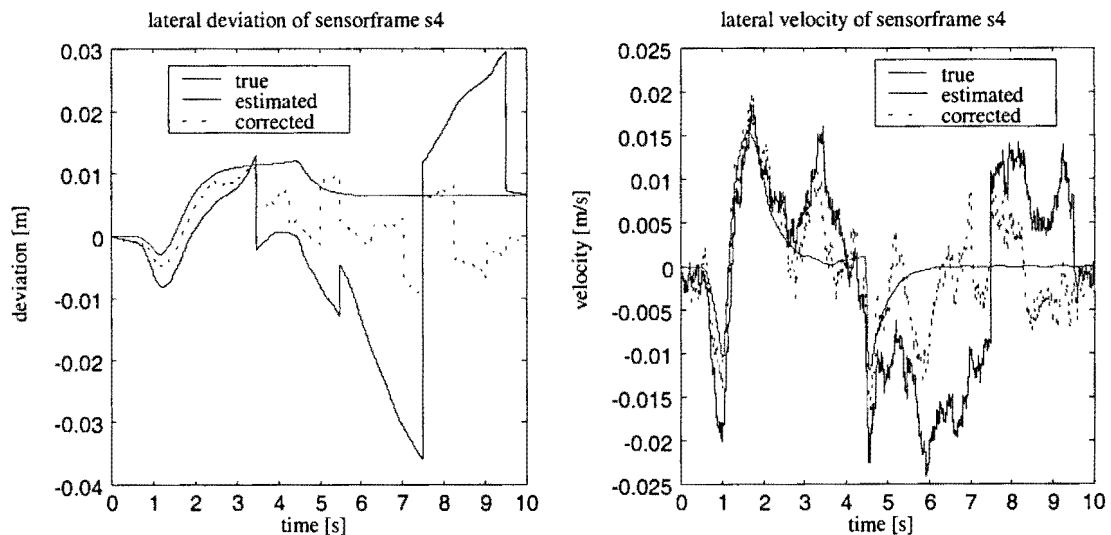


**Figure 6-13: True, estimated and rate gyro-corrected lateral deviation and velocity of sensorframe s4**

The simulation results show that the estimated states have large errors with respect to the true states. This is because the distance between the magnetic markers is large and the velocity of the vehicle is low, which implies that the time between updates from the magnetometers is large. This is the cause of the large errors in the estimated states. The rate gyroscopes can be used to do extra updates on the estimated states. The estimation of the lateral deviation and velocity (the states of the observer) becomes a lot better when the extra updates with the rate gyroscopes are implemented in the observer. This can be seen clearly in the figures, where the corrected states are depicted. The corrected states approximate the true states much closer than the estimated states before correction. Especially at points where the estimated states are really poor, the improvement of the corrected states is big.

### **6.1.2.2 Conclusions**

It has been shown that the observer can be extended with rate gyroscopes. The state estimates approximate the true states a lot better when the state estimates are extra updated with the measurement data coming from the rate gyroscopes. So, it is a good option to use rate gyroscopes for the improvement of the observer. Besides, rate gyroscopes have the advantage that their output is not integrated, so that the output of a rate gyroscope is much more reliable than the output of an integrating gyroscope. The calculation of the desired yaw rate at the path frames still has to be accurate enough to make the outcome of the yaw rate error a reliable value.

## **6.2 Conclusions**

In this chapter it has been described how to extend the observer with sensor measurements. The sensors which have been handled are the integrating and rate gyroscope. An integrating gyroscope provides the orientation and a rate gyroscope provides the rate of change in orientation of the object on which they are mounted. For both sensors, a method has been found to implement them in the observer. The estimated states of the observer can be extra updated and corrected with use of the measurement data coming from the sensors. In this way, the measurement system becomes more reliable and the estimated states approximate the true states a lot closer. The results obtained with the two different kinds of sensors are in close correspondence, but the rate gyroscope is the most reliable sensor of the two, for the reason that its output is not integrated.

One simulation has been run when both the correction steps are implemented in the observer, but this does not result in considerable improvements in comparison to the simulations where one of both correction steps is implemented in the observer.



# Chapter 7

## Sensor noise and covariance analysis

When the sensors which are described in the previous chapters are implemented in the observer, it is important to know their noise properties and that the noise can be characterized in the observer. The observer is designed according to a Kalman filter and the Kalman filter calculates the optimal Kalman gain when the right data is supplied to the observer. With the calculation of the Kalman gain, the covariances of the sensor noises are used. The Kalman gain will be optimal when the covariances used in the calculation are in close correspondence with the physical noises of the used sensors. Sensor noise and how to obtain its covariance are aspects which are dealt with in this chapter. Many sensors show bad low-frequency properties, such as bias and drift. These properties are very disadvantageous for the application which is described in this report which will become clear later. How to handle these low-frequency properties, is also described in this chapter.

### 7.1 Filtering of sensor noise

The measurements coming from the sensors are in the form of an analog signal. The measurements from the sensors are being processed by a computer. Therefore, the analog signal coming from the sensors has to be discretized by an A/D converter. The A/D converter takes samples of the analog output of the sensor at a certain sampling frequency. Before a continuous analog signal is sampled, it has to be filtered by an anti-aliasing filter. If this is not done, folding deformation or aliasing will occur during sampling and the original signal cannot be reconstructed. According to the sampling theorem of Nyquist, the sampling frequency has to be twice as high as the highest frequency appearing in the analog signal.

A global scheme of the system which is described in this report is given in **Figure 7-1**.

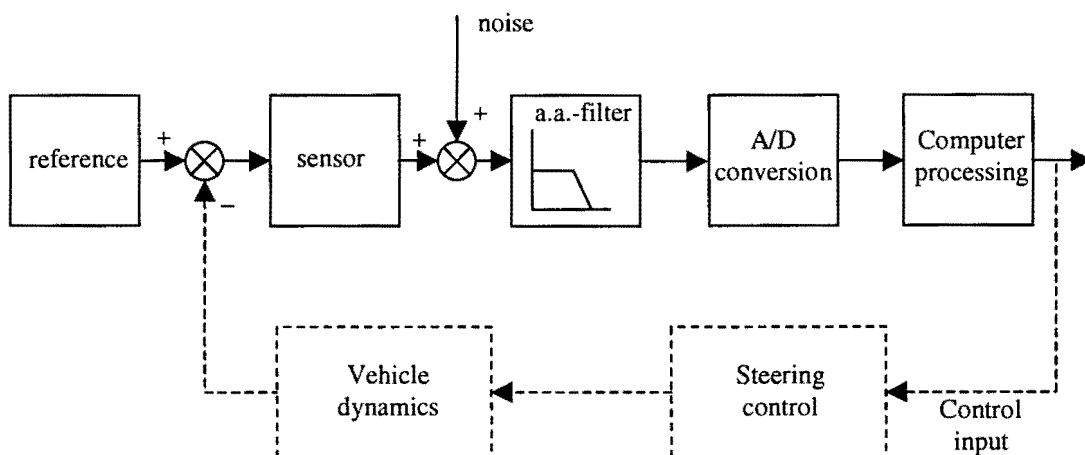


**Figure 7-1: The system schematic**

The anti-aliasing filter about which is talked before is denoted by the a.a.-filter in **Figure 7-1**.

The signals which are supplied to the observer are the signals coming out of the A/D converter. So, the properties of the noise coming out of the A/D converter and the covariance of this noise have to be determined. If the branch with the sensor, the filter and the A/D converter is cut out of **Figure 7-1** and is redrawn with adding the right signal names, the following figure can be obtained.

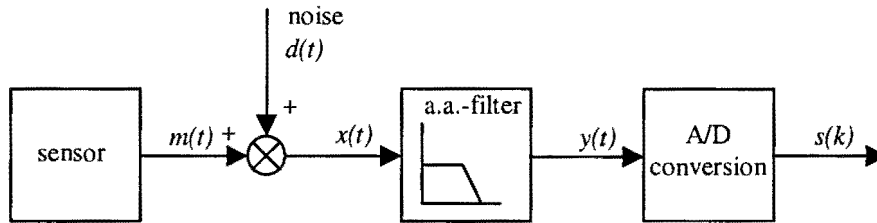
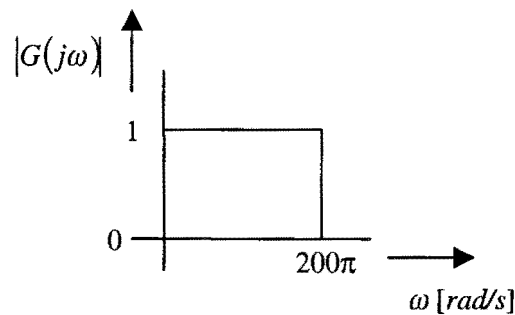


**Figure 7-2: Filtering and sampling of sensor noise**

The output of the sensor is denoted by  $m(t)$  and the noise signal is called  $d(t)$ . The input of the anti-aliasing filter is the signal  $x(t)$  and the output of the filter is the signal  $y(t)$ . The signal  $y(t)$  after it passed the A/D converter, which is the sampled version of  $y(t)$ , is denoted by  $s(k)$ .

The measurement signals coming from the accelerometers and the gyroscopes are sampled with a sampling time of 5 ms., that means a sampling frequency of 200 Hz. The sampling frequency of the magnetometer output signals depends on the velocity of the vehicle and is not known beforehand. That is why only the accelerometers and the gyroscopes are examined. The output signals of the sensors including the noise consist of signal contributions at much higher frequencies than 200 Hz. According to the Nyquist theorem the anti-aliasing filter has to have a cut-off frequency of 100 Hz. at highest. So, the anti-aliasing filter is an analog lowpass filter with the following idealized characteristic:



What has to be determined is the (co)variance of the noise in the signal  $s(k)$ . This can be determined as follows. Consider that the signal  $x(t)$  consists purely of noise, so the signal coming from the sensor  $m(t) = 0$ . From this, it follows that:  $x(t) = d(t)$ . The power spectral density of the signal  $d(t)$  is known. Namely, this can be obtained from the technical specifications of the noise of the concerning sensor. The mean power of the output process of the anti-aliasing filter can now be described as (ref. [5]):

$$P_y \triangleq R_{yy}(0) = \text{Var}(y(t)) = \sigma_y^2 = \frac{1}{2\pi} \cdot \int_{-\infty}^{\infty} S_{xx}(\omega) |G(\omega)|^2 d\omega \quad (7-1)$$

where  $R_{yy}(0)$  is the autocorrelation function  $R_{yy}(\tau) = E\{y(t)y(t+\tau)\}$  evaluated for  $\tau = 0$  and  $P_y$  is the mean power of the output signal  $y(t)$ . Furthermore,  $\sigma_y^2$  is another notation for the variance of the signal  $y(t)$  which is denoted by  $Var(y(t))$ . Besides,  $S_{xx}(\omega)$  is the Power Spectral Density (PSD) of the signal  $x(t)$  and  $G(\omega)$  is the transfer function of the anti-aliasing filter. Equation (7-1) can also be written as:

$$P_y \triangleq R_{yy}(0) = Var(y(t)) = \sigma_y^2 = \int_{-\infty}^{\infty} S_{xx}(f) |G(f)|^2 df \quad (7-2)$$

Now consider an ideal lowpass filter for which holds:

$$G(f) = \begin{cases} 1 & , \quad 0 < f < 100, \\ 0 & , \quad elsewhere . \end{cases} \quad (7-3)$$

Then the following can be said for the signal  $y(t)$ :

$$\begin{aligned} P_y \triangleq R_{yy}(0) &= Var(y(t)) = \sigma_y^2 = \int_{-\infty}^{\infty} S_{xx}(f) |G(f)|^2 df \\ &= \int_{-\infty}^0 S_{xx}(f) \cdot 0 df + \int_0^{100} S_{xx}(f) \cdot 1 df + \int_{100}^{\infty} S_{xx}(f) \cdot 0 df \\ &= \int_0^{100} S_{xx}(f) df \end{aligned} \quad (7-4)$$

The variance of the signal  $y(t)$  can be calculated now. From this the (co)variance of the output signal  $s(k)$  of the A/D converter has to be determined. In practice, the A/D converter is often formed by a switch followed by a zero-order-hold. This is illustrated in **Figure 7-3**.

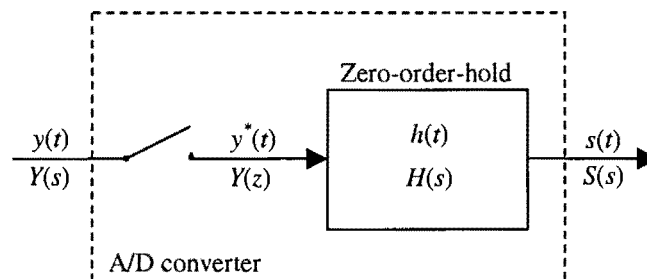


**Figure 7-3: Schematic of A/D converter**

The variance of the signal  $s(t)$  can be calculated with use of the following equation (ref. [6]):

$$\Phi_{ss}(s) = \Phi_{y^*y^*}(s) \cdot H(s) \cdot H(-s) \quad (7-5)$$

where  $\Phi_{ss}(s)$  and  $\Phi_{y^*y^*}(s)$  are the power spectral densities of the signals  $s(t)$  and  $y^*(t)$  respectively. The transfer function of the zero-order-hold circuit is denoted by  $H(s)$ . Transforming equation (7-5) back to the time domain yields the following equation (ref. [6]):

$$\varphi_{ss}(\tau) = \int_{-\infty}^{\infty} \psi_h(t) \varphi_{y^*y^*}(t+\tau) dt \quad (7-6)$$

In this equation  $\psi_h(t)$  is the system correlation function and is given by:

$$\psi_h(t) = \int_0^{\infty} h(t)h(t+\tau) dt \quad (7-7)$$

Further in equation (7-6),  $\varphi_{ss}(\tau)$  and  $\varphi_{y^*y^*}(\tau)$  are the autocorrelation functions of the signals  $s(t)$  and  $y^*(t)$  respectively. With use of:

$$\varphi_{y^*y^*}(\tau) = \frac{1}{T_a} \sum_{k=-\infty}^{\infty} \varphi_{yy}(kT_a) \delta(\tau - kT_a)$$

the variance can now be given by (ref. [6]):

$$\varphi_{ss}(0) = \sigma_s^2 = \frac{1}{T_a} \cdot \sum_{n=-\infty}^{\infty} \psi_h(nT_a) \varphi_{yy}(nT_a) \quad (7-8)$$

The transfer of the zero-order-hold circuit of **Figure 7-3** is:

$$h(t) = \begin{cases} 1 & , \quad 0 < t \leq T_a \\ 0 & , \quad t > T_a \end{cases} \quad (7-9)$$

According to [ref. 6],  $\psi_h(\tau)$  can also be written as:

$$\psi_h(\tau) = \begin{cases} \sigma_h^2 \left( 1 - \frac{|\tau|}{T_a} \right) & , \quad -T_a \leq \tau \leq T_a \\ 0 & , \quad otherwise \end{cases} \quad (7-10)$$

In this case is:

$$\begin{aligned} \sigma_h^2 = \psi_h(0) &= \int_0^{\infty} h(t)h(t) dt \\ &= \int_0^{T_a} 1 dt = t \Big|_0^{T_a} = T_a \end{aligned} \quad (7-11)$$

With use of equation (7-11), the system correlation function of equation (7-10) becomes:

$$\psi_h(\tau) = \begin{cases} T_a \left( 1 - \frac{|\tau|}{T_a} \right) & , \quad -T_a \leq \tau \leq T_a \\ 0 & , \quad otherwise \end{cases} \quad (7-12)$$

From this, it follows that the quantity  $\psi_h(nT_a)$  only has a value unequal to zero for  $n = 0$ , namely  $\psi_h(0) = T_a$ , so that the following holds:

$$\sigma_s^2 = \varphi_{yy}(0) = \sigma_y^2 \quad (7-13)$$

Concluding: The variance of the output signal  $s(t)$  of the zero-order-hold circuit is equal to the variance of the original signal  $y(t)$ .

## 7.2 White noise and colored noise

A Kalman filter considers the noise disturbances to be white noise with a Gaussian probability distribution function. Moreover, a Kalman filter can only handle with white Gaussian noise. However, the noise signals which are supplied to the observer are filtered noise signals, so the noise is not white, but it is colored noise. The coloring of the noise can be taken care of by adding an extra state to the observer for the representation of the coloring of the noise disturbance. But if the system is studied well, adding an extra state to the observer seems not to be necessary. The vehicle dynamics of the vehicle take place in the low-frequent area until 2 Hz. The signals of the sensors which measure the output of the vehicle dynamics are filtered by an anti-aliasing filter. So, the vehicle dynamics are also filtered by the same filter. This is shown in **Figure 7-4**.

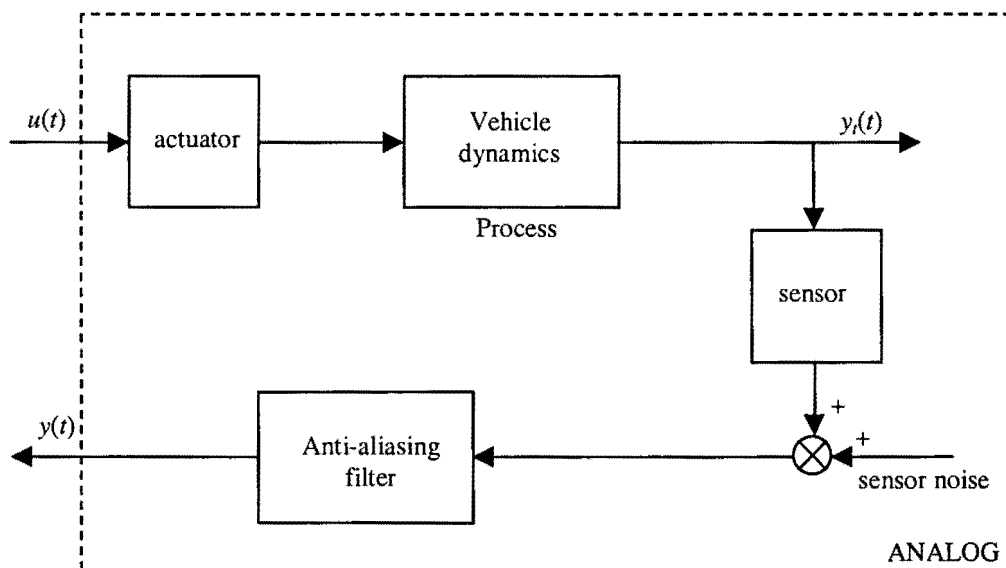


**Figure 7-4: Process and sensor filtering**

The sensor signals are being sampled with a sampling frequency of 200 Hz. Therefore, the anti-aliasing filter has a lowpass band with a cut-off frequency of 100 Hz. Then the following characteristic can be sketched.

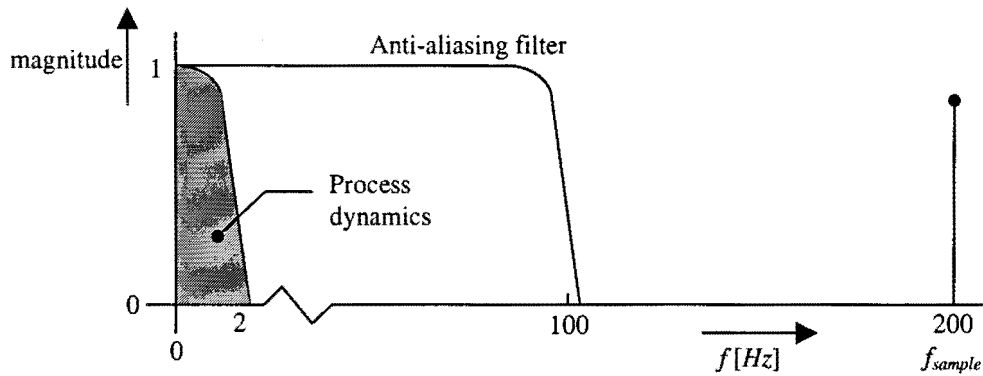


**Figure 7-5: Characteristic of filtered process dynamics**

It is assumed that the noise of the sensors has a flat spectrum in the passband of the anti-aliasing filter. Because the process dynamics are very lowfrequent, the filtered noise can be considered as white noise seen from the process. The sampling frequency is much higher than the fastest dynamics of the system, so that the filtered noise behaves itself as white noise as seen by the process. Therefore, the filtered noise signals as well as the covariance of the filtered noise can be applied to the observer without problems about that the observer considers the noise to be white.

Furthermore, the behaviour of the anti-aliasing filter will nearly not affect the behaviour of the process. Because the process dynamics are very lowfrequent, the poles of the process will all be located close to the point  $z = 1$  in the  $z$ -plane. Or in the  $s$ -plane, the poles will all be located close to the origin. The poles of the anti-aliasing filter in the  $s$ -plane will be located near the cut-off frequency of the filter. Since the cut-off frequency of the filter is  $100 \text{ Hz}$ ., the poles of the filter will be located near  $s = -200\pi$  in the  $s$ -plane. Thus, the poles of the filter and the poles of the process are so far apart that they almost will not influence each other. Therefore, the dynamics of the system will not be harmed by the behaviour of the anti-aliasing filter.

### ***7.3 Bias and drift properties of the sensors***

Most of the sensors used in practice possess bias and drift properties according to the specifications. Bias and drift are constant or very lowfrequent changing values which come on top of the desired signal of the sensor. Bias is a constant offset which is output by the sensor when the sensor measures no signal and drift is the drifting of the sensor signal according to temperature changes for example. These properties are very adversely, especially when the signal of the sensor has to be integrated, because big errors are introduced by integrating bias or drift. To get rid of these disadvantageous effects, the sensor signal can be filtered with a highpass filter. Because the sensors discussed here have to measure signals in the frequency range of the vehicle dynamics, which is a range until  $2 \text{ Hz}$ ., the cut-off frequency of the filter has to be very low. The cut-off frequency of the filter is very critical, because you may of course not lose any of the important vehicle dynamics. The cut-off frequency of the filter therefore has to be in the order of magnitude of  $0.1 \text{ Hz}$ . and the filter has to have a flank which is very steeply falling down below a frequency of  $0.1 \text{ Hz}$ . This is sketched in the following picture.

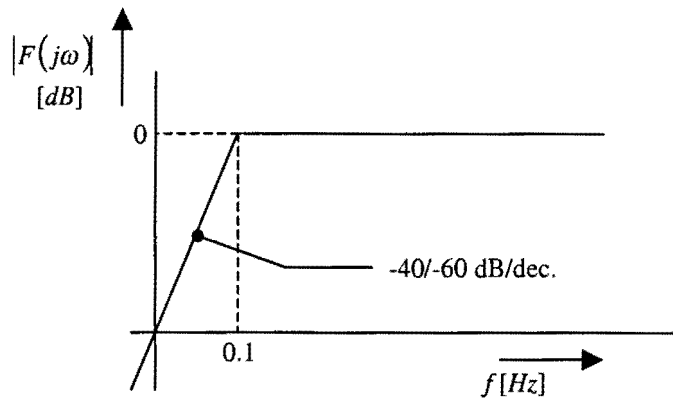


Figure 7-6: Characteristic of highpass filter

The design of the filter can be realized by a simple transfer function in the  $s$ -domain, so that it is a continuous and analog filter. The general form of the transfer function of the filter will be:

$$F(s) = \left( \frac{s}{s+a} \right)^n \quad (7-14)$$

where:

$n$  = the order of the filter, and  
 $a$  = the cut-off frequency of the filter.

The factors  $n$  and  $a$  are the design parameters of the filter. The cut-off frequency of the filter has to be in the order of magnitude of  $0.1 \text{ Hz}$ ., so that the behaviour of the vehicle dynamics will not be harmed. Therefore, the cut-off frequency of the filter is chosen as  $a = 0.1 \text{ Hz}$ . or  $a = 0.628 \text{ rad/s}$ . The order  $n$  of the filter is chosen to be 2, so that it is a second-order filter. It is chosen like this, because of a several reasons. The flank of a first-order filter falls down with a slope of  $-20 \text{ dB/dec}$ . below the cut-off frequency. For the application here, this is not enough because then the filtered signal is not enough suppressed at very low frequencies. Higher-order filters will have disadvantageous phase-effects, due to the phase response of the filter. A third-order filter will have worse phase-effects than a second-order filter, due to its phase response. Therefore, the filter is chosen to be a second-order filter. So, now the transfer function of the filter looks like:

$$F(s) = \left( \frac{s}{s+0.628} \right)^2 \quad (7-15)$$

where the cut-off frequency of the filter is given in radians per second. This is done, because Matlab/Simulink works with this dimension. The behaviour of the filter can be analyzed on the basis of its bodeplot. The bodeplot of the filter is shown in **Figure 7-7**.

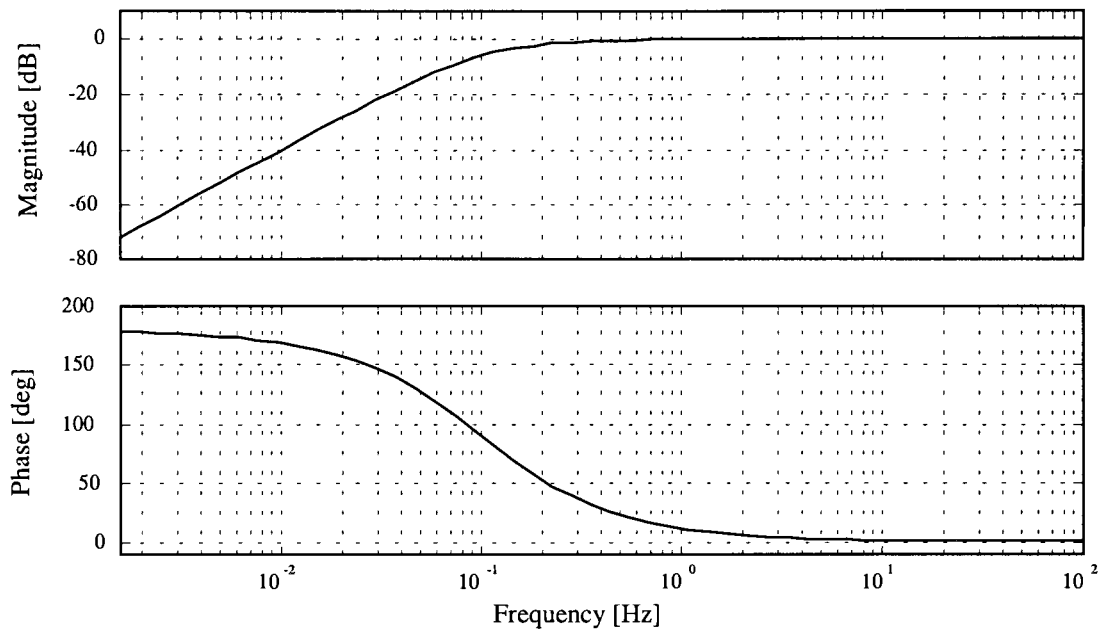


**Figure 7-7: Bodeplot of highpass filter**

As can be seen in **Figure 7-7**, signals with a frequency higher than the cut-off frequency of the filter are amplified with a factor of 1, so they are let through. On the other hand, signals with a frequency lower than the cut-off frequency are amplified with a factor much smaller than 1, so these signals are suppressed. The working of the filter can also be shown by a simulation. The simulation can be done by supplying the input of the filter with a sine wave of a certain frequency added to a constant. At the output of the filter, the constant should have been filtered out of the signal. The simulation is carried out with a sine wave of 1 Hz, and having an amplitude of 5 V. This sine wave is added up to the constant 3. The signal which forms the input of the highpass filter is shown in **Figure 7-8**.

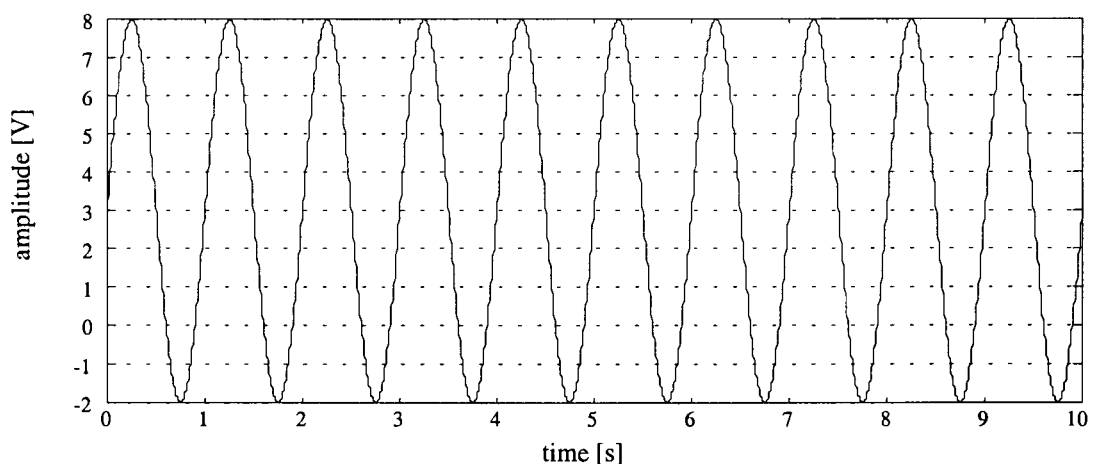


**Figure 7-8: Input signal of the highpass filter**

What can be seen in this figure is that the input signal of the highpass filter consists of a sinusoid and a d.c.-offset of 3 V. The sinusoid has an amplitude of 5 V, and the frequency of the sinusoid is 1 Hz. The output of the highpass filter looks like the signal which is illustrated in **Figure 7-9**.



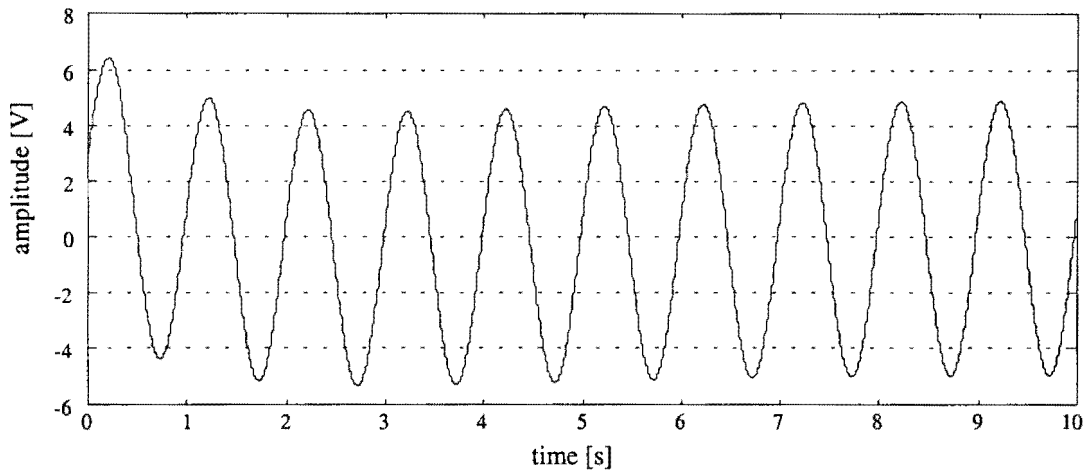


**Figure 7-9: Output signal of the highpass filter**

The filtered signal is shown in **Figure 7-9**. The figure illustrates that the d.c.-offset is filtered out of the signal and that the sinusoid passes the filter with a slight deformation. This is because the filter is not optimized for this application. However the filter is not optimal, it is shown that a highpass filter is a good option for the suppression of bias and drift in the sensor signals.

The highpass filter can also be implemented as a discrete-time filter. The transfer function of the discrete-time filter can be obtained by conversion of the continuous-time filter to the discrete-time domain. This can be done with the command `c2d` in the Matlab Command Window. The discretization method is chosen as 'zoh' which means zero-order hold on the inputs. The transfer function of the discrete-time filter after conversion of the continuous-time filter becomes:

$$F(z) = \frac{z^2 - 2z + 1}{z^2 - 1.994z + 0.9937} \quad (7-16)$$

The bodeplot of the discrete-time filter is the same as the bodeplot of the continuous-time filter, so they both have the same behaviour.

The highpass filter can be used to filter the signals which are supplied to the input of the observer. The signals which are supplied to the observer are the reference signals, which are derived from the desired states of the path, subtracted from the sensor signals. It is important that not the sensor signals are filtered, but that the sensor signals minus the reference signals are filtered. When the sensor signals are filtered, there exists a possibility that important information is lost. For the accelerometer this can be explained as follows. The acceleration which is measured by the accelerometer is given by equation (3-4) and is:

$$a_{y_{si}} = {}^{si}\dot{v}_{y_{si}} + {}^{si}v_{x_{si}} {}^w\dot{\epsilon}_{si} \quad (7-17)$$

In this equation  ${}^w\dot{\epsilon}_{si}$  is built up as:

$${}^w\dot{\epsilon}_{si} = {}^w\dot{\epsilon}_{pi} + {}^{pi}\dot{\epsilon}_{si} \quad (7-18)$$

Thus, equation (7-17) can be rewritten as follows:

$$a_{y_{si}} = {}^{si}\dot{v}_{y_{si}} + {}^{si}v_{x_{si}} \left\{ {}^w\dot{\epsilon}_{\rho_i} + {}^{pi}\dot{\epsilon}_{s_i} \right\} \quad (7-19)$$

The term  ${}^{si}v_{x_{si}} \cdot {}^w\dot{\epsilon}_{\rho_i}$  in this equation yields in a curve with a constant radius a constant acceleration which is not equal to zero. When the sensor signal of equation (7-19) is being highpass filtered, this constant acceleration is filtered out and lost. This is not desirable. This problem is taken care off by filtering the acceleration input signal of the observer. This signal is given by:

$${}^{pi}\ddot{y}_{si} = a_{y_{si}} - {}^{si}v_{x_{si}} \cdot {}^w\dot{\epsilon}_{\rho_i} \quad (7-20)$$

As can be seen, the term  ${}^{si}v_{x_{si}} \cdot {}^w\dot{\epsilon}_{\rho_i}$  is removed out of this signal, so this signal only contains the varying components of the lateral acceleration. If this signal is filtered by a highpass filter, only the bias and drift are filtered out and no important information is lost. The same can be said for the rate and integrating gyroscopes. The signal which is measured by a rate gyroscope is given by equation (7-18). In a curve with a constant radius, the term  ${}^w\dot{\epsilon}_{\rho_i}$  produces a constant yaw rate unequal to zero. This constant yaw rate would also be filtered out by a highpass filter and this again is not desirable. But if the signal of the yaw rate error which is supplied to the observer is filtered, then this problem does not exist anymore. The term  ${}^w\dot{\epsilon}_{\rho_i}$  is namely removed out of the signal of the yaw rate error, so that this signal only contains the varying yaw rate error. By highpass filtering this signal, no relevant information is lost. For the integrating gyroscopes the same can be said as for the rate gyroscopes with a slight modification. The output of an integrating gyroscope is built up as stated in the following equation:

$${}^w\epsilon_{s_i} = {}^w\epsilon_{\rho_i} + {}^{pi}\epsilon_{s_i} \quad (7-21)$$

The term  ${}^w\epsilon_{\rho_i}$  provides a constant growing yaw in a curve with a constant radius, and when the output signal of the integrating gyroscope is filtered by a highpass filter this constant growing yaw is lost. But instead of filtering the output signal of the integrating gyroscope, the signal of the yaw error which is input to the observer can be filtered. The constant growing yaw is removed from this signal, so that it only contains the varying yaw. The bias and drift present in this signal can be filtered out with the highpass filter, without losing any important information.

Concluding: When not the sensor signals, but the error signals are highpass filtered, no loss of important information will appear. The error signals are obtained by subtracting the reference signals from the sensor signals.

## 7.4 Covariance and PSD of the noise of used sensors

To simulate the effect of the noise of the used sensors it is necessary to determine the covariance and the PSD of the noise of the used sensors. The best and easiest way to do this is to measure the physical noise of the sensors. Then a characteristic can be

drawn of the density of the noise plotted out against the frequency. The covariance of the noise can be obtained from this characteristic. In the situation here, the choice of the sensors is not sure yet, so that the sensors are not present. Therefore, the physical noise of the sensors can not be measured in practice. Another way to obtain the covariance and PSD of the noise of the used sensors is to extract the noise properties from the datasheet of the concerning sensor. The datasheets of the sensors which are probably going to be used were present, so these datasheets are used to obtain some reliable values for the covariance and the PSD of the noise of the sensors.

### 7.4.1 Accelerometer noise

A good option for an accelerometer is the Micromachined Servo Accelerometer, model MSA100 from the Endevco Corporation. The datasheet of this sensor can be found in **Appendix B**. More information about this sensor or other sensors is present in ref. [7]. According to the technical specifications in the datasheet, the sensor has a typical scale factor of  $200 \text{ mV/g}$ . When the acceleration of gravity is taken as  $1 \text{ g} \approx 10 \text{ m/s}^2$ , the scale factor of the sensor can also be written as:

$$\text{scale factor} : \frac{200 \left[ \frac{\text{mV}}{\text{m/s}^2} \right]}{10 \left[ \frac{\text{m/s}^2}{} \right]} = \frac{20 \left[ \frac{\text{mV}}{\text{m/s}^2} \right]}{\left[ \frac{\text{m/s}^2}{} \right]}$$

The typical output noise of the sensor in the range of 0.5 to 500 Hz. is specified as  $4 \text{ } \mu\text{Vrms}/\sqrt{\text{Hz}}$ . With use of the scale factor, the output noise can be expressed in the dimension of  $\text{mg}/\sqrt{\text{Hz}}$ . This can be done by dividing the output noise by the scale factor. This results in:

$$\begin{aligned} \text{output noise} \left[ \frac{\text{mg}}{\sqrt{\text{Hz}}} \right] &= \frac{\text{output noise} \left[ \frac{\text{Vrms}}{\sqrt{\text{Hz}}} \right]}{\text{scale factor} \left[ \frac{\text{V}}{\text{m/s}^2} \right]} = \frac{4 \cdot 10^{-6} \left[ \frac{\text{Vrms}}{\sqrt{\text{Hz}}} \right]}{20 \cdot 10^{-3} \left[ \frac{\text{V}}{\text{m/s}^2} \right]} \\ &= 4 \cdot 10^{-6} \left[ \frac{\text{Vrms}}{\sqrt{\text{Hz}}} \right] \cdot \frac{1 \left[ \frac{\text{m/s}^2}{} \right]}{20 \cdot 10^{-3} \left[ \text{V} \right]} \\ &= 200 \cdot 10^{-6} \left[ \frac{\text{m/s}^2 \text{ rms}}{\sqrt{\text{Hz}}} \right] = 20 \cdot 10^{-6} \left[ \frac{\text{g rms}}{\sqrt{\text{Hz}}} \right] \\ &= 0.02 \left[ \frac{\text{mg rms}}{\sqrt{\text{Hz}}} \right] \end{aligned} \quad (7-22)$$

To obtain the height of the Power Spectral Density (PSD) of the noise of the accelerometer in the range of 0.5 to 500 Hz., the value which is calculated in equation (7-22) has to be squared. The height of the PSD of the noise of the accelerometer then becomes:

$$\text{height PSD} \triangleq S_{aa}(f) = (200 \cdot 10^{-6})^2 = 40 \cdot 10^{-9} \left[ \frac{m^2/s^4 \text{ rms}}{Hz} \right] \quad (7-23)$$

To determine the value of the accelerometer noise covariance, it is assumed that the spectrum of the noise is flat in the range of 0 to 500 Hz, and the height of the spectrum has the value calculated in equation (7-23). The covariance of the noise which is filtered by the anti-aliasing filter can then be calculated with use of equation (7-4). This gives:

$$\begin{aligned} P_a \triangleq R_{aa}(0) &= \text{Var}(a(t)) = \sigma_a^2 = \int_0^{100} S_{aa}(f) df \\ &= 40 \cdot 10^{-9} f \Big|_0^{100} = 40 \cdot 10^{-9} \cdot 100 = 4 \cdot 10^{-6} \left[ \frac{m^2}{s^4} \right] \end{aligned} \quad (7-24)$$

Equation (7-23) and (7-24) provide the values which are needed to simulate the noise coming from the accelerometers. Note that these values are determined theoretically and not practically and it might be possible that there is a difference in the theoretical and practical values. The same can be done for the noise of the gyroscopes.

## 7.4.2 Gyroscope noise

It is a good choice to choose for the Fiber Optic Gyroscope, model KVH E•Core 1000 from the KVH Industries, Inc. The datasheet of the sensor is depicted in **Appendix C**. More information about this sensor or other sensors can be found in ref. [8].

According to the technical specifications of the sensor, the output noise of the sensor is specified as the *Angle Random Walk* and it has the value of  $20 \text{ }^\circ/\text{hr}/\sqrt{\text{Hz}}$ . To simulate the noise, this value has to be transformed to the dimension  $\text{rad/s}/\sqrt{\text{Hz}}$ . The transformation yields:

$$20 \text{ } [^\circ/\text{hr}] = \frac{20 \cdot 0.01745}{3600} \approx 96.96 \cdot 10^{-6} \text{ } [\text{rad}/s] \quad (7-25)$$

With the use of this transformation, the value of the noise becomes:

$$20 \left[ \frac{^\circ/\text{hr}}{\sqrt{\text{Hz}}} \right] = 96.96 \cdot 10^{-6} \left[ \frac{\text{rad}/s}{\sqrt{\text{Hz}}} \right] \quad (7-26)$$

To obtain the height of the Power Spectral Density (PSD) of the noise of the gyroscope, the value which is calculated in equation (7-26) has to be squared. The height of the PSD of the noise of the gyroscope then becomes:

$$\text{height PSD} \triangleq S_{gg}(f) = (96.96 \cdot 10^{-6})^2 = 9.4 \cdot 10^{-9} \left[ \frac{(\text{rad}/s)^2}{Hz} \right] \quad (7-27)$$

To determine the value of the gyroscope noise covariance, it is assumed that the spectrum of the noise is flat and the height of the spectrum has the value calculated in equation (7-27). The covariance of the noise which is filtered by the anti-aliasing filter can then be calculated in the same way as is done for the accelerometer. This results in:

$$P_g \triangleq R_{gg}(0) = \text{Var}(g(t)) = \sigma_g^2 = \int_0^{100} S_{gg}(f) df \quad (7-28)$$

$$= 9.4 \cdot 10^{-9} f \Big|_0^{100} = 9.4 \cdot 10^{-9} \cdot 100 = 940 \cdot 10^{-9} \left[ \left( \frac{\text{rad}}{\text{s}} \right)^2 \right]$$

Equation (7-27) and (7-28) provide the values which are needed to simulate the noise coming from the gyroscopes. It has to be noted that these values are also determined theoretically and not practically and there might be a possibility that there is a difference in the theoretical and practical values.

## 7.5 Simulation results

The simulations carried out in the chapters 5 and 6 are carried out with intuitive values for the noise and the covariance of the noise of the sensors. The intuitive values were useful to show the principle of the observer. But to evaluate the performance of the observer with the sensors which are probably going to be used, it is necessary to implement the sensors in the observer with their true noise properties. This is done in the next simulations. The values for the noise of the accelerometers and magnetometers are adjusted to the values which are calculated in the previous section. The height of the PSD of the noise is implemented in the block *Band-Limited White Noise* in Simulink. The covariances of the noise from the sensors are defined in the Matlab-file which describes the observer. The noise source for simulating the effect of magnet misalignment and magnetometer noise was adjusted to result in a maximum measurement error of about 2 cm. To achieve this, the covariance of the noise from the magnetometers was set to  $0.0002 \text{ m}^2$  and the height of the PSD of the noise was adjusted to  $2 \cdot 10^{-6} \text{ m}^2/\text{Hz}$ .

Furthermore, the simulations are carried out for a vehicle entering a curve with a radius of 300 m. at a speed of  $20 \text{ ms}^{-1}$ . This is done to show that the observer can handle different road curvatures and vehicle velocities. The distance between the magnetic markers was set to 4 m. The states of the observer are estimated with use of measurement data coming from the accelerometers and magnetometers and the state estimates are extra updated with the measurement data from the integrating and rate gyroscopes, so an extra correction step is done to the yaw and yaw rate errors of the different vehicle carriages. The simulation results can be found in **Figure 7-10** until **Figure 7-13**. The figures show the true lateral deviation and velocity of the different sensor frames of the vehicle. The estimated states of the observer after correction with the integrating and rate gyroscopes, also referred to as the optimal estimated states, are also depicted in the figures.

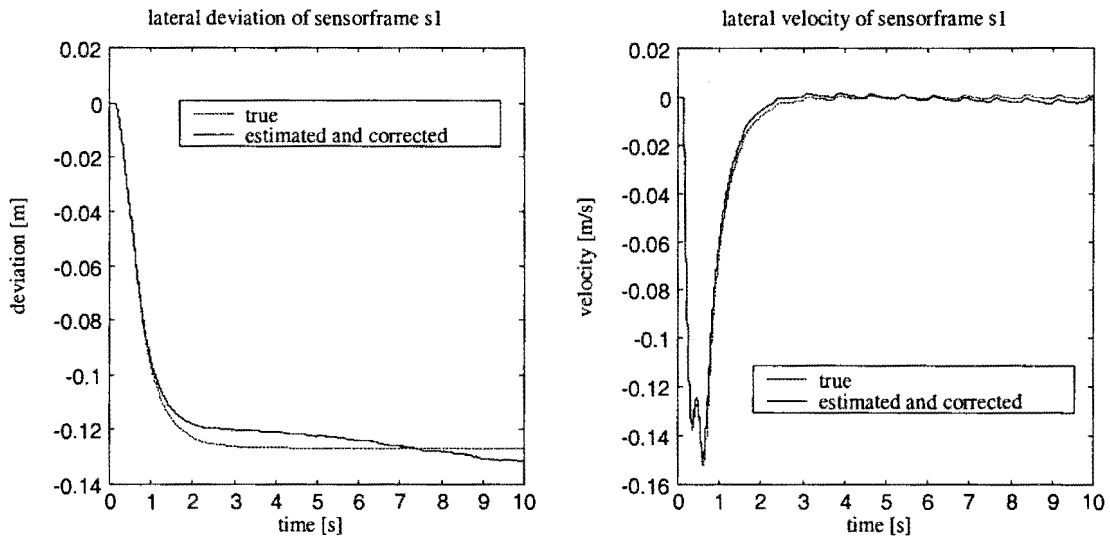


Figure 7-10: True and optimal estimated states of sensorframe *s1*

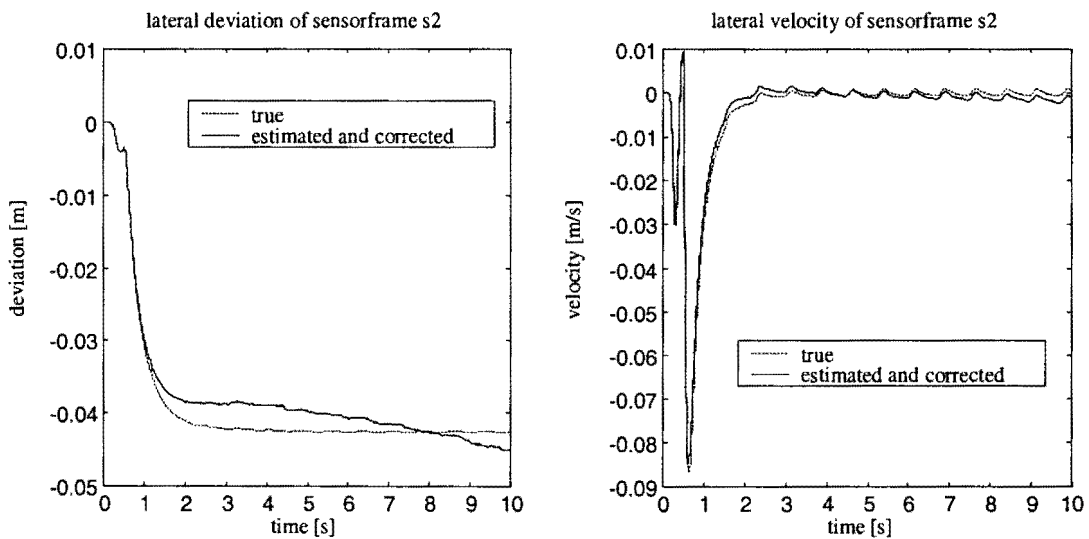


Figure 7-11: True and optimal estimated states of sensorframe *s2*

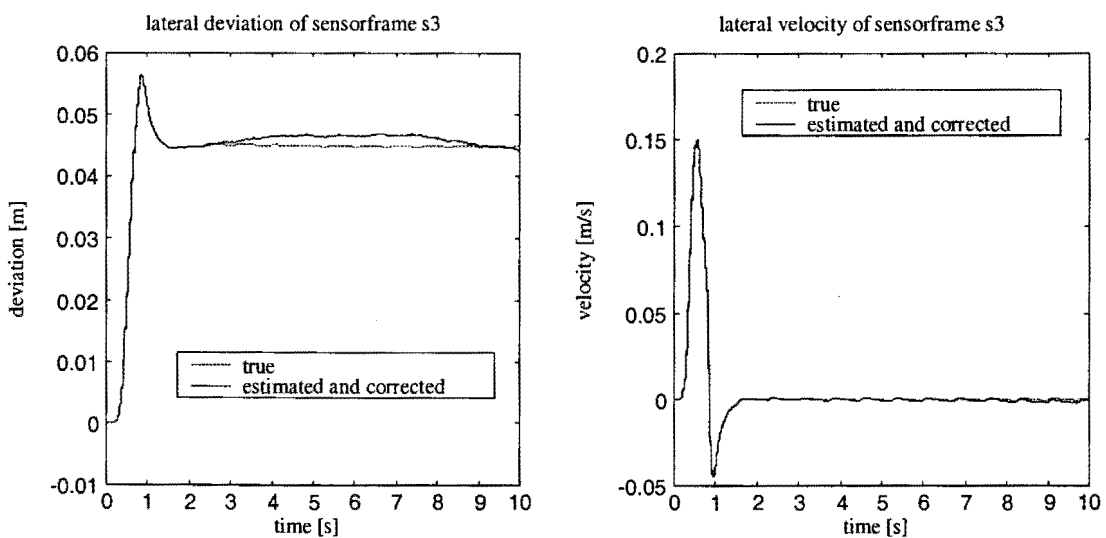
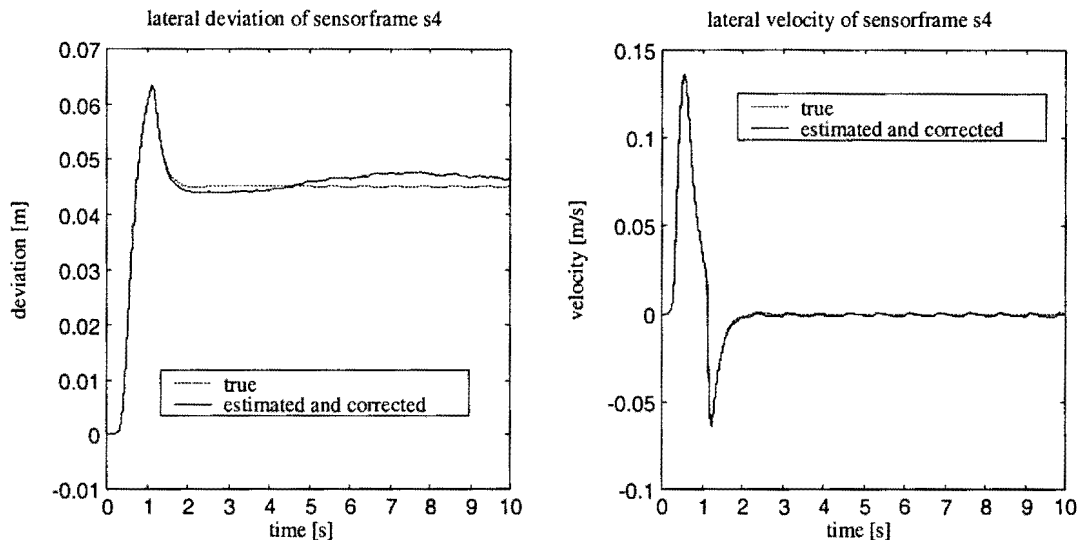


Figure 7-12: True and optimal estimated states of sensorframe *s3*



**Figure 7-13: True and optimal estimated states of sensorframe s4**

The simulation results show that the optimal estimated states are very close to the true states. The estimated lateral velocity fits even almost the true lateral velocity, whereas the estimated lateral deviation still shows some deviations with respect to the true lateral deviation. The estimated lateral deviation fluctuates around the true lateral deviation, but it will converge to the true lateral deviation. It also can be seen in the figures that the influence of noise is hardly visible anymore. This is because the true values of the noise taken in these simulations are much smaller than the intuitive values of the noise taken in the simulations of the previous chapters. The order of magnitude of the noise from the accelerometers and gyroscopes is so small in comparison to the order of magnitude of the sensor signals that the noise on the sensor signals will be almost not visible anymore. Furthermore, it is so that the covariance values of the noise used in the calculation of the Kalman gain are strongly related to the physical noise of the used sensors now, so that the Kalman gain will be optimal. When the Kalman gain is optimal, the state estimates will also reach their optimum. The estimated lateral deviations of the different sensor frames still show some errors with respect to the true lateral deviations of the different sensor frames because the lateral deviation is obtained by integrating the accelerometer readings twice. The double integration as well as magnetometer noise cause the small errors in the estimates of the lateral deviations. The magnitude of magnetometer noise is much bigger than the magnitude of accelerometer and gyroscope noise, so the influence of magnetometer noise is still visible. The estimates of the lateral velocity are obtained by integrating the accelerometer readings once, so the errors with respect to the true lateral velocities shown by these estimates are much smaller.

If the practical values of the sensor noise are the same as the theoretical values of the sensor noise, it can be said that the performance of the observer is of high quality and that it forms a reliable measurement system.

## 7.6 Conclusions

The sensor signals of the sensors described in this report consist of noise. Before the analog sensor signals can be processed by a computer, they have to be discretized. An analog signal has to be filtered by an anti-aliasing filter before it is discretized,

otherwise aliasing will occur. It is described how the sensor noise can be filtered and it is also explained how the covariance of the filtered sensor noise can be obtained. The filtered sensor noise is also called colored noise. It is discussed why the colored noise can be considered as white noise by the observer.

The sensors described here also possess bias and drift properties. It is shown how to deal with these properties and how the disadvantageous properties can be suppressed. Noise properties and values of the used sensors are extracted from their datasheets and simulations are carried out to show the behaviour of the observer with these sensors and their noise values.

When the practical values of the noise do not differ too much from the theoretical values, the estimated states of the observer are very close to the true states and the influence of noise is hardly visible anymore.



# Chapter 8

## Conclusions and recommendations

Here the most important conclusions found by the M.Sc. project are stated. Furthermore, some recommendations for future research are given.

### *8.1 Conclusions*

In this report a method is developed to design a measurement system for an Automatic Guided Vehicle. The measurement system or observer is designed according to the theory of Kalman filtering. The vehicle has to follow a certain roadway reference system. The reference system is formed by a track of magnetic discrete markers, which will be detected by magnetic sensing. Among other approaches, magnetic sensing appears to have some potential advantages. Although permanent magnetic markers are passive devices, they create magnetic fields. The magnetic field appears to be less influenced by environmental conditions than other reference systems. The life cycle of permanent magnets is several decades and they should not need any maintenance.

The observer estimates the lateral velocity and deviation of the vehicle with respect to the roadway reference system. The method of estimation which is used combines the discrete magnetic markers with acceleration measurements according to a Kalman filtering technique. In contrast to other techniques, this estimation technique is completely independent of all vehicle parameters. Another main advantage of this estimation technique is that the effects of disturbances are also taken into account by the observer.

To improve the estimation technique, the observer is extended with gyroscopes. Gyroscopes are instruments which are used to measure angular motion. There is chosen for these sensors, because angular velocity and orientation of a vehicle (which can be measured by these sensors) are main aspects for the lateral control system of the vehicle. A method to implement the rate and integrating gyroscopes in the observer is treated. The method is accurate for small road curvatures only.

One chapter is dedicated to sensor noise and covariance analysis. It is shown how to simulate sensor noise and a method to obtain noise covariances from sensor datasheets is introduced.

Simulation results throughout the report show that the estimated states of the observer are close to the true states of the vehicle. From the measurement results it also can be seen that the estimated states can be improved a lot when the observer is extended with the integrating and rate gyroscopes. The improvement is especially big when the distance between the magnetic markers is big and when the velocity of the vehicle is low. The estimation technique which combines the discrete magnetic markers with acceleration measurements is especially useful for high velocities of the vehicle and for small distances between the magnetic markers. For low velocities and large distances between the magnetic markers, the estimated states show large deviations with respect to the true states.

It can be said that the designed observer in this report forms a good basis for a reliable measurement system of an Automatic Guided Vehicle.

## 8.2 Recommendations

The presented method for a reliable measurement system of an Automatic Guided Vehicle (AGV) can be used for further research on a measurement system for an AGV. The estimation technique which combines the discrete magnetic markers with acceleration measurements is especially useful for high velocities of the vehicle and for small distances between the magnetic markers. It is recommendable to search for an estimation technique which produces reliable estimates for low velocities of the vehicle and large distances between the magnetic markers. Sensors which can be used for this estimation technique are pulse counters which can be mounted on the wheels of the vehicle and angular sensors which can be used to measure the steering angle of the wheels. When the measurements from these sensors are combined it is possible to obtain the lateral velocity of the vehicle with respect to the roadway reference system. The lateral deviation of the vehicle can be calculated out of the lateral velocity. The expectation is that this method is useful for low velocities of the vehicle. For high velocities of the vehicle this method becomes less reliable, because then slip of the wheels is going to play a part.

The presented method for the extension of the observer with gyroscopes is accurate for small road curvatures only. Commuter buses (where this vehicle is one of) however, might also drive on roads with small curves or large curvatures. Therefore, it is recommended to extend this method so that it is accurate for large road curvatures also.

At last, it is recommended that the covariance and the PSD of the noise of the used sensors are determined according to the physical measured noise of the sensors. Only then, reliable statements can be done about the true values of the noise. Thus, if it is known which sensors are going to be used, they have to be ordered so that the true physical noise can be measured. This is much more reliable than extracting the noise values from the datasheets of the sensors.

## References

- [1] Kwakernaak, H. and R. Sivan.  
*Linear Optimal Control Systems.*  
London: Wiley-Interscience, 1972.
- [2] Friedland, B.  
*Advanced Control System Design.*  
London: Prentice-Hall International, 1996.
- [3] Damen, A.  
*Modern Control Theory.*  
Department of Electrical Engineering, Measurement and Control Group,  
Eindhoven University of Technology, 1999.  
Syllabus.
- [4] Saraf, S. and M. Tomizuka.  
*Slip Angle Estimation for Vehicles on Automated Highways.*  
In: Proceedings of the American Control Conference.  
Albuquerque, New Mexico, June 1997, pp. 1588-1592.
- [5] Etten, W. van.  
*Stochastische Signaaltheorie.*  
Faculteit Elektrotechniek, Vakgroep Telecommunicatie,  
Technische Universiteit Eindhoven, januari 1996.  
Syllabus.
- [6] Grinten, P.M.E.M. van der and J.M.H. Lenoir.  
*Statistische Procesbeheersing.*  
Utrecht/Antwerpen: Het Spectrum B.V., 1973.
- [7] Endevco.  
*Products: Table of Contents.*  
<http://www.endevco.com>.  
Endevco Corporation.
- [8] KVH.  
*Innovative Solutions for Global Communications and Navigation.*  
<http://www.kvh.com>.  
KVH Industries, Inc.
- [9] Chen, C. and M. Tomizuka.  
*Passivity-based Nonlinear Observer for Lateral Control of Tractor-Trailer  
Vehicles in Automated Highway Systems.*  
13<sup>th</sup> Triennial IFAC World Congress,  
San Francisco, USA.



# Table of figures

FIGURE 1-1: PICTURE OF THE VEHICLE NAMED PHILEAS .....	1
FIGURE 2-1: FLOWCHART FOR A DISCRETE-TIME KALMAN FILTER .....	9
FIGURE 2-2: SAMPLING PATTERN INVOLVING THREE SENSORS .....	10
FIGURE 3-1: MODEL OF VEHICLE WITH SENSOR CONFIGURATION .....	13
FIGURE 3-2: PATH AND VEHICLE REFERENCED COORDINATES .....	15
FIGURE 4-1: BLOCK DIAGRAM OF THE SIMULINK MODEL .....	21
FIGURE 5-1: DISCRETE TIME KALMAN FILTER .....	26
FIGURE 5-2: FLOWCHART OF OBSERVER CYCLE.....	33
FIGURE 5-3: ESTIMATED AND TRUE LATERAL DEVIATION AND VELOCITY OF SENSORFRAME $s1$ .....	34
FIGURE 5-4: ESTIMATED AND TRUE LATERAL DEVIATION AND VELOCITY OF SENSORFRAME $s2$ .....	35
FIGURE 5-5: ESTIMATED AND TRUE LATERAL DEVIATION AND VELOCITY OF SENSORFRAME $s3$ .....	35
FIGURE 5-6: ESTIMATED AND TRUE LATERAL DEVIATION AND VELOCITY OF SENSORFRAME $s4$ .....	36
FIGURE 6-1: MODEL OF VEHICLE WITH EXTENDED SENSOR CONFIGURATION .....	38
FIGURE 6-2: DEFINITION OF YAW ANGLE ERROR OF VEHICLE CARRIAGE .....	38
FIGURE 6-3: TRANSFORMATION OF LATERAL DEVIATION ${}^p2y_{s2}$ TO LATERAL DEVIATION $y_{a1}$ .....	41
FIGURE 6-4: TRANSFORMATION OF LATERAL DEVIATION ${}^p3y_{s3}$ TO LATERAL DEVIATION $y_{a2}$ .....	43
FIGURE 6-5: ESTIMATED, TRUE AND CORRECTED LATERAL DEVIATION AND VELOCITY OF SENSORFRAME $s1$ .....	46
FIGURE 6-6: ESTIMATED, TRUE AND CORRECTED LATERAL DEVIATION AND VELOCITY OF SENSORFRAME $s2$ .....	46
FIGURE 6-7: ESTIMATED, TRUE AND CORRECTED LATERAL DEVIATION AND VELOCITY OF SENSORFRAME $s3$ .....	47
FIGURE 6-8: ESTIMATED, TRUE AND CORRECTED LATERAL DEVIATION AND VELOCITY OF SENSORFRAME $s4$ .....	47
FIGURE 6-9: FLOWCHART OF EXTENDED OBSERVER CYCLE.....	53
FIGURE 6-10: TRUE, ESTIMATED AND RATE GYRO-CORRECTED LATERAL DEVIATION AND VELOCITY OF SENSORFRAME $s1$ .....	54
FIGURE 6-11: TRUE, ESTIMATED AND RATE GYRO-CORRECTED LATERAL DEVIATION AND VELOCITY OF SENSORFRAME $s2$ .....	54
FIGURE 6-12: TRUE, ESTIMATED AND RATE GYRO-CORRECTED LATERAL DEVIATION AND VELOCITY OF SENSORFRAME $s3$ .....	55
FIGURE 6-13: TRUE, ESTIMATED AND RATE GYRO-CORRECTED LATERAL DEVIATION AND VELOCITY OF SENSORFRAME $s4$ .....	55
FIGURE 7-1: THE SYSTEM SCHEMATIC .....	57
FIGURE 7-2: FILTERING AND SAMPLING OF SENSOR NOISE.....	58
FIGURE 7-3: SCHEMATIC OF A/D CONVERTER .....	59
FIGURE 7-4: PROCESS AND SENSOR FILTERING .....	61
FIGURE 7-5: CHARACTERISTIC OF FILTERED PROCESS DYNAMICS.....	62
FIGURE 7-6: CHARACTERISTIC OF HIGHPASS FILTER .....	63
FIGURE 7-7: BODEPLOT OF HIGHPASS FILTER .....	64
FIGURE 7-8: INPUT SIGNAL OF THE HIGHPASS FILTER.....	64
FIGURE 7-9: OUTPUT SIGNAL OF THE HIGHPASS FILTER .....	65
FIGURE 7-10: TRUE AND OPTIMAL ESTIMATED STATES OF SENSORFRAME $s1$ .....	70
FIGURE 7-11: TRUE AND OPTIMAL ESTIMATED STATES OF SENSORFRAME $s2$ .....	70
FIGURE 7-12: TRUE AND OPTIMAL ESTIMATED STATES OF SENSORFRAME $s3$ .....	70
FIGURE 7-13: TRUE AND OPTIMAL ESTIMATED STATES OF SENSORFRAME $s4$ .....	71



# Appendices

Appendix 1: Observer.m

Appendix 2: Datasheet of MSA100

Appendix 3: Datasheet of KVH E•Core 1000





# Appendix 1: Observer.m

Matlab® file which describes the observer.

```
function [sys,x0,str,ts] = sfuntmpl(t,x,u,flag)
%
% The following outlines the general structure of an S-function.
%
switch flag,

    %%%%%%%%%%%%%%%%%%%%%%%%%%
    % Initialization %
    %%%%%%%%%%%%%%%%%%%%%%%%%%
    case 0,
        [sys,x0,str,ts]=mdlInitializeSizes;
        global counterf;           %Counter for number of samples.
        counterf = 0;             %Initialize sample-counter.
        global xd_f;              %States of the observer.
        xd_f = [0;0;0;0;0;0;0;0;0]; %Initialize states of the observer.
        global M_f;               %Variable for covariance of estimation
                                   %error.
        M_f=0;                    %Initialize covariance of estimation
                                   %error.
        global counter_front;     %Variables for counters to count how
        global counter_rear;     %many times the magnetometers
        global counter_st1;      %at the vehicle have passed
        global counter_st2;      %a magnetic marker.
        counter_front = 0;        %Initialize counter_front.
        counter_rear = 0;         %Initialize counter_rear.
        counter_st1 = 0;         %Initialize counter_st1.
        counter_st2 = 0;         %Initialize counter_st2.
        global correction_yaw;    %Variable for correction_yaw decision.
        global correction_yaw_rate; %Variable for correction_yaw_rate
                                   %decision.
        correction_yaw = 0;       %Variable for correction_yaw decision,
                                   %0 = FALSE, 1 = TRUE.
        correction_yaw_rate = 1;  %Variable for correction_yaw_rate
                                   %decision, 0 = FALSE, 1 = TRUE.

    %%%%%%%%%%%%%%%%%%%%%%%%%%
    % Outputs %
    %%%%%%%%%%%%%%%%%%%%%%%%%%
    case 3,
        sys=mdlOutputs(t,x,u);

    %%%%%%%%%%%%%%%%%%%%%%%%%%
    % GetTimeOfNextVarHit %
    %%%%%%%%%%%%%%%%%%%%%%%%%%
    case {1,2,4,9}
        sys=[];%unused flag;

    %%%%%%%%%%%%%%%%%%%%%%%%%%
    % Unexpected flags %
    %%%%%%%%%%%%%%%%%%%%%%%%%%
    otherwise
        error(['Unhandled flag = ',num2str(flag)]);
end
% end sfuntmpl
%
```

```

%=====
% mdlInitializeSizes
% Return the sizes, initial conditions, and sample times for the
% S-function.
%=====
%
function [sys,x0,str,ts]=mdlInitializeSizes

sizes = simsizes;

sizes.NumContStates = 0;    %Number of continuous states.
sizes.NumDiscStates = 0;    %Number of discontinuous states.
sizes.NumOutputs     = 8;    %Number of outputs of observer.
sizes.NumInputs      = 22;   %Number of inputs of observer.
sizes.DirFeedthrough = 1;    %Direct feedthrough is available.
sizes.NumSampleTimes = 1;    %At least one sample time is needed.

sys = simsizes(sizes);
%
% initialize the initial conditions
%
x0 = [];    %No continuous states.
%
% str is always an empty matrix
%
str = [];    %No state ordering.
%
% initialize the array of sample times
%
ts = [-1 0]; %Inherited sample time.

% end mdlInitializeSizes
%
%=====
% mdlOutputs
% Return the block outputs.
%=====
%
function sys=mdlOutputs(t,x,u)
global counterf;    %Sample-counter.
global xd_f;       %States of the observer.
global M_f;        %Covariance of estimation error.
global counter_front; %Variables for counters to count how
global counter_rear; %many times the magnetometers
global counter_st1; %at the vehicle have passed
global counter_st2; %a magnetic marker.
global correction_yaw; %Variable for correction_yaw decision.
global correction_yaw_rate; %Variable for correction_yaw_rate
                        %decision.

Lsf=2.5;    %Distance between tractor's centre of gravity and
            %frontsensor.
Lsr=5.217;  %Distance between tractor's centre of gravity and
            %rearsensor.
Lsst1=6.15; %Distance between articulation point of first
            %semitrailer and sensor on first semitrailer.
Lsst2=6;    %Distance between articulation point of second
            %semitrailer and sensor on second semitrailer.
Lst1=6.15;  %Length of first semitrailer.
dr1=5.217;  %Distance between tractor's centre of gravity and
            %articulation point.

```

```

ds1 = dr1 - Lsr; %Distance between tractor's rearsensor and
                %articulation point.
alfa = u(21); %Angle between tractor and first semitrailer.
beta = u(22); %Angle between first semitrailer and second
                %semitrailer.

a = [0 1;0 0]; %Definition of a-matrix for SISO representation.
b = [0;1]; %Definition of b-matrix for SISO representation.
c = [1 0]; %Definition of c-matrix for SISO representation.
A=[a zeros(2,6);zeros(2,2) a zeros(2,4); zeros(2,4) a zeros(2,2);...
   zeros(2,6) a]; %Definition of A-matrix for MIMO representation.
B=[0 0 0 0;1 0 0 0;0 0 0 0;0 1 0 0;0 0 0 0;0 0 1 0;0 0 0 0;0 0 0 1];
   %Definition of B-matrix for MIMO representation.
C = [1 0 0 0 0 0 0 0;...
     0 0 1 0 0 0 0 0;...
     0 0 0 0 1 0 0 0;...
     0 0 0 0 0 0 1 0;...
     1/(Lsf + Lsr) 0 -1/(Lsf + Lsr) 0 0 0 0 0;...
     0 0 1/(Lsst1*cos(alfa)) 0 -1/(Lsst1) 0 0 0;...
     0 0 0 0 1/(Lsst2*cos(beta)) 0 -1/(Lsst2) 0;...
     0 1/(Lsf + Lsr) 0 -1/(Lsf + Lsr) 0 0 0 0;...
     0 0 0 1/(Lsst1*cos(alfa)) 0 -1/Lsst1 0 0;...
     0 0 0 0 0 1/(Lsst2*cos(beta)) 0 -1/Lsst2];
   %Definition of C-matrix for MIMO representation.
t = u(9); %Simulation time.
dt = 0.005; %Definition of sample time.
w_d = 0.001; %Covariance of noise from accelerometer.
v_d = 0.00002; %Covariance of noise from magnetometer.
Wd = w_d*eye(4); %Covariance matrix of noise from
                %accelerometers at tractor and semitrailers.
Vd = v_d*eye(4); %Covariance matrix of noise from
                %magnetometers at tractor and semitrailers.
Vd(5,5) = 0.000005; %Covariance of noise from integrating
                %gyroscope at tractor.
Vd(6,6) = 0.000005; %Covariance of noise from integrating
                %gyroscope at first semitrailer.
Vd(7,7) = 0.000005; %Covariance of noise from integrating
                %gyroscope at second semitrailer.
Vd(8,8) = 0.000005; %Covariance of noise from rate gyroscope at
                %tractor.
Vd(9,9) = 0.000005; %Covariance of noise from rate gyroscope at
                %first semitrailer.
Vd(10,10) = 0.000005; %Covariance of noise from rate gyroscope at
                %second semitrailer.
Ad = expm(A*dt); %Calculation of discrete-time A-matrix.
Bd=eye(8)*dt*B+0.5*A*dt^2*B; %Calculation of discrete-time B-matrix.
Bw=Bd; %Definition of discrete-time Bw-matrix.
magnet_distance = 2; %Distance between magnetic markers.
timestep = 0.001; %Simulation timestep.

if t >= counterf*dt; %Start of observer cycle.
    t;
    xd_f = Ad*xd_f+Bd*[u(1);u(2);u(3);u(4)]; %Prediction of observer
                %states.
    M_f = Ad*M_f*Ad'+Bw*Wd*Bw'; %Propagation of the covariance
                %of the estimation error.

    %Correction step if measurement data of tractor's, semitrailer1's
    %and semitrailer2's integrating gyroscope (yaw) is available.
    %Assumed is that gyroscope data is available at the same time as
    %accelerometer data.

```

```

if correction_yaw == 1
    C = [0 0 0 0 0 0 0 0 0;...
         0 0 0 0 0 0 0 0 0;...
         0 0 0 0 0 0 0 0 0;...
         0 0 0 0 0 0 0 0 0;...
         1/(Lsf + Lsr) 0 -1/(Lsf + Lsr) 0 0 0 0 0;...
         0 0 1/(Lsst1*cos(alfa)) 0 -1/(Lsst1) 0 0 0;...
         0 0 0 0 1/(Lsst2*cos(beta)) 0 -1/(Lsst2) 0;...
         0 0 0 0 0 0 0 0 0;...
         0 0 0 0 0 0 0 0 0;...
         0 0 0 0 0 0 0 0 0];    %Observation matrix for integrating
                                %gyroscopes at the vehicle.
    K=M_f*C'*inv(C*M_f*C' + Vd);    %Calculation of Kalman gain.
    M_f=M_f-K*C*M_f;    %Update of covariance of estimation error.
    xd_f = xd_f + K * ([u(5); u(6); u(7); u(8); u(15); u(16);...
                       u(17); u(18); u(19); u(20)] - C * xd_f);
                                %Update of state estimate.
end

%correction step if measurement data of tractor's, semitrailer1's
%and semitrailer2's rate gyroscope (yaw rate) is available.
%Assumed is that gyroscope data is available at the same time as
%accelerometer data.
if correction_yaw_rate == 1
    C = [0 0 0 0 0 0 0 0 0;...    %Observation matrix for rate
         0 0 0 0 0 0 0 0 0;...    %gyroscopes at the vehicle.
         0 0 0 0 0 0 0 0 0;...
         0 0 0 0 0 0 0 0 0;...
         0 0 0 0 0 0 0 0 0;...
         0 0 0 0 0 0 0 0 0;...
         0 0 0 0 0 0 0 0 0;...
         0 1/(Lsf + Lsr) 0 -1/(Lsf + Lsr) 0 0 0 0;...
         0 0 0 1/(Lsst1*cos(alfa)) 0 -1/Lsst1 0 0;...
         0 0 0 0 0 1/(Lsst2*cos(beta)) 0 -1/Lsst2];
    K=M_f*C'*inv(C*M_f*C' + Vd);    %Calculation of Kalman gain.
    M_f=M_f-K*C*M_f;    %Update of covariance of estimation error.
    xd_f = xd_f + K * ([u(5); u(6); u(7); u(8); u(15); u(16);...
                       u(17); u(18); u(19); u(20)] - C * xd_f);
                                %Update of state estimate.
end

%Correction step if front magnetometer on tractor is on top of a
%magnetic marker.
if u(10)+timestep*u(14)> (counter_front+ceil(Lsf))*magnet_distance
    counter_front = counter_front+1;
    C = [1 0 0 0 0 0 0 0 0;...
         0 0 0 0 0 0 0 0 0;...
         0 0 0 0 0 0 0 0 0;...
         0 0 0 0 0 0 0 0 0;...
         0 0 0 0 0 0 0 0 0;...
         0 0 0 0 0 0 0 0 0;...
         0 0 0 0 0 0 0 0 0;...
         0 0 0 0 0 0 0 0 0;...
         0 0 0 0 0 0 0 0 0;...
         0 0 0 0 0 0 0 0 0];    %Observation matrix for front
                                %magnetometer on tractor.
    K=M_f*C'*inv(C*M_f*C'+Vd); %Calculation of Kalman gain.
    M_f=M_f-K*C*M_f;    %Update of covariance of estimation error.
    xd_f = xd_f + K * ([u(5); u(6); u(7); u(8); u(15); u(16);...
                       u(17); u(18); u(19); u(20)] - C * xd_f);

```

```

                                %Update of state estimate.
end

%Correction step if rear magnetometer on tractor is on top of a
%magnetic marker.
if u(11)+timestep*u(14)> (counter_rear-floor(Lsr))*magnet_distance
    counter_rear = counter_rear+1;
    C = [0 0 0 0 0 0 0 0;...
         0 0 1 0 0 0 0 0;...
         0 0 0 0 0 0 0 0;...
         0 0 0 0 0 0 0 0;...
         0 0 0 0 0 0 0 0;...
         0 0 0 0 0 0 0 0;...
         0 0 0 0 0 0 0 0;...
         0 0 0 0 0 0 0 0;...
         0 0 0 0 0 0 0 0]; %Observation matrix for rear
                                %magnetometer on tractor.
    K = M_f*C'*inv(C*M_f*C'+Vd); %Calculation of Kalman gain.
    M_f=M_f-K*C*M_f; %Update of covariance of estimation error.
    xd_f = xd_f + K * ([u(5); u(6); u(7); u(8); u(15); u(16);...
                       u(17); u(18); u(19); u(20)] - C * xd_f);
                                %Update of state estimate.
end

%Correction step if magnetometer on first semitrailer is on top
%of a magnetic marker.
if u(12)+timestep*u(14)>(counter_st1-...
    floor(Lsst1+drl))*magnet_distance
    counter_st1 = counter_st1+1;
    C = [0 0 0 0 0 0 0 0;...
         0 0 0 0 0 0 0 0;...
         0 0 0 0 1 0 0 0;...
         0 0 0 0 0 0 0 0;...
         0 0 0 0 0 0 0 0;...
         0 0 0 0 0 0 0 0;...
         0 0 0 0 0 0 0 0;...
         0 0 0 0 0 0 0 0;...
         0 0 0 0 0 0 0 0]; %Observation matrix for magnetometer
                                %on first semitrailer.
    K = M_f*C'*inv(C*M_f*C'+Vd); %Calculation of Kalman gain.
    M_f=M_f-K*C*M_f; %Update of covariance of estimation error.
    xd_f = xd_f + K * ([u(5); u(6); u(7); u(8); u(15); u(16);...
                       u(17); u(18); u(19); u(20)] - C * xd_f);
                                %Update of state estimate.
end

%Correction step if magnetometer on second semitrailer is on top
%of a magnetic marker.
if u(13)+timestep*u(14)>(counter_st2-...
    floor(drl+Lst1+Lsst2))*magnet_distance
    counter_st2 = counter_st2+1;
    C = [0 0 0 0 0 0 0 0;...
         0 0 0 0 0 0 0 0;...
         0 0 0 0 0 0 0 0;...
         0 0 0 0 0 0 1 0;...
         0 0 0 0 0 0 0 0;...
         0 0 0 0 0 0 0 0;...
         0 0 0 0 0 0 0 0;...
         0 0 0 0 0 0 0 0;...
         0 0 0 0 0 0 0 0];

```

```
    0 0 0 0 0 0 0 0;...
    0 0 0 0 0 0 0 0];      %Observation matrix for magnetometer
                           %on second semitrailer.
K = M_f*C'*inv(C*M_f*C'+Vd); %Calculation of Kalman gain.
M_f=M_f-K*C*M_f;          %Update of covariance of estimation error.
xd_f = xd_f + K * ([u(5); u(6); u(7); u(8); u(15); u(16);...
                   u(17); u(18); u(19); u(20)] - C * xd_f);
                           %Update of state estimate.

end
counterf = counterf+1;
end
sys=xd_f;
% end mdlOutputs
```

# Appendix 2: Datasheet of MSA100

## Micromachined Servo Accelerometer

**ENDEVCO  
MODEL  
MSA100**

### Model MSA100

- 3 mg Bias Composite Error
- Rugged, Low Vibration Rectification
- High Resolution
- Range Adjustable
- Self Test



Actual size

### DESCRIPTION

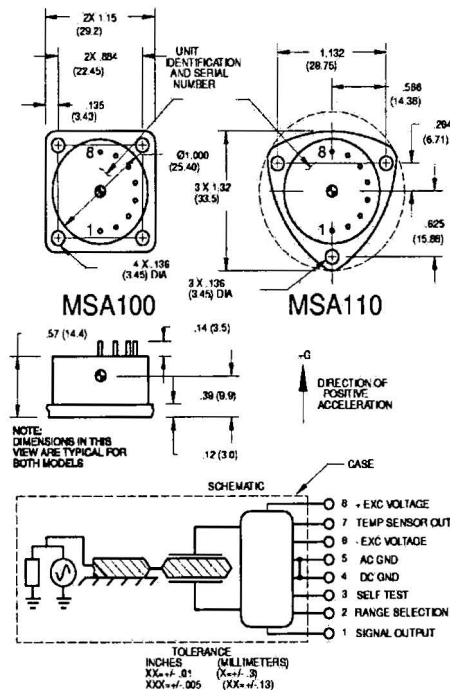
The ENDEVCO® Model MSA100 Servo Accelerometer utilizes a force rebalanced sensor that offers exceptional ruggedness, high resolution, and low vibration rectification. Temperature output and calibration coefficients are standard features allowing for modeling to 3 mg accuracies.

The Model MSA100 is designed for inertial motion studies in vehicles, tactical grade missile IMU's, flight tests, and tilt/angle measurements.

At the heart of the MSA100 is a three-layer micromachined silicon sensor. The middle layer includes the proof mass which, with applied acceleration, is electrostatically rebalanced to a null position between the upper and lower electrodes. This force rebalancing offers a wide bandwidth, minimal non-linearity and excellent performance in high shock and vibration environments. External resistors are used to adjust full scale range from the standard  $\pm 50$  g's to lower g levels without affecting the accelerometer's electronics. The MSA100 also has self-test capability which moves the proof mass and outputs a proportional signal.

The micromachined silicon sensor and hybrid electronics are hermetically sealed for environmental protection in a stainless steel case with an industry standard mounting pattern. The Servo Accelerometer is also available with a triangular mounting plate as a Model MSA110.

U.S. Patent 5,205,171



### SPECIFICATIONS

PERFORMANCE CHARACTERISTICS: All values are typical at +75 °F (+24 °C) and  $\pm 15$  Vdc excitation and with  $\pm 50$  g range unless otherwise stated. Calibration data, traceable to the National Institute of Standards, (NIST), is supplied. Reference Note [6] for definitions.

	Units	MSA100/MSA110
RANGE[1]	g	$\pm 50$ , Adjustable to $\pm 0.5$ [7]
BIAS	g Max	$\pm 1.5$
BIAS COMPOSITE ERROR [2]	mg rms Typ	3
	mg rms Max	5
BIAS TEMPERATURE SENSITIVITY	$\mu\text{g}/^\circ\text{F}$ Typ	330
	$\mu\text{g}/^\circ\text{C}$ Typ	600



**ENDEVCO**  
**MODEL**  
**MSA100**
**Micromachined Servo Accelerometer**
**SPECIFICATIONS—continued**  
**PERFORMANCE CHARACTERISTICS—continued**

	Units	MSA100/MSA110
SCALE FACTOR	mV/g	200 ±40
SCALE FACTOR COMPOSITE ERROR [2]	ppm Max	1000
SCALE FACTOR TEMPERATURE SENSITIVITY	ppm/°F Typ	-50
	ppm/°C Typ	-90
NON-LINEARITY	% FSO Typ	±0.1
FREQUENCY RESPONSE (±5% max, ref 100 Hz)	Hz	0 to 500
RESONANCE FREQUENCY	Hz Typ	2000
PHASE RESPONSE (0 to 500 Hz)	degree, Typ	-10
	degree, Max	-15
AXIS MISALIGNMENT	mrad Max	±10
VIBRATION RECTIFICATION COEFFICIENT [3] (0 to 2000 Hz)	µg/g <sup>2</sup> Max	30
VIBROPENDULOSITY	µg/g <sup>2</sup> Max	10
SELF-TEST	g/voIt Typ	2.5
TEMPERATURE SENSOR OUTPUT@ +75 °F (+24 °C) [4]	V Typ	0.630
TEMPERATURE SENSOR SENSITIVITY	mV/°F Typ	1.2
	mV/°C Typ	2.1
ACTIVATION TIME	sec Max	0.5
<b>ELECTRICAL</b>		
EXCITATION	±13 Vdc to ±18 Vdc	
Bias Voltage Sensitivity	< 1 µg/Vdc	
Scale Factor Voltage Sensitivity	<200 ppm/Vdc	
INPUT CURRENT	25 mA max per supply	
OUTPUT RESISTANCE	1000 ohms maximum	
INSULATION RESISTANCE	>20 Mohm at 50 Vdc	
OUTPUT NOISE [5] TYPICAL	0.5 to 10 Hz	0.4 µVrms/√Hz
	0.5 to 500 Hz	4 µVrms/√Hz
	0.5 to 10 kHz	40 µVrms/√Hz
<b>PHYSICAL</b>		
CASE, MATERIAL	304L Stainless Steel	
ELECTRICAL CONNECTIONS	Eight solder pins	
IDENTIFICATION	Manufacturer's logo, model number and serial number	
MOUNTING TORQUE	Holes for 4-40 or M3 mounting screws/ 6 lbf-in (0.7 Nm)	
WEIGHT	40 grams maximum	
<b>ENVIRONMENTAL</b>		
TEMPERATURE RANGE, OPERATING	-65 to +221 °F (-55 to +105 °C)	
VIBRATION	30 grms, 20 to 2000 Hz	
SHOCK (half-sine pulse)	5000 g min, 200 µsecond or longer	
HUMIDITY	Unaffected. Hermetically sealed	
ALTITUDE	Unaffected	
MAGNETIC SENSITIVITY ON BIAS	30 µg/Gauss at 15 Gauss field	
<b>CALIBRATION DATA SUPPLIED</b>		
BIAS	mV	
SCALE FACTOR	mV/g	
AXIS MISALIGNMENT	mrad	
TEMPERATURE MODELING	Coefficients for third order fit of Bias and Scale Factor	
FREQUENCY RESPONSE	20 to 10 kHz	

**ACCESSORIES**

EHW265	(4) Size 4, Flat Washers
EH409	(4) 4-40 X 3/8 inch Cap Screws
EHM464	(1) Hex Wrench

5. With 50 g full scale.

6. IEEE Std 337-1972. Standard Specification Format Guide and Test Procedure for linear, single axis, pendulous, analog and torque balance accelerometer.

 7. Range selection external resistor ( $R_s$ ) connected from pin 2 to pin 4.

**NOTES**

- For best results unit should be calibrated to required lower acceleration ranges when rescaling.
- RSS of temperature modeling residual and repeatability.
- Optional 10 µg/g<sup>2</sup> available on special order.
- Temperature modeling provides third order coefficients for bias and scale factor.

$$R_s = \frac{10,000 \text{ ohms}}{\left(\frac{S_u}{S_d} - 1\right)}$$

$S_d$  = desired scale factor, V/g.  
 $S_u$  = unadjusted scale factor, V/g.

Continued product improvement necessitates that Endevco reserve the right to modify these specifications without notice. Endevco maintains a program of constant surveillance over all products to ensure a high level of reliability. This program includes attention to reliability factors during product design, the support of stringent Quality Control requirements, and compulsory corrective action procedures. These measures, together with conservative specifications, have made the name Endevco synonymous with reliability.

ENDEVCO CORPORATION, 30700 RANCHO VIEJO ROAD, SAN JUAN CAPISTRANO, CA 92675 USA (949) 483-8181 fax (949) 661-7231

0298



## Appendix 3: Datasheet of KVH E•Core 1000



*KVH E•Core™ 1000 Fiber Optic Gyro (FOG) sensor offers unparalleled accuracy and precision at a fraction of the cost of competing products.*

### *Key Features & Attributes*

- No moving parts to wear out
- Excellent reliability – 50,000 hours MTBF
- Insensitive to vibration and linear acceleration
- Low noise, high bandwidth
- Exceptional stability – minimal temperature and power-up errors
- Digital or analog output
- Economical FOG solution



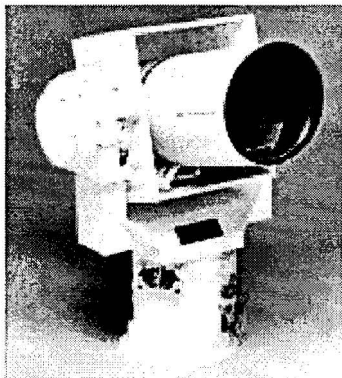
### *KVH E•Core™ 1000 –*

#### *Low Cost, High Performance Fiber Optic Gyro*

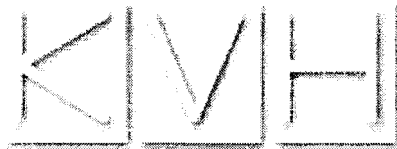
The new KVH E•Core 1000 fiber optic gyro is the perfect replacement for troublesome mechanical gyroscopes in applications such as antenna and optical stabilization, navigation, positioning, robotics, and instrumentation. Wide bandwidth, excellent resolution, and bias stability combined with resistance to shock and vibration fills a wide variety of system needs making the KVH E•Core 1000 the ideal upgrade solution for tracking, stabilization and GPS/FOG navigation.

Based on KVH's exclusive E•Core fiber and precision fiber optic gyro technology, the device precisely measures angular rates up to 100 degrees per second with a resolution of 0.05 degrees/sec in 100 Hz bandwidth. This exceptional dynamic rate is complemented with bias stabilities of better than 4° per hour. The unit never requires recalibration and has excellent time and temperature characteristics.

For replacement of mechanical gyros or new system design, the KVH E•Core 1000 series fiber optic gyros provide precision measurement of rotation with high reliability, ease of interface, and no need for preventive maintenance.



*KVH's fiber optic gyros are a principle component of Xybion's high accuracy positioning systems for optical and millimeter wave RF applications.*



**Applications**

- Antenna Stabilization
- Industrial Robotics
- Optical Stabilization
- Avionics – Attitude/Heading

**Precision, Performance, and Price**

Fabricated from KVH's proprietary E-Core polarization-maintaining fiber, the KVH E-Core 1000 delivers superior fiber optic precision and reliable performance for about the same price as a traditional gyro. Unlike mechanical gyros, the E-Core 1000 is a true single-axis rotation rate sensor insensitive to cross axis motion and errors. Its high bandwidth makes it particularly suitable for high dynamic applications. Additionally, the noise spectrum of the E-Core 1000 is exceptionally flat, lacking the discrete components of mechanical gyros. Aided by the unique properties of E-Core fiber, the KVH unit is intrinsically broadband and easily integrated into existing mechanical gyro applications. And, with no moving parts to maintain or replace, it lasts longer, functions better, and yields significant savings over the life of the product.

**Technical Specifications**

**Physical**

Input Voltage:	12 or 24 VDC nominal (9-18 VDC, 18-36 VDC) transient and reverse voltage protected
Power Consumption:	2 watts (analog) 3 watts (digital)
Weight:	0.55 lbs. (0.25 kg)
Size:	4.3" x 3.5" x 1.6" (109mm x 89mm x 41mm)
Connector Type:	15-pin subminiature D-sub (DA15P)

**Output**

Scale Factor:	20 mV/°/sec
Analog:	+2.5 VDC (zero rotation) ±2 V, into 10K Ohm
Digital:	16 bits, serial, RS232 9600 BPS, 10 values/sec
Sensor Output (Port 1):	analog, RS232 or RS422

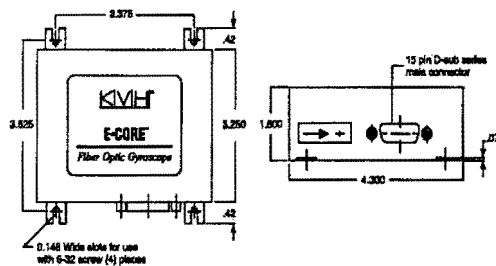
**Environmental**

Operating Temperature:	-40°C to +75°C
Storage Temperature:	-50°C to +85°C
Shock:	90 G
EMI/RFI:	CE, IEC 9081-2,3,4
MTBF:	50,000 hour

**Performance**

Bias Stability vs. Time:	2-4 °/hr, 1 sigma
Bias Stability vs. Temp <sup>1</sup> :	0.08 °/sec rms, typical 0.4 °/sec, peak to peak
Bias Drift Compensated (typical):	5-10 °/hr rms
Angle Random Walk (noise):	20 °/hr/rt-Hz 0.3 °/rt-hr
Rotation Rate:	±100 °/sec
Instantaneous Bandwidth:	100 Hz
Scale Factor Linearity:	<0.5% rms (constant temp.) <1% rms (full temp.)
Scale Factor Stability over Temp <sup>1</sup> :	0.5-1.0% rms
Turn-on Time:	1 sec

<sup>1</sup>Bias and scale factor stability specifications values are uncompensated. Calibration can reduce these errors by a factor of 10.



E-Core 1000 Bro. Sheet 4/98

KVH Industries, Inc. 50 Enterprise Center Middletown, RI 02842 U.S.A.  
 Phone: (401) 847-3327 Fax: (401) 849-0045 E-Mail: info@kvh.com Internet: http://www.kvh.com